

LIPID COMPOSITIONS OF MICROBIAL ORGANISMS ISOLATED  
FROM EXTREME ENVIRONMENTS AND THEIR IMPLICATION  
IN THERMO STABILITY OF BACTERIAL CELL  
MEMBRANE STRUCTURE

---

A Dissertation  
Submitted to  
the Temple University Graduate Board

---

In Partial Fulfillment  
of the Requirements for the Degree  
DOCTOR OF PHILOSOPHY

---

by  
SIDDHARTH SHAH  
DECEMBER 2016

Examining Committee Members:

Dr. Susan A. Jansen-Varnum, Advisory Chair, Department of Chemistry  
Dr. Robert Stanley, Department of Chemistry  
Dr. Michael Zdilla, Department of Chemistry  
Dr. Parkson Lee-Gau Chong, External Member, Department of Biochemistry,  
Temple University

©  
Copyright 2016

By

Siddharth Shah  
All Rights Reserved

## ABSTRACT

Microorganisms with an ability to thrive in harsh environments are referred as “extremophiles”. With advances in biotechnology, interest has grown in the extremophile research because of their unique macromolecules’ characteristics due to their growth environments. Over last decade, researchers have isolated many extremophiles from environments like volcano, salt lakes, hydrothermal vents, deep oceans, Antarctica glaciers etc. Macromolecules of these extremophiles are responsible for their survival in extreme environments. In this research work we have isolated lipid molecules from three different microorganisms.

- 1) *GWEI* strain, a thermophilic bacterium, isolated from dark crusty material from sterilization ovens.
- 2) *7L* strain, a thermophilic bacterium, isolated from Chilean Copahue Volcano.
- 3) *IIP* strain, a facultative anaerobe of the family Enterobacteriaceae, recently isolated from Antarctica.

Complex lipid arrangement and/or type in the cell membrane are known to affect thermostability of microorganisms and efforts were made to understand the chemical nature of the polar lipids of membrane. In this work, we extracted total lipids from cell membrane, separated them by TLC into various fractions and characterize the lipid structures of fractions with analytical tools such as  $^1\text{H}$ ,  $^{13}\text{C}$ ,  $^{31}\text{P}$  and 2D NMR spectroscopy, ATR-FTIR spectroscopy and  $\text{MS}^n$  spectrometry.

In *GWEI* strain, we were able to identify glycerophosphoethanolamine, glycerophosphate, glycerophosphoglycerol and cardiolipin lipid classes and an unknown

glycerophospholipid class with novel MS/MS spectra pattern. We have also noticed the presence of saturated iso-branched fatty acids with NMR spectra in individual lipid classes. In case of *IIP* strain, we have identified glycerophosphoglycerol, glycerophosphoethanolamine, glycerophosphate, and acyl glycerophosphoglycerol lipid classes with unsaturated fatty acids in their structure, which could be one of the many reasons for survivability at lower temperatures. In case of *7L* strain, we were able to identify glycerophosphoglycerol, cardiolipin, glycerophosphoethanolamine and glycerophosphate lipid classes with saturated iso branched fatty acids. FAME analysis revealed iso-15:0 (52.29 %) and iso-17:0 (18.64 %) as major fatty acyl chains.

We did not observe major difference in polar head group composition of lipid classes between thermophiles (*GWE1* and *7L*) compare to psychrophiles (*IIP*). Major difference among these three strains was in fatty acid composition of lipid molecule. Both thermophiles showed presence of lipids with long chain saturated fatty acids while *IIP* showed presence of lipid molecule with unsaturated fatty acid chain. Lipids made of unsaturated fatty acids have lower melting points and they introduce kink in the cell membrane structure. At lower temperatures, these effects allow membrane to maintain fluidity and its functionality, which in turn allows the microorganism to grow at lower temperature. Lipids made with saturated iso branched fatty acid chain have higher melting points and they pack together densely in cell membrane. At high temperature because of higher melting point and dense packing, membrane fluidity is not affected and this effect allows microorganism to grow at the higher temperature. We believe that change in fatty acid composition is one of the many reasons for these microorganisms to

survive the extreme condition. Thermostability of the other macromolecules (DNA, enzyme) of these extremophiles is not studied in this dissertation.

## **ACKNOWLEDGEMENTS**

My graduation study at Temple University has been a wonderful journey. I am feeling deep gratitude for the support and assistance provided by many people. First I would like to thank my parents who supported my decision to come for further study in USA and provided me with all the resources so I can achieve success in my life. I will always be grateful for their love and support that has led me to this point.

I would like to express my deepest gratitude to my advisor Professor Susan Jansen-Varnum for the continuous support of my PhD study. Her guidance has made this a thoughtful and rewarding journey. I could not have imagined having a better advisor and mentor for my PhD study. Moreover, I am very grateful to Professor Parkson Lee-Gau Chong for his valuable suggestions and guidance for the research work. I will always appreciate the time that he volunteered to proofread my research articles. My sincere thanks also go for other committee members Professor Robert Stanley, Professor Michael Zdilla for their willingness to serve in my committee and for the assistance they provided at all levels of my PhD study.

I would also like to take this opportunity to thank all the teachers from Zenith High school, Maharaja Sayajirao University and Fairleigh Dickinson University. Special thank you for Yadav Sir, Balaraman Sir, Professor Richard Thompson, who encouraged me and increased my interest in research. I am here because of what they have taught me. I will forever be indebted to them.

I would also like to thank Dr. Jeff Mihalic (Amgen Inc.), Dr. Satyakala Ganti (Wes Pharma) and Dr. Xingwang Liu (Taro Pharmaceuticals) for providing me

opportunity to work under their guidance in the pharmaceutical field, which provided me valuable knowledge about the industrial atmosphere. I would also like to acknowledge my colleagues from Taro Pharmaceutical (Parminder, Ming Jiang, Shanjun Liu, Deepal, Sandeep, Shilpa, and Sanjay), from Wes Pharma (Silpa, Shyam, Anuja, Kamleshbhai) and from Amgen (Manny and Jeff), for assisting me.

I must also acknowledge fellow PhD students Dr. Venkata Velvadapu Muralidhar for teaching me basics of NMR interpretation, Dr. Soujanya Singireddy for helping me with ATR-FTIR experiments, Dr. Mohit Patel for all the valuable discussions. I would also like to thank my group members, Michael Puppolo, Tiffany Giles, Dr. Guoxiu Wei, and Dr. Deepti Varma for making suggestions at all the group meeting presentations. I would also like to mention other friends Sudipto Munshi, Sandeep Kondaveeti, Vijay Chatare, Praveen Kokkonda, Hairong Wang and many others for their support. I would also like to mention my friends for all the support and providing me with valuable friendship. Special thanks to Talla group (Mohak, Bhavik, Sinchan, Shailesh, Ritesh, Jaimin, Mehul Jai, Preeti, Jalpa, Vaibhavi and Archana) from Maharaja Sayajirao University made the difficult transition from school to university easy. I would also like to mention my friends Tapan, Nainesh, Pavan, Sanket, Jigish, Dhiren and Nishit for their great friendship.

I would like to thank Department of Chemistry for providing all the resources during my PhD. I would specially like to thank Ms. Sharon S. Kass and Ms. Tanya Santiago for helping with all the paper work. I would also like to thank Dr. John

Michel and Dr. Roy Keyer for giving me the opportunity to teach under their assistance.

Finally I would like to thank my parents for providing me with all the resources and being there for me whenever I needed help and my brother Malav Shah for his caring nature. Lastly and most importantly I would like to thank my lovely wife Urja Shah for unconditional love and being patient with me and for standing strong besides me in difficult times.

## **DEDICATION**

To my family particularly my Father Prakashchandra N. Shah, Mother

Smitaben P. Shah, and Wife Urja S. Shah

# TABLE OF CONTENTS

ABSTRACT.....	iii
ACKNOWLEDGMENTS .....	vi
DEDICATION .....	ix
LIST OF FIGURES .....	xiii
LIST OF TABLES.....	xvi
Chapter	
<b>1. INTRODUCTION.....</b>	<b>1</b>
1.1 Introduction.....	1
1.2 Extremophiles .....	2
1.3 Bacterial Cell Envelope: Structure.....	4
1.3.1 Gram Positive.....	4
1.3.2 Gram Negative.....	5
1.4 Cell Membrane: Architecture .....	6
1.5 Archaea–Monolayer vs. Bacteria-Bilayer cell membrane .....	8
1.6 Adaptation in cell membranes .....	9
1.6.1 Thermophiles and their adaptations .....	10
1.6.2 Psychrophiles and their adaptations.....	17
1.7 References.....	21
<b>2. ANALYTICAL TECHNIQUES AND INSTRUMENTATION .....</b>	<b>25</b>
2.1 Introduction.....	25
2.2 ATR-FTIR.....	25
2.2.1 Theory .....	25
2.2.2 Modes of Vibrations .....	27
2.2.3 ATR-FTIR Instrument .....	29
2.3 Shotgun lipidomics with High resolution mass spectrometer.....	32
2.3.1 Mass Spectrometry.....	32
2.3.2 Electro spray Ionization .....	33
2.3.3 Mass analyzers .....	37
2.3.4 Ion Detector: Electron Multiplier (EM).....	39
2.4 NMR spectroscopy.....	40
2.4.1 Basics .....	40
2.4.2 Energy levels.....	41

2.4.3 Components of NMR spectrometer .....	42
2.4.4 Pulsed mode for signal acquisition .....	43
2.4.5 Complex Pulse sequences .....	44
2.5 Reference .....	57
<b>3. LIPID COMPOSITION OF THERMOPHILIC <i>GEOBACILLUS</i> SP. STRAIN GWEI, ISOLATED FROM STERILIZATION OVEN.....</b>	<b>59</b>
3.1 Introduction.....	59
3.2 Materials and Methods.....	62
3.2.1 Cell growth.....	62
3.2.2 Materials .....	62
3.2.3 Extraction of polar lipids .....	63
3.2.4 Attenuated total reflection- Fourier transform infrared (ATR-FTIR) spectroscopy.....	65
3.2.5 NMR Spectroscopy.....	65
3.2.6 Mass Spectrometry.....	66
3.3 Results and Discussion .....	67
3.3.1 ATR-FTIR Spectroscopy.....	67
3.3.2 NMR spectroscopy.....	70
3.3.3 Mass Spectrometry.....	80
3.4 Conclusion .....	102
3.5 Reference .....	103
<b>4. EFFORTS TO IDENTIFY UNKNOWN LIPID MOLECULE FROM <i>GWEI</i> STRAIN .....</b>	<b>107</b>
4.1 Introduction.....	107
4.2 Materials and methods .....	107
4.2.1 Materials .....	107
4.2.2 Cell Growth and Extraction of polar lipids.....	107
4.2.3 Methods.....	107
4.3 Results and Discussion .....	108
4.3.1 MS-MS Scan.....	109
4.3.2 MS-MS-MS Scan.....	111
4.4 Conclusion .....	118
4.5 References.....	119
<b>5. LIPID COMPOSITION OF PSYCHROTOLERANT <i>SERRATIA</i> SP. STRAIN <i>IIP</i>, ISOLATED FROM ANTARCTICA.....</b>	<b>120</b>
5.1 Introduction.....	120
5.2 Materials and Methods.....	123
5.2.1 Cell growth.....	123
5.2.2 Materials .....	123

5.2.3 Extraction of polar lipids .....	123
5.2.4 Gas Chromatography .....	124
5.2.5 Mass Spectrometry.....	124
5.3 Results and Discussion .....	125
5.3.1 Gas Chromatography .....	125
5.3.2 Mass Spectrometry.....	127
5.4. Conclusion .....	140
5.5 References.....	142
<b>6. LIPID COMPOSITION OF THERMOPHILIC ANOXYBACILLUS SP. STRAIN 7L, ISOLATED FROM CHILEAN COPAHUE VOLCANO .....</b>	<b>146</b>
6.1 Introduction.....	146
6.2 Materials and Methods.....	147
6.2.1 Cell growth.....	147
6.2.2 Materials .....	147
6.2.3 Extraction of polar lipids .....	148
6.2.4 Gas Chromatography .....	150
6.2.5 Mass Spectrometry.....	150
6.3 Results and Discussion .....	151
6.3.1 Gas Chromatography .....	151
6.3.2 Mass Spectrometry.....	153
6.4. Conclusion .....	170
6.5 References.....	171
<b>7. LIPID COMPOSITION SUMMARY.....</b>	<b>174</b>
7.1 Introduction.....	174
7.2 Lipid Composition .....	174
7.3 Contribution to the field.....	179
7.4 Reference .....	180
<b>BIBLIOGRAPHY.....</b>	<b>181</b>

## LIST OF FIGURES

Figure 1.1 Fluid mosaic model of the plasma membrane.....	6
Figure 1.2 Structures of thermophilic lipid candidates.....	16
Figure 2.1 Symmetric and Asymmetric stretching for water molecule.....	28
Figure 2.2 Different types of bending vibrations.....	28
Figure 2.3 Schematics of Ge multiple bounce ATR.....	31
Figure 2.4 Schematic diagram of the principle of electrospray ionization in positive-ion mode.....	34
Figure 2.5 Ionization efficiency comparisons for analytes.....	36
Figure 2.6 Basic $^1\text{H}$ NMR pulse sequence.....	45
Figure 2.7 Selective spin Inversion.....	46
Figure 2.8 $^{13}\text{C}$ Decoupled experiment pulse sequence.....	47
Figure 2.9 J Modulated Spin Echo (JMOD) experiment pulse sequence.....	49
Figure 2.10 Vector diagram for J Modulated Spin Echo (JMOD) experiment pulse sequence.....	49
Figure 2.11 Homonuclear COSY pulse sequence.....	52
Figure 2.12 HSQC pulse sequence.....	53
Figure 2.13 Vector diagram for HSQC pulse sequence.....	54
Figure 3.1 Thin layer chromatography of lipids extracted from <i>GWEI</i> gave 6 different bands.....	64
Figure 3.2 ATR-FTIR spectra of fraction I-IV.....	70

Figure 3.3 a) Structure of phosphatidyl ethanolamine lipid b) Proton NMR spectrum of fraction IV lipids .....	73
Figure 3.4 2-D COSY spectrum of fraction IV lipids.....	75
Figure 3.5 a) Proton decoupled $^{13}\text{C}$ NMR spectrum of fraction IV b) J-Modulated spin echo $^{13}\text{C}$ NMR spectrum.....	77
Figure 3.6 $^1\text{H}$ - $^{13}\text{C}$ heteronuclear single quantum coherence (HSQC) lipid profile of <i>GWE1</i> strain fraction IV .....	78
Figure 3.7 a) Positive ion ESI-MS spectrum for fraction IV b) Negative ion ESI-MS spectrum for fraction IV.....	81
Figure 3.8 Positive (a) and negative (b) ESI-MS-MS spectra for m/z 692.5.....	82
Figure 3.9 ESI-MS-MS (+ve) Fragmentation spectra of lipids in fraction IV .....	87
Figure 3.10 ESI-MS (-ve) spectrum for fraction III .....	90
Figure 3.11 ESI MS-MS (-ve) fragmentation spectra of lipid molecules from fraction III and IV.....	98
Figure 3.12 ESI-MS (-ve) spectrum for fraction II.....	100
Figure 3.13 ESI MS-MS spectra of unknown lipid like molecule from fraction II.....	101
Figure 4.1 MSMS scan of m/z 821.4 molecule using linear trap quadrupole mass analyzer .....	110
Figure 4.2 MS-MS-MS Scan for daughter ion m/z 645.....	112
Figure 4.3 MS-MS-MS Scan for daughter ion m/z 565.....	113
Figure 4.4 MS-MS-MS Scan for daughter ion m/z 407.....	115

Figure 5.1 ESI-MS scan of fraction C, obtained by LC-6520B Q-TOF high resolution Mass Spectrometer .....	128
Figure 5.2 Negative ESI- MS/MS analysis of PG lipid at m/z 719.48 .....	129
Figure 5.3 ESI MS-MS (-ve) fragmentation spectra of lipids in fraction C .....	134
Figure 5.4 Negative ESI- MS/MS analysis of acyl PG lipid at a) m/z 957.71 b) m/z 983.72 c) Structure of acyl PG lipid .....	137
Figure 6.1 Thin layer chromatography of lipids extracted from 7L strain.....	149
Figure 6.2 Negative ESI-MS spectrum of fraction II a) Shows region from m/z range 600-900 b) Shows region from m/z range 1200-1450 .....	155
Figure 6.3 ESI MS-MS (-ve) fragmentation spectra of PG lipids .....	159
Figure 6.4 Negative ESI- MS-MS analysis of Cardiolipin lipid at m/z 1323.9 .....	161
Figure 6.5 ESI MS-MS (-ve) fragmentation spectra of cardiolipin lipids .....	163
Figure 6.6 ESI MS-MS (-ve) fragmentation spectra of PA lipid at m/z 647.49 .....	164
Figure 6.7 ESI MS-MS (-ve) fragmentation spectra of fraction III lipids .....	167

## LIST OF TABLES

Table 1.1 Principal classes of extremophiles .....	3
Table 2.1 Classification of lipid classes based on their electrical propensities .....	37
Table 3.1 <sup>1</sup> H and <sup>13</sup> C NMR spectral data and 2D NMR correlations for fraction IV .....	79
Table 3.2 lipid analysis and lipid composition of major phospholipids from <i>GWEI</i> strain fraction I-IV .....	83
Table 3.3 Comparison of observed mass with exact mass of the predicted molecule.....	88
Table 4.1 Possible chemical formulas for fatty acyl like molecule at 253.0945 .....	116
Table 4.2 Possible Chemical formula generated for head group .....	117
Table 5.1 Whole cell fatty acid Profile for <i>IIP</i> strain .....	126
Table 5.2 lipid composition of major polar lipids from <i>IIP</i> strain fraction C .....	138
Table 5.3 Comparison of observed mass with exact mass of the predicted molecule.....	139
Table 6.1 Whole cell fatty acid Profile for <i>7L</i> strain .....	152
Table 6.2 Lipid analysis and lipid composition of major phospholipids from <i>7L</i> strain fraction II and III.....	154
Table 6.3 Comparison of observed mass with exact mass of the predicted molecule.....	168
Table 7.1 Fatty acyl composition for microorganism <i>7L</i> , <i>GWEI</i> and <i>IIP</i> .....	177
Table 7.2 Summary of fatty acyl composition.....	178
Table 7.3 Fatty acyl composition for mesophilic strains A. <i>B. pumilus</i> ; B. <i>Bacillus sp.</i> ( <i>XI</i> ); C. <i>B. licheniformis</i> .....	179
Table 7.4 Fatty acyl composition for thermophilic strains D. <i>B. stearotherophilus FJW</i> ; E. <i>B. stearotherophilus 10</i> ; F. <i>B. stearotherophilus 2184</i> .....	179

# CHAPTER

## 1. INTRODUCTION

### 1.1 Introduction

Robert Koch and his associates isolated the first pure cultures of bacteria more than 100 years before, since then microbiologists worldwide started isolating laboratory cultures of literally thousands of different bacteria. Some of these bacteria are causative agents of infectious diseases and some of them carry out critical chemical reactions and form the life support for plants and animals. Bacteria are example of prokaryotic cells and they do not have a nucleus or other membrane bound organelles, while eukaryotic cells (animal or plant cell) have membrane bound organelles and a nucleus which contains genetic information of the cell. Eukaryotic cells could be unicellular or multicellular in contrast to prokaryotes which are unicellular. With diversity already found in bacterial classifications, it is now clear that we have seen only the tip of the iceberg. Most bacteria that exist in nature have not yet been obtained in laboratory culture. Microbiologists are exploring variety of microbial habitats to find different microorganisms to learn about their basic biology, to harness their genetic resources for benefit of mankind and more importantly to determine the evolutionary relationships of bacteria. As per one theory, they are considered as primitive forms of life when the earth's atmosphere was not suitable for eukaryotic cells to thrive (1, 2).

In this dissertation, our focus is identification of lipid structures present in the cell membrane of bacteria that thrive in extreme high and low temperature conditions (Extremophiles).

## 1.2 Extremophiles

Microbiologists discover numbers of prokaryotic microorganisms every year by exploring hostile environments, in which the physical parameters such as temperature, salinity, pH or pressure are extreme with respect to the conditions in which mesophilic microorganisms live preferentially. The microorganisms that live in these extreme environments are termed extremophiles. Most extremophiles belong to the kingdom of the archaea, but also certain bacteria and even some eukaryotic cells can tolerate some of these extreme conditions (3).

Many different physical and chemical parameters can determine the optimal habitat for such microorganisms. High or low temperatures, high pressures, high ionic strength, acidic or alkaline pH, strict anaerobiosis, desiccation or radiations are only some of the typical conditions in which extremophiles can survive and thrive. Interestingly, many obligate extremophiles are not only characterized by the skill of surviving in harsh habitats, but they require such conditions to survive (4, 5). On the basis of the physical or chemical parameters these microorganisms can stand, further divisions have been recognized among the wide class of extremophiles. In particular, thermophiles are able to stand extremely high temperatures, ranging from 40 °C up to 100 °C; psychrophiles are able to survive in frozen habitats, i.e. glaciers or polar seas; acidophiles and alkalophiles can cope with extreme pH values; halophiles stand extreme salinity and barophiles require elevated pressure for proliferation (4, 5).

<b>Class</b>	<b>Growth Requirement</b>
Thermophiles	Temperature from 40 °C to 100 °C.
Psychrophiles	Temperature from 10 °C to -20 °C.
Mesophiles	Moderate temperature condition.
Barophiles (Piezophiles)	Pressure up to 40 MPa
Halophiles	Salt concentrations from 3 M to saturation of NaCl.
Organic Tolerant Bacteria	Toxic organic substances up to supersaturating conditions.
Acidophiles	Low pH values (2- 6)
Alkalophiles	High pH values (10-13)

**Table 1.1 Principal classes of extremophiles**

Often, extremophiles are found in isolated environments, i.e. deep-sea habitats, where two or more of such conditions (high ion concentration, high pressure, low temperature) can be encountered. Thus, they are referred to as polyextremophiles, belonging to two or more of the above categories at the same time. Besides the classical definition above given for extremophiles, it is actually possible to define another class of microorganisms able to thrive in harsh conditions. The industrial development has generated a variety of contaminated sites with the accumulation of highly toxic substances. Bacteria have been isolated from these environments, which cannot strictly be considered extremophiles, although exhibiting a pronounced tolerance towards organic substances. These bacteria are able to metabolize various toxic organic substances and moreover, these bacteria are often endowed with the ability to metabolize a wide range of highly toxic compounds, thus they are central in the development of the environmental biotechnology (6).

Together with the development of stable enzymes, extremophiles often show structural modifications of their biomolecules in order to obtain stable cell physiology in

unhospitable environments. The extraordinary stability shown by extremophilic cells is associated with development of extreme environment resistant macromolecules, which are different in structure and/or content than mesophilic macromolecules (7, 8, 9). As we are focused in difference in lipid structure only, we will be discussing only cell wall and membrane physiology in this next section.

### **1.3 Bacterial Cell Envelope: Structure**

The cytoplasm in bacteria is separated from the external environment by a complex series of layers, which makes the cell envelope. Difference in the cell envelope nature divides prokaryotes in two different families: Gram Positives and Gram Negatives.

#### **1.3.1 Gram Positive**

In gram positive bacteria, the cytoplasm is separated from the surrounding environment by the cytoplasmic membrane (composed of lipid bilayer and proteins). This membrane is surrounded by a thick cell wall (20-80 nm), composed of peptidoglycan also known as murein. Peptidoglycan is a polymer of sugar and amino acids. The sugar component contains a residue of  $\beta$ -(1,4) linked N acetylglucosamine and N-acetylmuramic acid. Peptide chains of three to five amino acids is cross linked to N-acetylmuramic acid components of two strands and forms the 3D mesh-like layer (10). This cell wall provides strength and protection to the cell from outer environment. From this cell wall Teichoic Acids (TAs) and Lipoteichoic acids (LTAs) protrude (Fisher, 1990). TAs and LTAs are polyanionic in nature and gives antigenic function to the bacterial cell. TAs are directly linked to a muramic acid component of peptidoglycan and LTAs are embedded in the membrane through a lipid anchor (10). Other polysaccharides are also bound to the cell

wall by a covalent linkage (11), often referred as “Secondary Cell Wall Polymers” (SCWPs), since they play a secondary role in the assembly of the cell wall. Recent investigations have pointed out the existence of non-classical SCWPs, in correspondence with the bacterial cell surface-layer (S-layers). These are typically composed of protein and glyco-protein species (12). The S-layers, together with the SCWPs, creates a microenvironment, in which the microorganisms can survive under unfavorable conditions.

### **1.3.2 Gram Negative**

In contrast, in Gram-negative bacteria, the cytoplasmic membrane is surrounded by the peptidoglycan layer. In this case, the thickness of the murein layer is considerably lower (5-10 nm) than in Gram-positive bacteria and a second membrane, the Outer Membrane (OM) encloses the cell wall. The OM constitutes a distinctive feature of Gram-negative bacteria, and is connected to the PG layer through peculiar lipoproteins, the Braun Lipoproteins (BLP). The OM has a peculiar asymmetrical organization, and it is composed of glycerophospholipids and lipoproteins in the inner side and by Lipopolysaccharides (LPSs) in the outer side. The OM hosts several proteins (Outer Membrane Proteins, OMPs), among which the Porins, responsible for the formation of pores, carry out transportation functions (13).

The cell envelope plays crucial role in the survival of both archaea and bacteria. It acts as a barrier and prevents permeation of nutrients, ions and toxic substances. Through integral proteins within the structure, it also allows permeation of certain molecules across the membrane via either active or passive transport. Peptidoglycan, TAs and LTAs

for Gram positives and LPs for Gram-negative bacteria act as antigens and are recognized by specific receptors of the host immune system cells and are responsible for virulence of the bacterial cells.

#### 1.4 Cell Membrane: Architecture

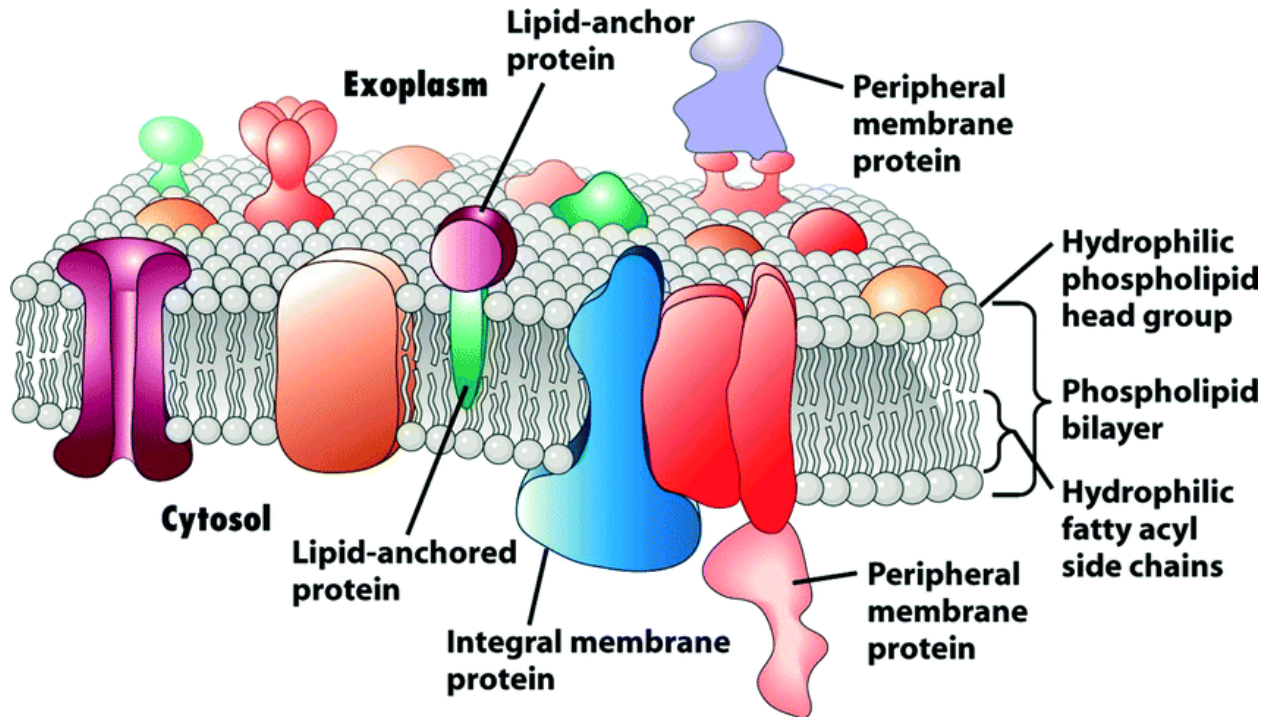


**Figure 1.1 Fluid mosaic model of the plasma membrane.**

Integral membrane proteins are inserted into lipid bilayer (mostly, transmembrane proteins). Peripheral Proteins are attached to membrane with Protein-Protein Interaction. Reproduced from (15) with permission of The Royal Society of Chemistry.

The cell wall covers the cell membrane. The cell membrane structure is a peculiar characteristic for the microorganism (figure 1), and therefore plays a very important role in resistance and survival of extremophiles in unfriendly environments. Extremophiles possess adaptations to survive against diverse stressors, depending on the disrupting potential of the stressor. The barrier function of cell membrane is very important in both the structural organization and function of all prokaryotic and eukaryotic cells (16). The cell membrane consists of two fundamental components, 1) Phospholipid mono-/bi-layers and 2) Integral proteins. Within the cell membrane, intact polar lipids (IPLs) bury their hydrophobic tails in the interior and expose their hydrophilic heads to the exterior. Phospholipid layer separates the two compartment and integral proteins embedded within the lipid layer takes part in selective transport of molecules and cell-cell recognition. There are two types of membrane proteins, first Integral proteins which are mostly transmembrane proteins and Peripheral proteins which are bound to the membrane by protein-protein interaction. The Extracellular portions of these proteins are glycosylated (17).

Two general features of these mono/bilayers are critical for the cell functionality, first the interior of these layer is made of hydrophobic chains, making the membrane impermeable for an aqueous solute, and second the phospholipid layers of naturally occurring phospholipids are viscous fluids (liquid crystalline state), which forms a sort of two-dimensional solvent matrix for membrane proteins, as described in the fluid mosaic model (18). Both phospholipids and proteins are free to diffuse laterally within the membrane, which is critical for many membrane functions (18, 19), such as maintaining

solutes concentration gradient across the membrane, which is necessary to maintain the correct physiology of the cell. Thus, the maintenance of a liquid crystalline state of a plasma membrane appears as a vital importance in every microorganism (19). The difference in lipid structure at extreme condition is observed to maintain this liquid crystalline state of a bilayer cell membrane, which is required for the survival of bacteria (9). In this next section we will compare the difference between archaeal and bacterial cell membrane lipid components.

### **1.5 Archaea–Monolayer vs. Bacteria-Bilayer cell membrane**

In most cases, prokaryotes and eukaryotes cell membranes consist of lipid bilayers which are made of ester phospholipids. Some of the archaea have similar features, a polar head coupled to two hydrophobic tails and they respond to the hydrophobic forces in a similar way by forming a lipid bilayer membrane. However, there are differences in the nature of the linkage. In Archaea, the hydrocarbon chain is linked to glycerol backbone via ether linkage (Figure 2a). Thermoacidophilic archaea contains unique lipid structure not observed in other two domains. They contain a dimerized diether molecule (Figure 2d). There are several possibilities with regard to its orientation in the cell membrane. These dimerized diether lipids could form a monolayer, in which the molecule is completely stretched, and spans the entire thickness of membrane or bilayer. Here, two polar heads are anchored on same side of membrane due to bending of hydrophobic chains (20). DeRosa confirmed presence of monolayer through computer simulations and evidences such as, the structure and dimensions of the lipids, the absence of a preferential freeze-fracture plane in the middle of the lipid membrane layer (as found in ester-based lipid

bilayers), the extreme rigidity of the thermophilic archaeal membrane, the properties of liposomes prepared with C<sub>40</sub> archaeal tetraether lipids, and the chemical labeling of the lipids on the outer surface of intact cells with nonpenetrating reactives (20). Archaeal lipids are distinctively different than prokaryotic lipids, with regard to following features,

- 1) Hydrocarbon chains are linked to the glycerol backbone with an ether linkage rather than an ester linkage,
- 2) Hydrocarbon tails are derived from isoprenoid units rather than fatty acid alkyls.
- 3) The chirality of the glycerol is sn-glycerol-1-phosphate, rather than sn-glycerol-3-phosphate.

The first feature is not exclusive as some bacteria also contain ether lipids, often in combination with ester lipids in their cell membrane but archaeal cell membrane does not contain an ester linkage (9). The second feature is also not exclusive for archaea as some prokaryotes have isoprenoid chains. However, third feature is exclusive for the archaeal cell membrane (21).

## **1.6 Adaptation in cell membranes**

Without a functional membrane, many types of molecules would freely move between the inside and the outside of the cell and maintenance of a stable and self-regulating system will become impossible. On the other hand, without sufficient permeability, the molecular movement across the membrane would become very difficult, and cells would fail to change their composition for required metabolic functions. Obviously, life could not be sustained in either case. Thus, both the barrier function of cell membrane and permeability of required molecules are of a vital importance. Depending on nature of

molecule, the bacterial cell has developed many methods to regulate permeation. In the case of very large, hydrophilic or charged molecules, the lipid bilayer itself presents too much resistance, and special mechanisms are required to allow the membrane permeation of such molecules (9). These mechanisms involve transport proteins or carrier molecules, which moves freely in the membrane and allows permeability of molecules either actively or passively. Many smaller lipophilic molecules, however, are able to permeate across the membrane without any specific transport mechanism. This is called the basal permeation process or passive diffusion. To maintain this permeation, it is necessary to maintain the liquid crystalline state of lipid bilayer even in the extreme conditions (9).

Microbiologists have found wide array of lipids in cell membrane with different polar head groups, different composition of hydrocarbon chain, ester or ether linkage between polar head groups and hydrocarbon chain. These compositions are obvious in a qualitative sense as it optimizes physical properties like, membrane fluidity, lipid polymorphism and other physicochemical properties which ultimately leads to survival of the fittest in extreme environment.

### **1.6.1 Thermophiles and their adaptations**

High (up to more than 100 °C) or low (to -20 °C) temperatures define the habitat for thermophiles and psychrophiles respectively. Thermophiles are mainly found in hot environments such as terrestrial or submarine heated soils, deep sea hot vents and hot springs, which are present in active volcanic areas along tectonic fracture zones and hot spots (22). These conditions impose a burden on the organisms to maintain the

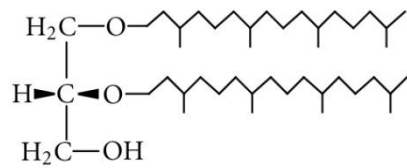
functioning of cellular metabolism and high stability is required for enzymes and other macromolecules.

In bacteria, exposure to heat shock transiently induces the synthesis of "Heat Shock Proteins (HSPs)", following the release of intracellular  $\sigma^{32}$  (the prokaryotic initiation enzyme factor for heat shock). HSPs rate of synthesis is mainly observed in case of heat shock, however its synthesis can be induced by change in several other conditions such as, pH, osmolarity, UV irradiation and presence of toxic material like ethanol, antibiotics, aromatic compounds or heavy metals (23). Ramos et al. suggested that HSPs synthesis is triggered by accumulation of misfolded proteins within the cell under stress condition. HSPs act like chaperones for biomolecules and assure their correct folding and translocate them into the right cell compartment. Presence of heat shock proteins also affects the structure of cell membrane composition of lipids. Changes in growth conditions leads to several adaptations such as, increasing the length of the acyl chains in lipid molecule, the ratio of iso branching acyl chain (Figure 2k) to anteiso branching acyl chains (Figure 1.2L) and increase in degree of saturation of the fatty acids to maintain the liquid crystalline state of membrane and to preserve all the functions within cell (9). These changes balances heat increased reaction rate of basal ion permeation across the membrane, with immediate consequences on the bioenergetic equilibrium of the cell (24).

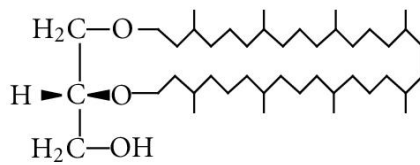
Another survival strategy is to maintain structure of other macromolecules like, proteins and nucleic acids. Pack *et al.* compared 20 different mesophilic and thermophilic proteins and suggested differences in amino acid arrangement between fully exposed

areas and fully buried areas (7). Other strategies in preservation of protein structure at higher temperature include increasing ion-pair content, forming higher-order oligomers, decreasing flexibility at room temperature and decreasing the length of surface loops that connect elements of secondary structure and optimizing electrostatic and hydrophobic interactions (8). Nucleic acids are subject to denaturation (disassociation of double stranded DNA) at high temperature. The DNA of thermophiles has greater thermal stability compared to that of mesophiles, due to the presence of mono-divalent salts stabilizing charge on phosphate and/or due to changes in base pair. More G-C base pairs instead of A-T or A-U pairs have been found in nucleic acids of thermophilic prokaryotes compared to mesophilic nucleic acids (8).

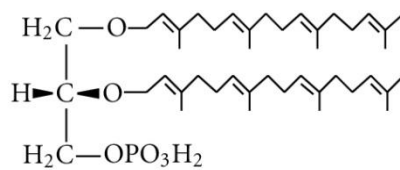
In archaeal cell, the main characteristic of phospholipid is presence of ether bonds (Figure 2a-e), which are difficult to hydrolyze compare to an ester bond of bacteria and membrane spanning nature of the ether phospholipids, which allows preservation of liquid crystalline state even at higher temperatures. However scientists have observed ether bonds in mesophilic archaea as well, which lead us to believe that ether bond has minimal role in thermostability (25). Few lipid structures that are observed in thermophilic bacteria and archaea are shown in Figure 2. Archaeal lipids and their adaptations are described elsewhere in detail (9) and it will not be repeated in this dissertation.



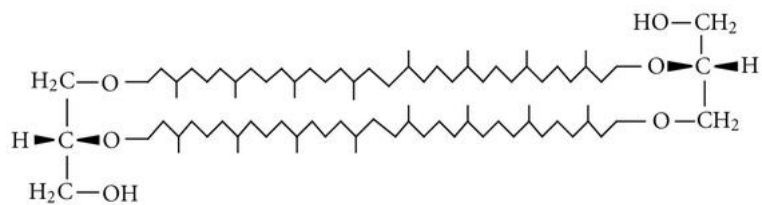
(a)



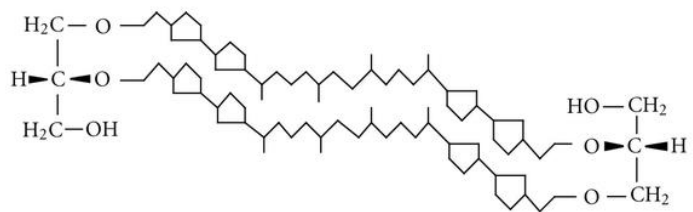
(b)



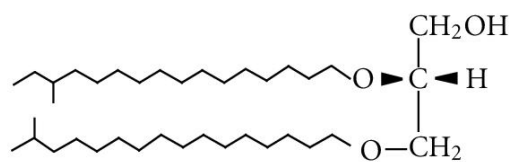
(c)



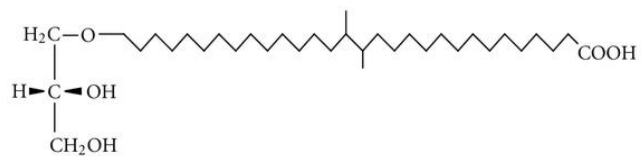
(d)



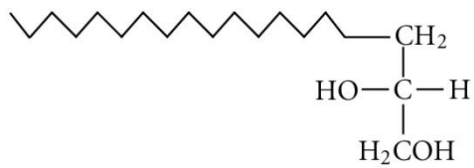
(e)



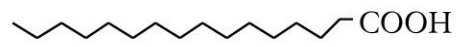
(f)



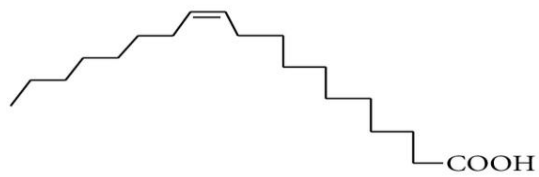
(g)



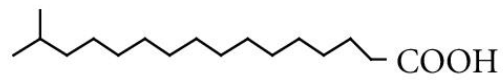
(h)



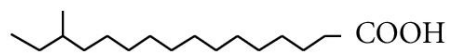
(i)



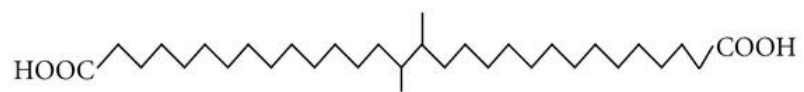
(j)



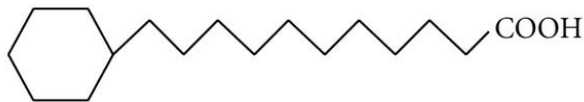
(k)



(l)



(m)



(n)

### Figure 1.2 Structures of thermophilic lipid candidates

(a) diphytanylglycerol (archaeol: archaeal diether lipid); (b) cyclic archaeol; (c) digeranylgeranylglycerophosphate (DGGGP); (d) caldarchaeol (archaeal tetraether lipid); (e) cyclopentane-containing caldarchaeol; (f) bacterial dither lipids; (g) 15,16-dimethyl-30-glyceryloxytriacontanoic acid; (h) 1,2-di-hydroxynonadecane (long-chain diol lipid); (i) palmitic acid (saturated straight chain fatty acid); (j) cis-vaccenic acid (monounsaturated straight chain fatty acid); (k) iso-C17 fatty acid; (l) anteiso-C17 fatty acid; (m) 15,16-dimethyltriacontandioic acid (diabolic acid); (n) 11-cyclohexylundecanoic acid. (a)–(e) Archaeal lipids; (f)–(o) bacterial lipids. Part of image is reproduced with permission from (9).

### 1.6.2 Psychrophiles and their adaptations

The effect of cold shock on cells is opposite to that attained due to heat shock.

Psychrophiles are naturally encountered in water environment in the polar regions.

Compared to regular growth temperature, lowering the survival temperature affects the cell physiology by decreasing rate of biochemical reactions and changes the viscosity of cell fluid, which changes by factor of higher than two between 37 °C and 0 °C (26).

Lower temperature affects cell membrane by enhancing the weak interactions holding the lipid layer and enhances rigidification associated with low temperature. Due to this, permeability of ions and essential nutrients is strongly decreased (26). A down temperature shift induces the synthesis of the so called Cold Shock Proteins (CSPs) similarly to HSPs. In mesophiles, CSPs function as chaperones to assure the correct functioning of several processes such as transcription, translation, protein folding and the regulation of membrane fluidity itself (27).

Carty et al. reported, increase in acyl chain unsaturation within the Lipid A structure as a part of cold adaptation in *E. Coli* (28). Change in the fatty acids branching profile is observed in the Gram positive microorganism *Bacillus subtilis* (29).

Chintalapati et al. 2004 reported change in fatty acids chain length within the lipid structure (30). All these strategies introduce steric constrains, change the packing order of lipid bilayer or reduce the interactions within the membrane and maintains liquid crystalline state of the membrane at lower temperature.

Proteins synthesis and DNA/RNA functions are also compromised due to cold shock. Cold shock causes stabilization of the nucleic acid secondary structure and impairs

RNA transcription, RNA degradation and translation. The main function of the cold-induced proteins involved in RNA metabolism is to prevent secondary structure formation or to facilitate degradation of structured RNA. Proteins from the Cold Shock Protein (CSPs) family are nucleic acid chaperones and this activity prevents the formation of secondary structures. Secondary structures of nucleic acid can impair RNA metabolism at different stages (27),

1. It affects degradation by hampering progress of the nucleases;
2. It affects translation by preventing the formation of translation initiation complex by ribosome subunits;
3. It affects transcription by causing premature termination of RNA polymerase (RNAP).

The chaperone activity of CSPs prevents these undesirable effects (27). Obligated psychrophiles, which can only survive at cold temperatures express analogous of the CSPs, the so-called Cold-Aclimation Proteins (CAPs). Although structurally and functionally related to CSPs, the CAPs are constitutively rather than transiently expressed by the psychrophiles. Obligated psychrophiles also express Antifreeze Protein (AFPs) (26). AFPs bind to small ice crystals through a large complementary surface and create difference between melting and freezing temperature, which is also known as thermal hysteresis. This prevents growth of ice crystals and allows the microorganism to grow at subzero temperatures. These proteins have been recently isolated and described in Antarctic lake bacteria (31). Few cold adapted bacteria synthesize disaccharide trehalose or other exopolysaccharides (EPSs). Trehalose is a nonreducing disaccharide ( $\alpha$ -D-glucopyranosyl-1,1- $\alpha$ -D-glucopyranoside). Accumulation of trehalose in the cell is

thought to have a colligative effect, and it probably helps also in preventing cold-induced protein denaturation and aggregation (32). The occurrence of high concentrations of EPSs around the bacterial cell modifies the physico-chemical environment of bacterial cells, participating in cell adhesion to surfaces and in water retention. Moreover, EPS matrices can favor the sequestration and local concentration of nutrients, retain and protect extracellular enzymes against cold denaturation and act as cryoprotectants as well. (33).

To maintain the biochemical processes within the cell, psychrophiles have also evolved cold-adapted enzymes, endowed with specific activities at low temperature, comparable, and sometimes even higher, than mesophilic enzymes (34). They undergo structural modifications in order to attenuate the strength and the number of conformation stabilizing factors. Common trends in such direction include the reduction of the number of ion pairs, hydrogen bonds and hydrophobic interactions, the weakening of inter-subunits interactions, higher interaction with the solvent and higher accessibility to the active site (34).

The primary focus of this thesis is the complete structure elucidation of the membrane constituents of several extremophile bacteria. All of the presented microorganisms were isolated in extreme environments characterized by high and low temperature. The aim is to establish a parallel between the membrane constituents of diverse classes of extremophiles, in order to understand adaptive structure changes in the classical cell membrane under these extreme environmental conditions. We have identified lipid structures and fatty acid profile of two thermophilic strains and one psychrophilic strain and explained how it would help the organism to survive under these

stress condition. Adaptations occurring under other stress conditions are not discussed here.

## 1.7 References

- 1) Brock, T. Life at high temperatures. *Science* **230**, 132-138 (1985)
- 2) Brown, J.R. & Lupas, A.N. 1998. What makes a thermophile?. *Trends in Microbiology* **6**, 349-351 (1998).
- 3) Konings, W.N., Albers, S.V., Koning, S. & Driessen, A.J.M. The cell membrane plays a crucial role in survival of bacteria and archaea in extreme environments. *Antonie van Leeuwenhoek* **81**, 61-72 (2002).
- 4) Danson, M.J. & Hough, D.W. Structure, function and stability of enzymes from the Archaea. *Trends Microbiol.* **6**, 307-314 (1998).
- 5) Morell, V. Microbiology's Scarred Revolutionary. *Science* **276**, 669-702 (1997).
- 6) Sardesai, Y. N. & Bhosle, S. Organic solvent-tolerant bacteria in mangrove ecosystem. *Curr. Sci.* **82**, 622-623 (2002).
- 7) Pack, S.P. & Yoo, Y.J. Protein thermostability: structure-based difference of amino acid between thermophilic and mesophilic proteins. *Journal of Biotechnology* **111**, 269-277 (2004).
- 8) Rothschild, L.J. & Mancinelli, R.L. Life in extreme environments. *Nature* **409**, 1092-1101 (2001).
- 9) Koga, Y. Thermal adaptation of bacterial and archaeal lipid membranes. *Archaea* **2012**, 1-6 (2012).
- 10) Neuhaus, F. C. & Baddiley, J. A continuum of anionic charge: structures and functions of d-alanyl-teichoic acids in gram-positive bacteria. *Microbiol Mol Biol Rev* **67**, 686-723 (2003).

- 11) Araki, S., Sakurai, T., Oohusa, T. & Kayama, M. Distribution of phosphatidylcholine in brown algae. *Nippon Suisan Gakkaishi* **55**, 2049 (1989).
- 12) Schäffer, C. & Messner, P. The structure of secondary cell wall polymers: how Gram-positive bacteria stick their wall together. *Microbiology* **151**, 643-651 (2005).
- 13) Beveridge, T.J. Structures of gram-negative cell walls and their derived membrane vesicles. *J. Bacteriol.* **181**,4725-4733 (1999).
- 14) Ellen, A.F., Zolghadr, B., Driessen, A.J.M. & Albers, S.V. Shaping the Archaeal Cell Envelope. *Archaea* **2010**, 1-13 (2010).
- 15) Nan, L., Zhuangde, J. & Xueyong, W. Emerging microfluidic devices for cell lysis: a review. *The Royal Society of Chemistry* **14(6)**, 1060-1073 (2013).
- 16) Gennis, R.B., *Biomembranes. Molecular Structure and Function.* (Springer-Verlag, New York, 1989).
- 17) Cooper G.M., *The Cell: A Molecular Approach. 2nd edition.* (Sinauer Associates, Sunderland (MA), 2000).
- 18) Singer, S.J. & Nicholson, G.L. The fluid mosaic model of the structure of cell membranes. *Science* **175**, 720-731 (1972).
- 19) Bloom, M., Evans, E. & Mouritsen, O.G. Physical properties of the fluid lipid-bilayer component of cell membranes: A perspective. *Q. Rev. Biophys.* **24**, 293-297 (1991).
- 20) De Rosa, M., Trincone, A., Nicolaus, B. & Gambacorta A. Archaeobacteria: lipids, membrane structures, and adaptation to environmental stresses. In *Life under Extreme Conditions.* pp.61-87. (Springer, Heidelberg, 1991).
- 21) Gambacorta, A. *et. al.* Unique features of lipids of archaea. *Systems of Applied*

- Microbiology* **16**, 518-527 (1994).
- 22) Stetter, K. A brief history of the discovery of hyperthermophilic life. *Biochemical Society Transactions* **41(1)**, 416-420 (2013).
- 23) Ramos, J.L, Gallegos, M.T., Marques, S., Ramos-Gonzalez, M.I., Espinosa-Urgel, M. & Segua, A. Responses of Gram-negative bacteria to certain environmental stressors. *Curr. Opin.Microbiol.* **4**,166-171 (2001).
- 24) Van de Vossenberg, J. *et. al.* The essence of being extremophilic: the role of the unique archaeal membrane lipids. *Extremophiles* **2**,163-170 (1998).
- 25) Koga, Y. & Nakano, M., A dendrogram of archaea based on lipid component parts composition and its relationship to rRNA phylogeny, *Systematic and Applied Microbiology* **31(3)**, 169-182 (2008).
- 26) D'Amico, S., Collins, T., Marx, J.C., Feller, G. & Gerday, C. Psychrophilic microorganisms: challenges for life. *EMBO reports* **7**, 385-389 (2006).
- 27) Barria, C., Malecki, M. & Arraiano, C. Bacterial adaptation to cold. *Microbiology* **159(12)**, 2437-2443 (2013).
- 28) Carty, S.M., Sreekumar, K.R. & Raetz, C.R.. Effect of cold shock on lipid A biosynthesis in *Escherichia coli*. Induction At 12 degrees C of an acyltransferase specific for palmitoleoyl-acyl carrier protein. *J. Biol. Chem.* **274**, 9677-9685 (1999).
- 29) Klein, W., Weber, M.H. & Marahiel, M.A. Cold shock response of *Bacillus subtilis*: isoleucine-dependent switch in the fatty acid branching pattern for membrane adaptation to low temperatures. *J. Bacteriol.* **181**, 5341-5349 (1999).
- 30) Chintalapati, S., Kiran, M.D. & Shivaji, S. Role of membrane lipid fatty acids in cold

adaptation. *Cell Mol Biol (Noisy-le-grand)* **50**, 631-642 (2004).

31) Gilbert, J.A., Hill, P.J., Dodd, C.E. & Laybourn-Parry, J. Demonstration of antifreeze protein activity in Antarctic lake bacteria. *Microbiology* **150**, 171-180 (2004).

32) Phadtare, S. & Inouye, M. Genome-wide transcriptional analysis of the cold shock response in wild-type and cold-sensitive, quadruple-csp-deletion strains of *Escherichia coli*. *J Bacteriol.* **186**, 7007-7014 (2004).

33) Mancuso-Nichols, C.A.; Guezennec, J. & Bowman, J.P. Bacterial exopolysaccharides from extreme marine environments with special consideration of the southern ocean, sea ice, and deepsea hydrothermal vents. *Mar. Biotechnol.* **7**, 253-271 (2004).

34) Johns, G.C. & Somero, G.N. Evolutionary convergence in adaptation of proteins to temperature: A4-lactate dehydrogenases of Pacific damselfishes (*Chromis* spp.). *Mol Biol Evol.* **21**, 314-320 (2004).

## CHAPTER

### 2. ANALYTICAL TECHNIQUES AND INSTRUMENTATION

#### 2.1 Introduction

The primary focus of this chapter is to understand the techniques and instruments involved to identify unknown lipid molecules in these extremophiles. In particular, emphasis has been given to the underlying principles of Attenuated Total Reflectance Fourier Transformed Infrared (ATR-FTIR) Spectroscopy, Tandem Mass Spectrometry ( $MS^n$ ), and Nuclear Magnetic Resonance (NMR) Spectroscopy.

#### 2.2 ATR-FTIR

One of the major complications in these projects was limited amount of material. We have used ATR-FTIR at the beginning for the screening purpose to confirm that extracted material contains lipid like molecule. ATR-FTIR helped us identify carbonyl functional group and terminal methylene and methyl symmetric and asymmetric vibrations confirming long chain fatty acid like structure. ATR-FTIR is non-destructive technique and very limited amount of material was required for the screening purpose. Because of these advantages, ATR-FTIR was used for quick screening of fractions, before using complex, destructive and time consuming techniques.

##### 2.2.1 Theory

Infrared (IR) Spectroscopy is one of the most important analytical techniques available. One of the biggest advantages of the newly developed IR Spectrophotometer is that

virtually any sample in any state may be studied. Liquids, solutions, pastes, powders, films, fibers, gases and surfaces can all be examined with a judicious choice of sampling technique.

The infrared (IR) region is the part of the electromagnetic spectrum between the visible and microwave regions, which is further divided in three categories the near, mid, and far IR. The mid IR region (MIR) is a region of interest for chemical analysis. This is the region of wavelengths between  $4000\text{-}400\text{ cm}^{-1}$  ( $2.5\text{-}25\text{ }\mu\text{m}$ ). Infrared light imposed on a molecule will not create electronic transitions but it does contain enough energy to interact with a molecule causing vibrational and rotational changes (1).

During the 20th Century, Einstein, Planck and Bohr indicated that in many ways electromagnetic radiation could be regarded as a stream of particles (or quanta) for which the energy,  $E$ , is given by the Bohr equation, as follows:

$$E = h\nu \quad (2.1)$$

where  $h$  is the Planck constant ( $h = 6.626 \times 10^{-34}\text{ J s}$ ) and  $\nu$  is equivalent to the classical frequency (1).

Vibration and rotation changes associated with infrared spectroscopy can be represented in terms of quantized discrete energy levels  $E_0, E_1, E_2$ , etc. and each atom or molecule in a system must exist in one or other of these levels. Whenever a molecule interacts with radiation, a quantum of energy (or photon) is either emitted or absorbed. In each case, the energy of the quantum of radiation must exactly fit the energy gap  $E_1 - E_0$  or  $E_2 - E_1$ , etc. The energy of the quantum is related to the frequency by the following:

$$\Delta E = h\nu \quad (2.2)$$

Hence, the frequency of emission or absorption of radiation for a transition between the energy states  $E_0$  and  $E_1$  is given by:

$$\nu = (E_1 - E_0)/h \quad (2.3)$$

For molecules to be IR active it must possess a specific feature, i.e. an electric dipole moment of the molecule must change during the vibration. This is the selection rule for infrared spectroscopy. In heteronuclear triatomic molecule ( $\text{CO}_2$ ), The dipole moment of such a molecule changes as the bond expands and contracts. By comparison, an example of an ‘infrared-inactive’ molecule is a homonuclear diatomic molecule ( $\text{O}_2$ ) because its dipole moment remains zero no matter how long the bond. An understanding of molecular symmetry and group theory is important when initially assigning infrared bands. Detail description of this is beyond the scope of thesis (1).

### **2.2.2 Modes of Vibrations**

There are two types of molecular vibrations, stretching and bending. Some bonds can stretch in-phase (symmetrical stretching) or out-of-phase (asymmetric stretching) as shown in Figure 2.1. If a molecule has different terminal atoms such as HCN, then the two stretching modes are no longer symmetric and asymmetric vibrations of similar bonds, but will have different proportions of the stretching motion from each atom.

Bending vibrations also occurs due to IR absorbance and generates band in infrared spectra and these are summarized in Figure 2.2. It is best to consider the molecule being cut by a plane through the hydrogen atoms and the carbon atom. The hydrogens can move in the same direction or in opposite directions in this plane, or they can move in and out of the plane (1).

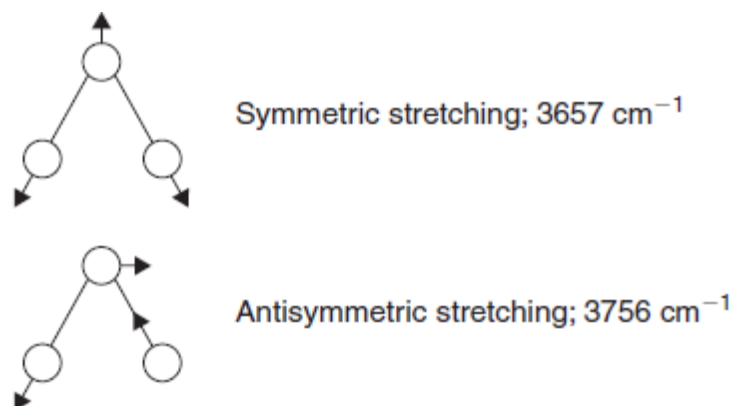


**Figure 2.1: Symmetric and Asymmetric stretching for water molecule (2)**  
 (Reprinted with permission from Elsevier)

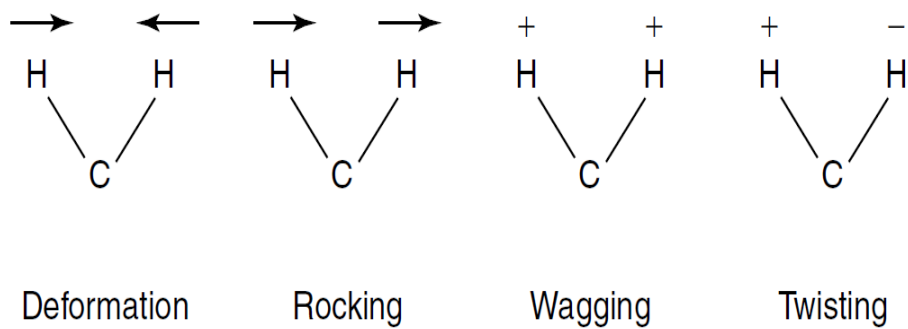


**Figure 2.2: Different types of bending vibrations (1).** Reprinted with permission from John Wiley & Sons Inc.

In general, the bonds between light atoms vibrate at higher frequencies than the bonds between heavy atoms. It is observed for carbon atom bound to another atom Vibrations of C–H, C–D, C–O, C–Cl, and C–Br bonds are 3000, 2280, 1100, 800, and 550  $\text{cm}^{-1}$  respectively. As already mentioned, for a vibration to give rise to the absorption of infrared radiation, it must change the dipole moment of the molecule. Higher the change in dipole moment, more intense band is observed. Indeed, the -C=O group, formed by different atoms and highly polarized, strongly absorbs in the MIR region, while C-C bond absorbance in the MIR region is much weaker. Since the energies involved with the vibration will be different for each kind of bond, each different bond will absorb a different frequency of infrared radiation in order to make this jump from one state to higher one, and each functional group in molecule will give rise to specific absorption band which will be fingerprint for that functional group and would help us to identify that functional group (1).

### **2.2.3 ATR-FTIR Instrument**

Attenuated Total Reflectance (ATR) is today the most widely used FTIR sampling tool. ATR generally allows qualitative or quantitative analysis of samples with little or no sample preparation, which greatly speeds sample analysis (3). The main benefit of ATR sampling is very thin sampling path length and depth of penetration of the IR beam into the sample. This is in contrast to traditional FTIR sampling by transmission where the sample must be diluted with IR transparent salt, pressed into a pellet or pressed to a thin film, prior to analysis to prevent totally absorbing bands in the infrared spectrum. ATR-FTIR is used to detect the species that are near or on the surface of a

diamond with minimal sample preparation (3). The infrared beam coming from IR source, passes through the dense medium (ATR crystal) to a less dense medium (sample) and gets reflected internally from the surface of the crystal and creates an evanescent wave, and extends into the sample. Some of the energy of the evanescent wave is absorbed by the sample and remaining is reflected. The parameters that affect the ATR spectrum are refractive indices of the crystal, sample and depth of penetration of the evanescent wave (4, 5). Refractive indices of the crystal and the sample are related by the following equation

$$\theta_c = \sin^{-1}(n_2/n_1) \quad (2.4)$$

Where  $n_2$  is the refractive index of the sample and  $n_1$  is the refractive index of the crystal, and  $\theta_c$  is the critical angle.

The refractive indices of the crystal must be significantly higher than the refractive index of the sample to get a good quality spectrum. Also a good contact between the sample and the ATR crystal is required as the depth of penetration of evanescent wave into the sample is only up to specific microns. In an ATR spectrum, the penetration depth ( $d_p$ ) of the evanescent wave depends on the wavelength ( $\lambda$ ), the refractive indices of the sample ( $n_2$ ) and the crystal ( $n_1$ ) and on the angle of reflection ( $\theta$ ) according to the following equation (4, 5):

$$d_p = \lambda / (n_1^2 \sin^2 \theta - n_2^2)^{1/2} \quad (2.5)$$

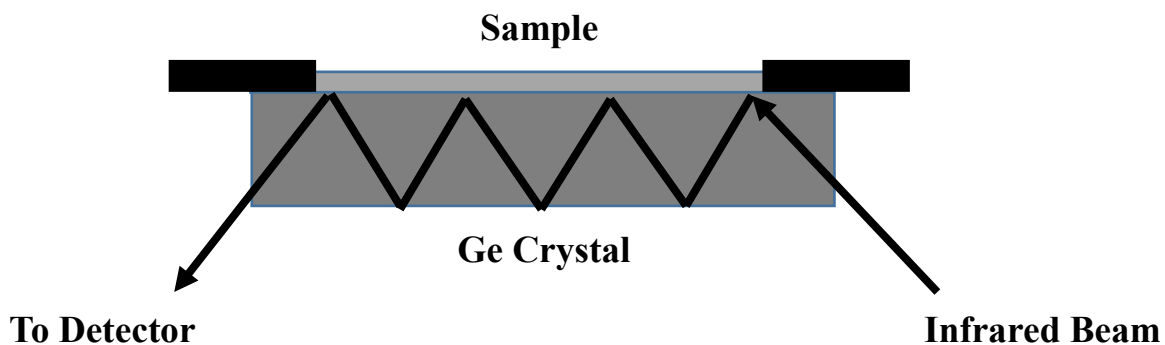


**Figure 2.3: Schematics of Ge multiple bounce ATR (3).**

The ATR crystals are usually made of diamond, zinc selenide (ZnSe), and Germanium (Ge) (4, 5). Diamond crystals are used to make single reflection ATR crystals and ZnSe and Ge crystals are used to make multibounce ATR crystals. Increasing the number of reflections increases the sensitivity of instrument due to more absorbance of IR beam compare to single bounce ATR crystals. While using single bounce diamond ATR crystals, external pressure is applied to collect good spectrum. For soft and liquid samples ZnSe crystals are used. ZnSe crystals require to be used carefully as they scratch easily. Compare to ZnSe crystals, diamond crystals are inert and scratch resistant. They can be used for small size samples and have good durability. Also, Diamond is ideal for high temperature and pressure studies. Schematics of multiple bounce ATR is shown in Figure 2.3.

In this work, ATR-FTIR experiments were performed on a Germanium (Ge) multibounce ATR accessory mounted in a Nicolet Magna 750 FTIR spectrometer that was equipped with a mercury cadmium telluride A (MCTA) detector.

### **2.3 Shotgun lipidomics with High resolution mass spectrometer.**

Lipids isolated from microorganisms have different functional groups and different length of fatty acyl chain length. Extracted lipids also contain isobaric lipids (same molecular mass but different acyl chain lengths). It is difficult to separate these diverse lipid structures with HPLC.

High resolution mass spectrometry is fast and highly sensitive technique. Using high resolution mass spectrometer we can identify hundreds of lipids, even at very low concentration without need of chromatographic separation. Using fragmentation analysis we can also identify headgroup fragments, different acyl chain fragments of isobaric lipids and assign position for acyl chain based on relative abundance of acyl chain.

Sample requirement for mass spectrometry is low but it is a destructive technique and sample recovery is not possible.

#### **2.3.1 Mass Spectrometry**

Mass spectrometer detects analyte based on their mass to charge ratio. Analysis of molecules using mass spectrometer is comprised of following steps:

- 1) Production of gas phase ions of analyte using ion source.
- 2) Separation of the ions according to their masses.
- 3) Fragmentation of parent molecule by collision.
- 4) Detection and data processing

Mass spectrometry analysis requires high vacuum to function, this allows ions to reach the detector without undergoing collisions with other molecules. It is required to avoid these collisions as they deviates the ion trajectory and which makes ions to lose their

charge against walls of the instrument. Collisions could also increase the complexity of spectrum as collision of ions with other ions may produce unwanted reactions. As per the kinetic theory of gases mean free path (the average distance traveled by a moving particle between successive impacts), is given by,

$$L = \frac{kT}{\sqrt{2}p\sigma} \quad (2.6)$$

where  $k$  is the Boltzmann constant,  $T$  is the temperature (in K),  $p$  is the pressure (in Pa) and  $\sigma$  is the collision cross-section (in  $m^2$ );  $\sigma = \pi d^2$  where  $d$  is the sum of the radii of the stationary molecule and the colliding ion (in m). In a mass spectrometer, the mean free path should be at least 1 m and hence the maximum pressure should be 66 nbar (6). In this chapter, focus is on explaining the ESI-ion source, analyzer and detector used in this research.

### **2.3.2 Electro spray Ionization**

Electro spray ionization technique has been extensively used to analyze broad range of compounds since developed by Fenn et al. (7). The principles of the ESI process as a schematical diagram is shown in Figure 2.4. Initially, a solution containing the analytes of interest is introduced into the ESI ion source through capillary tubing. The narrowed orifice at the end of the capillary tubing and the mechanical forces imparted as the solution passes through the narrow orifice facilitate the formation of sprayed small droplets in the ionization chamber. The electric field is applied (3–6 kV) is applied between the capillary and the counter-electrode. The distance between capillary and counter electrode is about 0.3–2 cm (6). Due to the applied field, charge accumulation occurs at the end of the capillary. At low voltage the drop at the end of capillary appears

spherical and then it elongates under the pressure of the accumulated charges at the tip in the stronger electric field and when the surface tension is broken, the shape of the drop changes to a ‘Taylor cone’ and the spray appears.

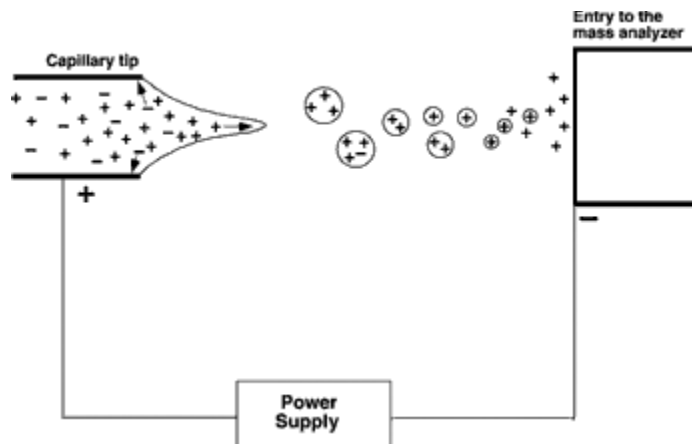


**Figure 2.4 Schematic diagram of the principle of electro spray ionization in positive-ion mode (7). Reprinted with permission from John Wiley & Sons Inc.**

Dispersion of the spray remains in a limited in space due to gas injected coaxially at a low flow rate. These droplets then pass through a curtain of heated inert gas, most often nitrogen, to remove the last solvent molecules. The droplets can carry net charges and are directed into the mass analyzer by the applied electric field. As shown in Figure 2.4, if a positive electric potential is applied to the end of capillary tube and a negative electric potential is present at the entrance of the mass analyzer in the positive-ion mode, droplets carry net positive charges. Droplet surface tension and the spatial proximity of surface charges on sprayed droplets are critical determinants of the ionization process (7).

Ionization efficiency of an analyte depends on the analyte's ability to lose or gain a charge in its own micro environment in the presence of electric field. Principles of the relationship between ion formation, ionization efficiency, and the electrical properties of specific analytes are illustrated in figure 2.5.

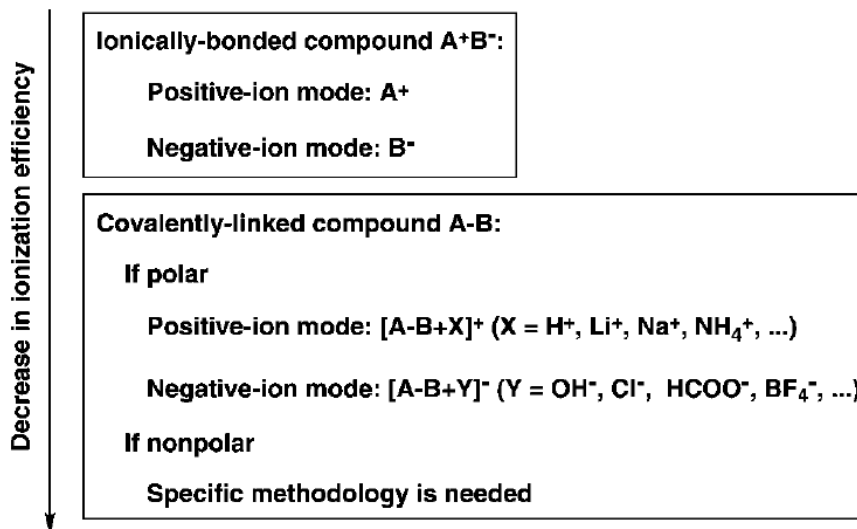


**Figure 2.5 Ionization efficiency comparisons for analytes.**

The formation of analyte with adduct ion X or Y depends on the availability of small cation or anion in the solution and the affinity of the adduct ion with the polar compound (7). (Reprinted with permission from John Wiley & Sons Inc.)

Cationic and anionic moieties carry inherent charges that can be readily separated in the ESI ion source. The ionization efficiency for these ions is much higher relative to that for compounds that do not carry an inherent charge. Ions can also be formed by addition of adduct ions. If sufficient dipole potential is present, an analyte can be induced to interact with either anion or cation in the ESI ion source and thus is potentially suitable for analysis by ESI/MS. Table 2.1 shows different type of lipids based on their electrical propensities.

Group	Electrical Propensity	Lipid Classes
Anionic lipids	Carry net negative charge(s) at physiological pH	Cardiolipin, acylCoA sulfatide, PI, PG, PS, PA
Weak anionic lipids	Carry net negative charge(s) at alkaline pH	PE, ceramide, NEFA, eicosanoids
Neutral polar lipids	Neutral at alkaline pH	PC, SM, glycolipid, TAG
Special lipids	Vary	Acylcarnitine, sterol

**Table 2.1: Classification of lipid classes based on their electrical propensities.**

(PI: phosphatidyl inositol, PG: phosphatidylglycerol, PS: phosphatidylserine, PA: phosphatidic acid, PE: phosphatidylethanolamine, NEFA: non esterified fatty acids, PC: phosphatidylcholine, TAG, triacylglycerol, SM: sphingomyelin)

### 2.3.3 Mass analyzers

Once the ions are produced, they are separated according to their masses in the mass analyzers. In this work we have used hybrid mass analyzer, which is a combination of Triple quadrupole mass analyzer and time of flight (TOF mass analyzer).

#### 2.3.3.1 Triple quadrupole mass analyzer

The quadrupole analyzers are made up of four cylindrical rods and each pair of rods is connected electrically. Stability of the ion trajectories is used by quadrupole analyzers to separate ions according to the mass/ charge ratio. A time dependent direct current (DC) and oscillating radio frequency RF voltages are applied to the rods. The RF voltages applied to the each pair of the rods are 180° out of phase. Typically, the DC voltage will vary from 5000 to 200 V whereas the RF voltage varies from zero to 3000 V (from -3000 to +3000 V peak to peak). The ions travelling in the center of quadrupole (Z axis) are subjected to forces induced by electric fields in the x and y directions. This will cause the ions to travel in a three-dimensional sine wave through the center of the quadrupole. These quadrupoles also focus the trajectory of the ions towards the center of the

quadrupole. For example if the potential energy of the positive ion located at the center of the rods of a quadrupole increases if it comes nearer a positive rod and it decreases if it comes nearer to a negative rod. However, as the RF field actually switches the potentials, if the frequency is sufficient, an ion that starts coming down the slope towards a negative barrier is caught in the positive potential well and is thus brought back to the center of the quadrupole rods. Only ions with certain  $m/z$  have stable trajectory through the quadrupole. The other ions will strike the rods and discharge itself and will not be detected (6, 8).

A linear arrangement of three quadrupoles is known as a triple quadrupole mass analyzer. The first and third quadrupoles act as mass filters, and the middle quadrupole is employed as a collision cell. The collision cell is a RF-only quadrupole and generally uses Ar, He, or  $N_2$  gas for collision induced dissociation. Kinetic energy of inert gas molecule is transferred to selected parent ion which leads to fragmentation and these fragments are analyzed in third quadrupole. Collisions could be high energy ( $>100$  eV) or low energy ( $<100$  eV) (6, 8). In this work, we have used low energy (25-45 eV) collisions.

### **2.3.3.2 Time of flight mass analyzer**

The TOF mass analyzer has higher resolution power and after the fragments are filtered in third quadrupole, they will enter the TOF mass analyzer for higher resolution. TOF analyzer separates ions, according to their velocities when they drift in a free-field region that is called a flight tube. Before entering the free-field region they are accelerated towards the flight tube by a difference of potential applied between an electrode and the

extraction grid. As all the ions acquire the same kinetic energy, ions are characterized by a distribution of their velocities. Mass-to-charge ratios are determined by measuring the time that ions take to move through a field-free region between the source and the detector. Reflectron TOF analyzer uses ion mirror to reflect ions from the end of the flight tube and sends it back to the flight tube and enters the detector which is parallel to ion source (6).

#### **2.3.4 Ion Detector: Electron Multiplier (EM)**

After separation of ions in mass analyzers, it enters the detector. There are several methods for ion detection. But the most common detector is the electron multiplier (EM). Agilent 6500 series use microchannel plate (MCP) type electron multiplier detector. When an ion hits the front surface of the MCP, an electron escapes and begins the process of electrical signal amplification. Free electrons collide with the walls of the microscopic tubes and ever-increasing cascade of electrons travels to the rear of the plate. Roughly 10 times more electrons come out the MCP than incoming ions contact the surface. These electrons are then focused onto a scintillator, which, when struck by electrons, produces a flash of light. The light from the scintillator is focused through two small lenses onto a photomultiplier tube (PMT), which produces the electrical signal read by the data system (6).

In this work, we have used Agilent 6500 series qTOF mass spec, which uses quadrupole as mass analyzer, hexapole as a collision cell and TOF analyzer to separate ions.

## 2.4 NMR spectroscopy

We have performed NMR experiment for structure identification of unknown lipid initially, because of nondestructive nature of the technique. 1D and 2D NMR spectra of lipids allowed us to identify coupling of C-H and C-C bonds and helped us identifying multiplicity of  $^{13}\text{C}$  atom. Main complication was the sensitivity issue, because of the low concentration of the lipid in isolated lipid fractions.

### 2.4.1 Basics

Physicist P. Zeeman in 1902 discovered that nuclei of certain items behave strangely when exposed to external magnetic field. Based in this knowledge, F. Bloch and E. Purcell constructed first NMR spectrometer. Nuclear magnetic resonance (NMR) spectroscopy works based on the principle of spin of the nucleus. Just like electrons protons have spin quantum number ( $m$ ).  $m$  can assume value of  $+\frac{1}{2}$  or  $-\frac{1}{2}$ . Such nucleus is described with a nuclear spin ( $I$ ) value of  $\frac{1}{2}$ . As nucleus is spinning charged particle, this gives rise to magnetic moment ( $\mu$ ). These two spin states degenerate in absence of magnetic field. All up spins are cancelled by down spins and nucleus have net zero magnetic moment. If we apply external field in positive direction, considering opposite charge of nucleus with respect to electron, nucleus with  $+\frac{1}{2}$  whose magnetic moment is aligned with magnetic field has the lower energy. Isotopes with odd numbers of proton and/or neutrons possess non zero nuclear spin and they can be detected by NMR methods. Isotopes with even protons and neutrons have zero nuclear spin ( $I=0$ ) and cannot be detected. Nucleus with nuclear spin  $I$  adopts  $2I + 1$  non degenerative spin orientation in the magnetic field (9). The energy of the particular spin state is given as

$$E = -m \frac{\gamma h B}{2\pi} \quad (2.7)$$

In this equation  $m$  is spin quantum number of the state,  $h$  is Planck's constant,  $B$  is magnetic field strength and  $\gamma$  is magnetogyric ratio, describes how much spin state energies of a given nucleus vary with changes in external field. Negative sign is used to keep positive  $m$  (stable) value corresponds to a lower energy. As magnetic strength increases difference between any two spin states, for example  $+1/2$  and  $-1/2$  increases and makes NMR spectroscopy more sensitive. Nuclei do not stay parallel or antiparallel to applied field. They wobble around the axis of the field at a fixed frequency called Larmor frequency which is a function of  $\gamma$  and  $B$ . It is independent of  $m$ , so all spin orientations of a given nucleus precess at same frequency (9).

#### 2.4.2 Energy levels

When frequency is applied to nucleus under the influence of external magnetic field, spin flip occurs and low energy spin state ( $m=+1/2$ ) becomes high energy spin state ( $m=-1/2$ ). Difference can be calculated using equation 2.7. For absorption of frequency more particles needed to be in lower energy state compare to high energy state. If particle in both states are equal than transition can also occur from high to low state during the absorption process causing net zero absorption, a condition called saturation (9).

There will always be more particles in lower state compare to higher state. Distribution of particles between these two states is given by Boltzmann distribution as follows.

$$\frac{P(+1/2)}{P(-1/2)} = e^{-\Delta E/kT} \quad (2.8)$$

Where  $P$  is population in each state,  $\Delta E$  is difference in energy between two states and  $T$  is absolute temperature in Kelvin and  $k$  is the Boltzmann constant. As seen from

equation higher energy difference between the states (depends on magnetic field strength), a larger magnetogyric ratio or a lower temperature all contribute to a larger population difference and lead to an intense NMR signal (9).

### **2.4.3 Components of NMR spectrometer**

NMR spectrometer is made up of, NMR magnet to generate magnetic field, rf Oscillator to generate  $B_1$  in the transmitter coil, a receiver coil to pick up the signal, the electronics to turn the signal into spectrum (9).

Most important characteristics of the NMR magnet include their strength, stability and homogeneity of field. Precessional frequency of identical and nonidentical nuclei depends directly on strength of magnet, so it is advantageous to use the strongest magnet available to obtain the greatest separation between the NMR signals. Stronger field also increases energy difference between spin states and generates more intense signal (9).

Superconducting magnets are generally used for the routine applications. Each superconducting magnet is designed to provide specific field strength, currently in the range of 6-18 T, corresponding to  $^1\text{H}$  operating frequencies in the range of 250-750 MHz. The cylindrical solenoid of NMR spectrometer is made up of unique niobium-tin alloy which becomes superconducting when cooled to 4 K by immersion into liquid helium in a cryostat which is covered by outer jacket of liquid nitrogen. Appropriate current is established using DC current. Then two ends of solenoid loop are short circuited and DC source is removed. As solenoid circuit has zero resistance, DC continues to coursing through the solenoid and maintains a strong and stable magnetic field (9).

Stability of the field is monitored and controlled by electronic feedback technique known as locking. Substance selected (usually solvent) that gives rise to strong signal at a different frequency from those of the nuclei of interest. Lock signal is continuously monitored and compared to a fixed reference frequency. Any difference between these two frequencies generates micro current that passes through secondary coil and generates small magnetic field parallel or antiparallel to magnetic field until lock and reference frequency matches (9).

After obtaining the stable field, homogeneity is required to maintain across the sample which is achieved by a process called spinning and shimming. Sample is centered along the center of the field called the probe, whose temperature is separately controlled. Tube is spun around its axis at 100 Hz by means of an air stream which averages out any slight inhomogeneity. Contour of the field can be varied by passing extremely small current through shim coils around the probe cavity. This process is called shimming or tuning of magnet (9).

#### **2.4.4 Pulsed mode for signal acquisition**

Pulsed mode NMR experiment is performed at both constant magnetic field and constant rf frequency and rf radiation is supplied by a brief but powerful computer controlled pulse of rf current via transmitter coil. This pulse centered at operating frequency  $\nu_0$ , is characterized by a power and pulse width. It is applied for microseconds and as per uncertainty principle, covers a range of frequencies from  $\nu_0 - \Delta\nu$  to  $\nu_0 + \Delta\nu$ . Shorter the pulse, the greater the range of frequencies covered. The power of pulse must be sufficient to cause all sets of nuclei precessing at frequencies within the spectral width to become

phase coherent. Closer the nuclei's frequency to  $\nu_0$ , more excitation energy the nucleus receives and increases the flip angle which gives more intense signal (9).

After applying pulse, induced ac signal is monitored in receiver coil. Excited nucleus decays at constant frequency and this free induction decay (time domain spectrum) is measured. The data obtained is fourier transformed to convert time domain spectrum to frequency domain spectrum. Frequency of each spectrometer varies and to get uniformity in frequency new parameter chemical shift (ppm) is introduced which is defined as

$$\delta_i = 10^6 \delta \nu_i / \nu_0. \quad (2.9)$$

#### **2.4.5 Complex Pulse sequences**

Before understanding the pulse sequences, it is necessary to understand the spin orientation of net magnetization. Net magnetization vector is observed by laboratory frame of reference, the normal X, Y, Z coordinate system. At equilibrium, Net magnetization M is aligned with static magnetic field at Z axis. Individual magnetization vectors still precess around Z axis. After applying RF pulse ( $90^\circ_x$ ), Net magnetization vector flips and precess around Z axis in XY plane forming a disk like shape.

In rotating frame of reference we introduce rotating axes X', Y' and Z', in which X' and Y' precess around Z axis at same frequency as net magnetization vector. If the observers are precessing around Z axis at same frequency as the net magnetization vector, they will see the net magnetization vector stationary (9).

### 2.4.5.1 $^1\text{H}$ NMR Pulse Sequence

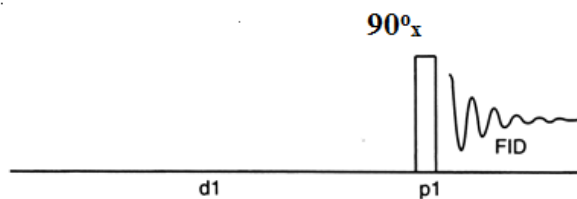


**Figure 2.6 Basic  $^1\text{H}$  NMR Pulse Sequence. Figure adapted by author from (10)**

#### Setting up the experiment

Figure 2.6 explains typical  $^1\text{H}$  NMR pulse sequence. Interpulse delay (d1) allows the spin system to relax back to the equilibrium status, after obtaining Free Induction Decay (FID) signal. This is important to obtain maximum signal to noise ratio. The Longer the relaxation delay the closer the spin system gets to equilibrium status, which will give maximum signal. However, increasing the time for relaxation delay leads to longer experiment time and compromise is made in practice to achieve maximum signal with minimum delay time. Typical relaxation time for  $^1\text{H}$  spin system is 2-4 seconds. Spin system is also relaxing during the acquisition time, so typical value for d1 is in range of 100 msec (9, 10).

The rf oscillator aligned around the X axis is turned on for 1-10  $\mu\text{seconds}$  to apply  $90_x$  pulse (p1) and then turned off. This irradiates range of frequencies and flips net magnetization vector in Y axis, and it starts precessing around Z axis in XY plane. After sufficient dead time, we start collecting FID in receiver coil around the Y axis. Dead time is necessary for electronics to stabilize after irradiation (9, 10).

### 2.4.5.2 Spin Inversion Effect and NOE effect

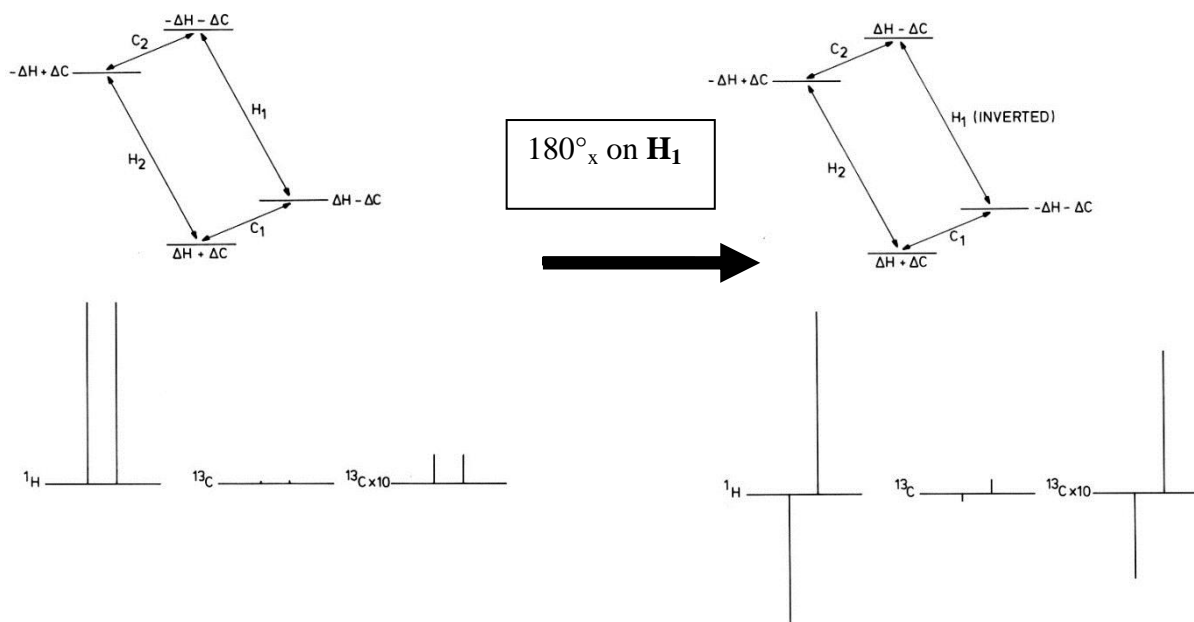


**Figure 2.7 Selective spin Inversion. Figure adapted by author from (10)**

Consider CH spin system with four energy levels as shown in figure 2.7. At initial stage difference between  $C_1$  and  $C_2$  transition is  $2\Delta C$  and difference between  $H_1$  and  $H_2$  transition is  $2\Delta H$ . If we apply selective  $180^\circ_x$  pulse for  $H_1$  transition and invert the population, energy difference for  $C_1$  and  $C_2$  transition becomes  $-2\Delta H + 2\Delta C$  and  $2\Delta H + 2\Delta C$  respectively and signal enhancement in  $^{13}\text{C}$  NMR signal is observed (9,10).

In NOE, we saturate  $H_1$  and  $H_2$  transition, so first energy state  $\Delta H + \Delta C$  becomes same as third and second energy state  $\Delta H - \Delta C$  becomes same as fourth. Energy difference between first and second and third and fourth energy state is still  $2\Delta C$ , but difference between first and fourth decreased to  $2\Delta C$ . To compensate for this decrease in energy some population is transferred from fourth energy state relax to state one and this

increase the population in state one and decrease population in fourth and this increase signal of  $^{13}\text{C}$  NMR (9).

### 2.4.5.3 $^{13}\text{C}$ Decoupled NMR Pulse Sequence

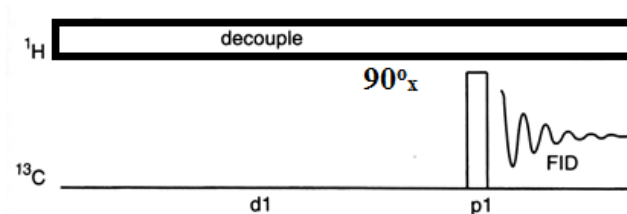


**Figure 2.8  $^{13}\text{C}$  Decoupled Experiment Pulse Sequence. Figure adapted by author from (10)**

$^{13}\text{C}$  nuclei have nuclear spin of  $\frac{1}{2}$  like  $^1\text{H}$  nuclei, but it resonates at lower frequency because of lower magnetogyric ratio of  $^{13}\text{C}$  nuclei. Also, because of low natural abundance and lower sensitivity of  $^{13}\text{C}$  nuclei, we use  $^{13}\text{C}$  decoupled pulse sequence. This pulse sequence enhance signal through Nuclear Overhauser Effect (NOE effect) and by removing coupling of  $^1\text{H}$  nuclei. The NOE effect is defined by change in intensity of  $^{13}\text{C}$  nuclei by irradiating coupled  $^1\text{H}$  nuclei. For C-H spin system if we saturate  $^1\text{H}$  transition, this increases the lower energy state population of  $^{13}\text{C}$  nuclei by relaxation through different pathway (cross polarization) and increases the signal of  $^{13}\text{C}$  NMR (9).

Pulse sequence of  $^{13}\text{C}$  channel (Figure 2.8) is similar to  $^1\text{H}$  NMR pulse sequence, which includes  $90^\circ_x$  pulse, which will flip the net magnetization vector for  $^{13}\text{C}$  nuclei ( $M_c$ ) on Y axis, which will precess around Z axis. If decoupler is off, one component of  $M_c$  vector will precess faster than precession frequency by  $+J/2$  value and other will precess slower by  $-J/2$  value because of up and down spin states of nearby proton nuclei and this will generate doublet peak with coupling value of  $J_{\text{CH}}$ . If we have decoupler on,

which will irradiate the sample at average precessional frequency of  $^1\text{H}$  nuclei and this pulse will irradiate all  $^1\text{H}$  nuclei in system and they will precess around X axis in YZ plane and this will cause protons to rapidly change their up and down state (From +Z to -Z and vice versa). As protons are saturated, their up and down states does not affect magnetization of  $M_c$  and this generates single peak for -CH- spin system. Decoupler must be on during acquisition for decoupling to occur. Keeping the decoupler on before applying pulse causes NOE effect and increases the intensity of signal (9, 10).

### 2.4.5.4 J Modulated Spin Echo (JMOD) NMR Pulse Sequence

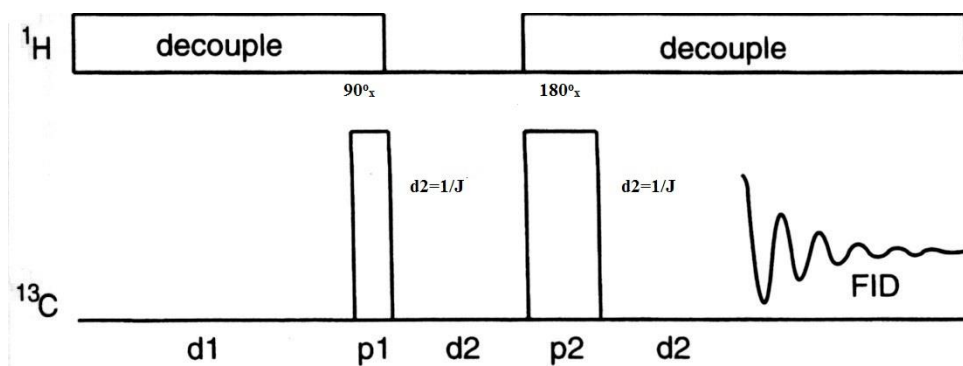


Figure 2.9 J Modulated Spin Echo (JMOD) experiment pulse sequence. Figure adapted by author from (10).

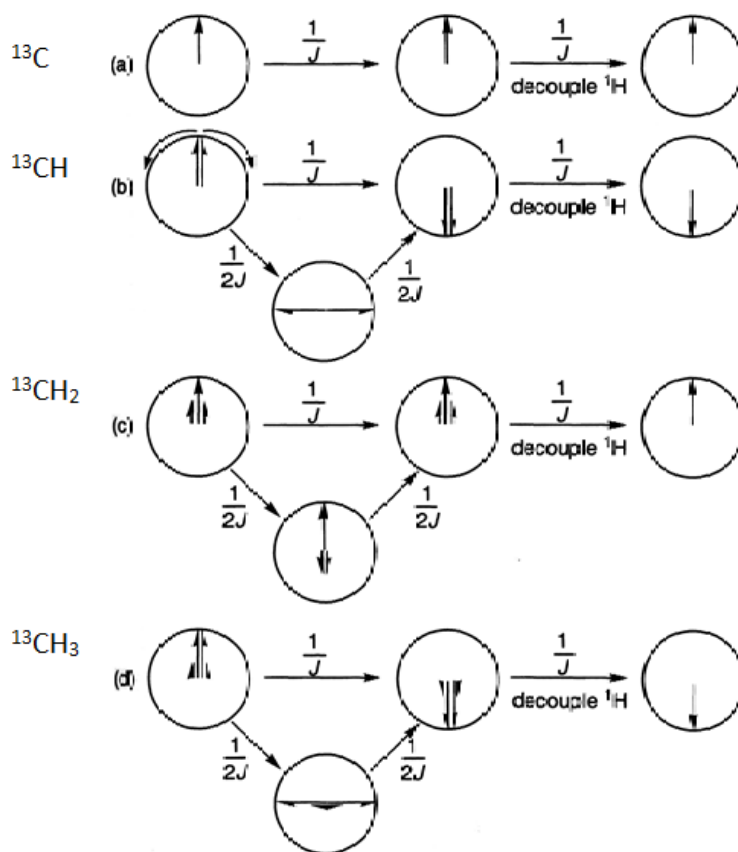


Figure 2.10 Vector diagram for J Modulated Spin Echo (JMOD) Experiment Pulse Sequence. Figure adapted by author from (10).

J Modulated Spin Echo experiment is 1D NMR method to assign C-H multiplicities.

Pulse sequence for this experiment is shown in figure 2.9 which is further explained by vector diagram at each pulse in figure 2.10. It is also known as attached proton test.

The first  $90^\circ_x$  pulse rotates magnetization vector for  $^{13}\text{C}$  ( $M_c$ ) on  $+y'$  axis. After this we turn decoupler off on  $^1\text{H}$  channel to allow evolution of coupling for  $d_2=1/J$  seconds (9, 10).

a) Quarternary carbon ( $^{13}\text{C}$ ) does not have any coupling to proton therefore after  $d_2=1/J$ ,  $M_c$  remains on  $+y'$  axis. After next  $180^\circ_y$  pulse and second  $d_2=1/J$  period,  $M_c$  remains on  $+y$  axis and decoupler is turned back on and FID is collected and this gives positive peak in  $^{13}\text{C}$  NMR spectra (9, 10).

b) Methine carbon ( $^{13}\text{CH}$ ) observes proton spin up and down and therefore generates doublet. In rotating frame of reference, one peak moves clockwise at  $+J/2$  Hz and other at  $-J/2$  Hz. After  $d_2=1/J$  seconds, these peaks completes half revolution and comes to  $-y'$  axis. After next  $180^\circ_y$  pulse and second  $d_2=1/J$  period,  $M_c$  refocus on  $-y$  axis and decoupler is turned back on and  $M_c$  freezes on  $-y'$  axis and this gives negative peak in  $^{13}\text{C}$  NMR spectra (9, 10).

c) Methylene Carbon ( $^{13}\text{CH}_2$ ) generates three vectors with decoupler off. In rotating frame of reference, these peaks will move at  $+J$ ,  $0$  and  $-J$  Hz. After  $d_2=1/J$  they will complete one full revolution and comes back to  $+y'$  axis After next  $180^\circ_y$  pulse and second  $d_2=1/J$  period,  $M_c$  refocus on  $+y$  axis and decoupler is turned back on and  $M_c$  freezes on  $+y'$  axis and this gives positive peak in  $^{13}\text{C}$  NMR spectra (9, 10).

d) Methyl carbon, generates four vectors, which will rotate at  $+3J/2$ ,  $+J/2$ ,  $-J/2$  and  $-3J/2$  in rotating frame of reference. After  $d2=1/J$ , they will end up at  $-y'$  axis. After next  $180^\circ_y$  pulse and second  $d2=1/J$  period,  $M_c$  refocus on  $-y$  axis and decoupler is turned back on and  $M_c$  freezes on  $-y'$  axis, which gives negative peak in  $^{13}\text{C}$  NMR spectra (9, 10).

#### **2.4.5.5 2D NMR Spectroscopy**

All 2D-NMR experiments have four well-defined stages: (i) preparation; (ii) evolution; (iii) mixing; and (iv) detection. Preparation and detection phase are similar to 1D NMR experiment. Evolution and mixing period varies with the complexity of the pulse sequence (9, 12).

In 2D NMR, multiple FIDs are collected at different evolution time ( $t_1$ ) increments.

During this  $t_1$  period peak intensity (phase) will modulate at a frequency corresponding to the correlated chemical shift and/or coupling constant and then all the obtained FIDs are fourier transformed with respect to  $t_1$  and  $t_2$  time domain, which converts time domain into frequency domain  $F_1$  and  $F_2$ . Generated FIDs are fourier transformed in  $t_2$  domain to generate frequency domain  $F_2$ , which contains information about chemical shift. After that data is fourier transformed into  $t_1$  domain to generate frequency domain  $F_1$  to obtain information about offsets and coupling (9, 12).

### A) $^1\text{H}$ - $^1\text{H}$ correlation Spectroscopy (Homonuclear COSY)

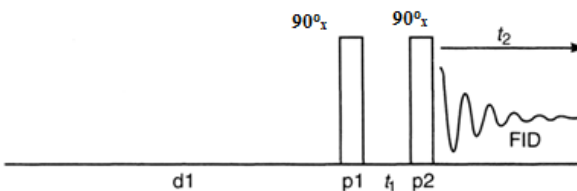


**Figure 2.11 Homonuclear COSY pulse sequence. Figure adapted by author from (11).**

To understand  $^1\text{H}$ - $^1\text{H}$  correlation Spectroscopy pulse sequence (figure 2.11), Consider two spin system A-X with vectors  $M_A$  and  $M_X$ . After the first pulse they rotate in  $y'$  plane and with evolution  $t_1$ , they get split into four vectors because of coupling. Two of them will move clockwise and other two will move counter clock wise. Each of these vectors now has one component in X plane and one component in Y plane. After the second pulse, y component will move to  $z'$  axis and will not be detected and other component will decay to equilibrium and generate FID (11).

In a COSY spectrum, the signals along the diagonal reflect the normal 1D proton spectrum and the off-diagonal peaks provide correlation due to two to three bond  $^1\text{H}$ - $^1\text{H}$  coupling (9, 11).

### B) Heteronuclear Single Quantum Coherence Spectroscopy (HSQC)

HSQC experiment provides information about the correlations of the protons with the carbon atoms to which they are directly attached. It provides valuable information to solve the structure of unknown organic compounds. Figure 2.12 provides information about HSQC pulse sequence and 2.13 provides information about position of vectors during this pulse sequence (11).

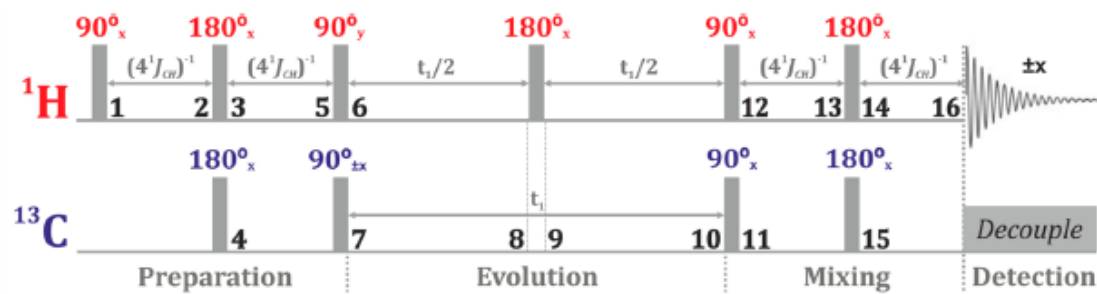
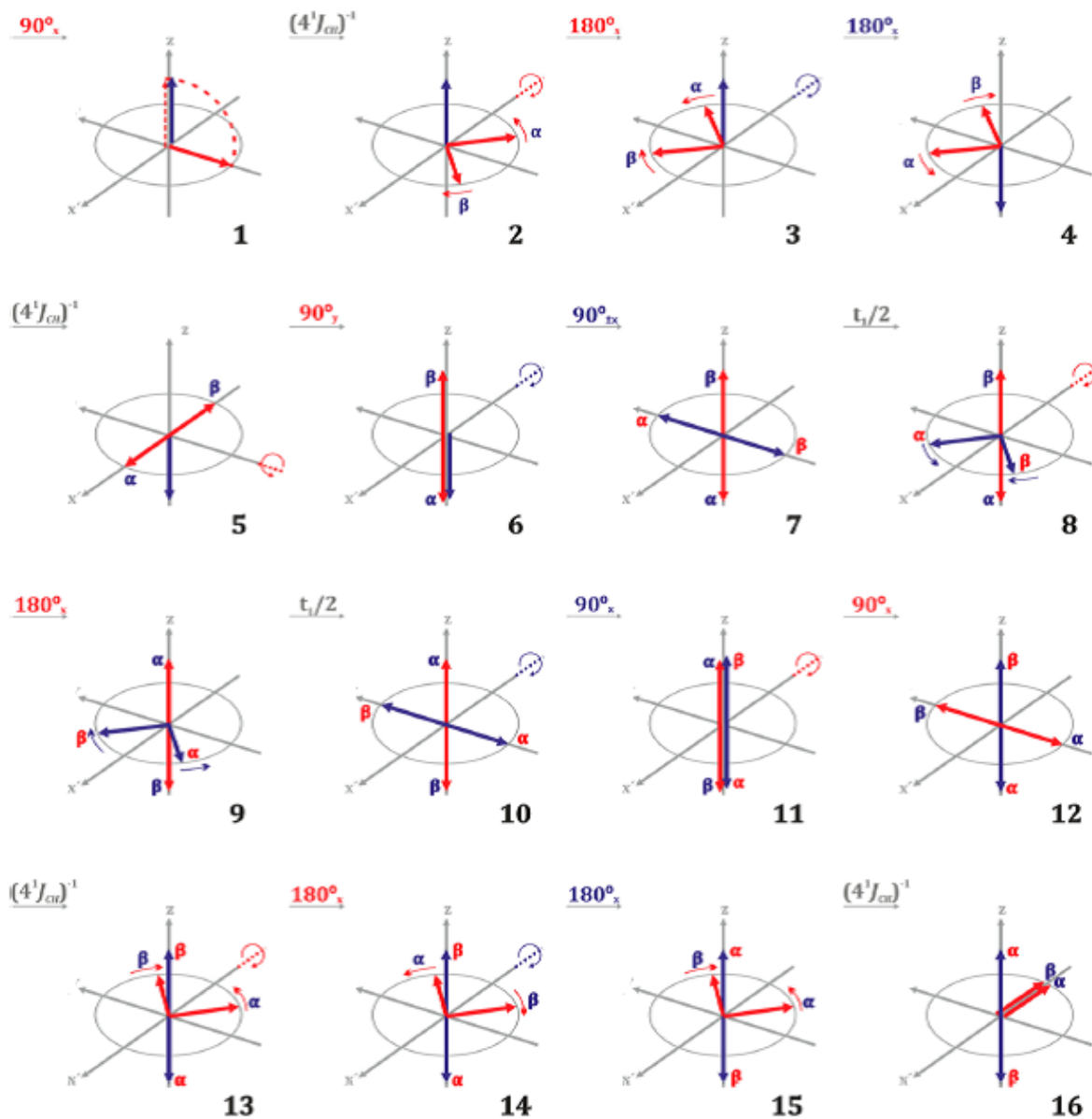


Figure 2.12 HSQC pulse sequence. Reprinted with permission from (12). Copyright (2014) American Chemical Society.



**Figure 2.13 Vector diagram for HSQC pulse sequence. Reprinted with permission from (12). Copyright (2014) American Chemical Society.**

In figure 2.13, protons ( $^1\text{H}$ ) magnetization vector is represented by red color and carbon ( $^{13}\text{C}$ ) magnetization vector is represented by blue color.

### 1) Preparation:

The first  $90^\circ_x$  pulse flips proton magnetization on  $y'$  axis (Scheme 1). After that system is allowed to evolve for  $1/4J_{1CH}$  seconds.  $J_{1CH}$  stands for single bond carbon proton coupling constant. After this time the two vector component travels  $1/4^{\text{th}}$  distance (Scheme 2). Next  $180^\circ_x$  proton pulse rotates magnetization to  $180^\circ$  axis (Scheme 3). Simultaneously, another  $180^\circ_x$  pulse is applied on carbon channel which inverts magnetic vector of carbon into  $-z$  axis. This pulse on carbon channel causes spin inversion effect by changing energy level of CH spin system. This effect converts  $H_\alpha$  into  $H_\beta$  and vice versa (Scheme 4). After  $1/4J_{1CH}$  seconds they evolve and end up at  $x'$  axis (scheme 5), forming an angle of  $180^\circ$ . The  $90^\circ_y$  pulse on proton channel moves these magnetization vectors into  $+z$  and  $-z$ . (Scheme 6). This is the inversion of proton which permits polarization transfer to carbon after  $90^\circ_x$  pulse on carbon channel is applied (Scheme 7) (12).

### 2) Evolution:

There is no evolution of homonuclear coupling because proton magnetization vector is in  $\pm z$  axis. Instead Carbon magnetization vector evolves due to heteronuclear coupling with proton in  $t1/2$  period (Scheme 8). At this point another  $180^\circ_x$  pulse on proton again inverts their position and this causes inversion of carbon magnetization vector and they change their direction and become antiphase on  $\pm y$  axis (Scheme 9). At the end of evolution period, with different  $t1$  value carbon magnetization vector always end up in  $\pm z$  axis. This experiment is repeated with different value of  $t1$  which allows carbon coupling to proton to develop and this provides us valuable information about indirect F1 domain (12).

### 3) Mixing:

$90^\circ_x$  pulse on carbon channel flips these carbon magnetization vector into  $\pm z$  axis (Scheme 11). Another  $90^\circ_x$  pulse on proton channel brings proton magnetization vectors into  $x'y'$  plane and causes the reverse polarization transfer (Scheme 12). Now this homonuclear coupling of proton evolves (Scheme 13) in  $x'y'$  plane for  $1/4J_{1CH}$  seconds and  $180^\circ_x$  pulse to proton interchanges the vector (Scheme 14) and then simultaneous  $180^\circ_x$  pulse to carbon interchanges the carbon and proton magnetization vector respectively (Scheme 15). Then proton vector evolves for  $1/4J_{1CH}$  seconds and become in-phase (Scheme 16). Now decoupler is turned on on carbon channel and proton signal is measured. Proton homonuclear couplings are observed in F2 domain and heteronuclear coupling evolved during  $t_1$  period are measured in indirect F1 domain (12).

## 2.5 Reference

- 1) Stuart, B. *Infrared Spectroscopy: Fundamentals and Applications*, John Wiley & Sons Inc., Hoboken (NJ), 2004).
- 2) Dufour, E. *Infrared Spectroscopy for Food Quality Analysis and Control*, (Elsevier Inc., Burlington (MA), 2009).
- 3) "FT-IR Spectroscopy - Attenuated Total Reflectance (ATR)". *Perkin Elmer Life and Analytical Sciences*. 2005.
- 4) Mirabella, FM Jr. *Practical Spectroscopy Series; Internal reflection spectroscopy: Theory and applications*, (Marcel Dekker, Inc., New York, 1993).
- 5) Milosevic, M. *Internal Reflectance near Critical Angle, in Internal Reflection and ATR Spectroscopy*. (John Wiley & Sons, Inc., Hoboken(NJ), 2012).
- 6) Hoffmann, E.De, Charette, J. & Stroobant, V. *Mass spectrometry: Principles and applications*. (John Wiley and Sons Inc., Hoboken(NJ), 1996).
- 7) Fenn, J.B., Mann, M., Meng, C.K., Wong, S.F. & Whitehouse, C.M. Electrospray ionization-principles and practice. *Mass Spectrom Rev* **9**, 37–70 (1990).
- 8) March, R. An Introduction to Quadrupole Ion Trap Mass Spectrometry, *Journal of Mass Spectrometry* **32(4)**, 351-369 (1997).
- 9) Macomber, R.S. *A complete introduction to modern NMR spectroscopy*. (John Wiley and Sons Inc., Hoboken(NJ), 1998)
- 10) Roberts, P. Chapter 8: One-Dimensional (1D) NMR Experiments [PowerPoint slides]. Retrieved from <http://www.bionmr.unl.edu> (2014).

11) Roberts, P. Chapter 9: 2D NMR Experiments [PowerPoint slides]. Retrieved from <http://www.bionmr.unl.edu> (2014).

12) De la Vega-Hernandez, K. & Antuch, M., The Heteronuclear Single-Quantum Correlation (HSQC) Experiment: Vectors versus Product Operators. *J. Chem. Educ.* **92**, 482-487 (2015).

## CHAPTER

### 3. LIPID COMPOSITION OF THERMOPHILIC *GEOBACILLUS* SP. STRAIN *GWE1*, ISOLATED FROM STERILIZATION OVEN

(Note: Content of this Chapter is adapted from the publication “Siddharth P. Shah, Susan A. Jansen, Leeandrew Jacques-Asa Taylor, Parkson Lee-Gau Chong, Daniela N. Correa-Llantén, Jenny M. Blamey, Lipid composition of thermophilic *Geobacillus* sp. strain *GWE1*, isolated from sterilization oven. Chemistry and Physics of Lipids, 2014, 180:61–71” with permission)

#### 3.1 Introduction

*GWE1* is a thermophilic Gram-positive bacterium, belonging to the genera *Geobacillus* according to phylogenetic analysis based on 16S rRNA sequences (1). *GWE1* requires optimum temperature of 70 °C. This extreme thermophile was isolated from a sterilization-drying oven (1), which had different extreme conditions like high temperatures as well as dehydration and rehydration cycles. This strain shows remarkable stability both against autoclaving and UV irradiation, characteristics uncommon to genus *Geobacillus*. This strain remains viable for 60 min at 136 °C under autoclaving conditions and shows stability under UVA, UVB and UVC irradiation for 40 h, 36 h and 28 h respectively. It also shows a high resistance to desiccation, for up to 120 days (1, 2).

It is of interest to understand why *GWE1* strain is able to sustain these harsh conditions. It is known that thermophilic prokaryotes adapt to the extreme environments by modifying their macromolecules, such as proteins, nucleic acids and lipids. Several

survival strategies of prokaryotes have been proposed. Pack et al. compared 20 different mesophilic and thermophilic proteins and suggested differences in amino acid arrangement between fully exposed areas and fully buried areas (3). Other strategies in preservation of protein structure at higher temperature include increasing ion-pair content, forming higher-order oligomers, decreasing flexibility at room temperature and decreasing the length of surface loops that connect elements of secondary structure and optimizing electrostatic and hydrophobic interactions (4). Nucleic acid is subject to denaturation at high temperature, but the DNA of thermophiles has greater thermal stability compared to that of mesophiles, due to the presence of mono-divalent salts stabilizing charge on phosphate and/or due to changes in base pair. More G-C base pairs instead of A-T or A-U pairs have been found in RNA of thermophilic prokaryotes compared to mesophile RNA (4).

Lipid also plays an important role in thermostability by maintaining liquid crystalline state of membrane and by acting as barrier to decrease permeability of solutes (4). At higher growth temperature, thermophilic bacteria are adapted to meet both conditions require for thermostability by changing lipid amount and type to counteract the thermo-induced increase in membrane fluidity. Adaptations for thermostability in bacterial lipid membrane include increasing hydrocarbon chain length and the degree of saturation as well as increasing the ratio of iso/anteiso branching (4, 5, 6). For example a mesophilic strain of *Bacillus megaterium* (7) has been shown to have 25% iso-C15 and nearly 50% anteiso-C15 fatty acids at 20°C growth temperature and 35% iso-C15 and

15% anteiso-C15 at 60°C. This suggests that the iso-C15 fatty acid is thermophilic and the anteiso-C15 fatty acid is psychrophilic in this bacterial species.

Archaeal lipids have a different mechanism of adaptation. Archaea have shown to increase proportion of dibiphytanylglycerol tetraether lipids in compare to diphytanylglycerol diether lipids to adapt to thermal stress. In *Arhcaeoglobus fulgidus* ratio increases from  $0.3 \pm 0.1$  to  $0.9 \pm 0.1$  with increase on growth temperature from 70 °C to 89 °C (8). In *Thermoplama acidophilum* increase in growth temperature and decrease in growth pH, leads to increase in number of cyclopentane rings in hydrocarbon chain of tetraether lipids (9). Different mode of adaptation of bacteria and archaea (10) to thermal stress lead to development of theory of “lipid divide”, which is described in depth elsewhere (11) and will not be repeated here.

Some other examples of lipids found in thermophilic bacteria include, monobranched fatty alcohol-containing diether lipids from *Thermodesulfobacterium commune* (70 °C) (11) and *Aquifex pyrophilus* (85 °C) (11), long chain dicarboxylic fatty acids (diabolic acid), and 15,16-dimethyl 30-glycerloxytriacontanoic acid from *Thermotoga maritima* (90 °C) (11) and *Fervidobacterium islandicum* (75 °C) (11), a long chain 1, 2-diol from *Thermomicrobium roseum* (75 °C) (11); cyclohexyl fatty acid from *Bacillus acidocaldarius* (65 °C) (11); novel glycolipids and phosphoglycolipid from *thermophilus* Samu-SA1 (75 °C) (12). These have been assumed to be thermophilic lipids because of their unhydrolyzability (diether or saturated long-chain diols) or membrane-spanning nature (dicarboxylic acid) like tetraether lipids. However, thermostability of

bacteria is not limited to diether containing lipids. Some ester bond lipids also have shown thermostability in extreme environment (11-12).

In the present study, we extracted and identified certain lipids present in *GWEI* cell membrane, as the start point to understand the stability of *GWEI* strain against high temperature and irradiation. We have used shotgun lipidomics, 1D and 2D NMR spectroscopy and ATR-FTIR spectroscopy to answer the question of high stability of *GWEI* strain. We were able to identify glycerophosphoethanolamine (PE), glycerophosphoglycerol (PG), glycerophosphate (PA), glycerophosphocholine (PC) and cardiolipins (CL) classes in the TLC fractions of extracted lipids. These lipids are rich in saturated, long, and iso-branched fatty acids, which may attribute to some extent the cell membrane stability.

## **3.2 Materials and Methods**

### **3.2.1 Cell growth**

*GWEI* cells were isolated as previously described (1). In brief, samples of dark crusty material were collected from the corners and cracks of a sterilization oven. These samples were enriched in modified marine medium and plated for colony isolation. *GWEI* cells were isolated under aerobic conditions. Optimum growth was obtained using 70 °C, pH 5.8, and 2% NaCl.

### **3.2.2 Materials**

HPLC grade acetonitrile, water, triphenyl phosphine, chloroform, methanol and formic acid were obtained from either Sigma (St. Louis, MO, USA) or Fisher Scientific

(Waltham, MA, USA). Deuterated methanol and deuterated chloroform were ordered from Acros Organics (Fair Lawn, NJ, USA). All standards were used as received.

### **3.2.3 Extraction of polar lipids**

Total polar lipids were extracted by the method of Lo and Chang (13). In brief, dried cells were soxhlet-extracted with chloroform/methanol (1:1, v/v) for 24 h. The crude lipids were fractionated by reversed-phase column chromatography using C-18 PrepSep columns (Fisher Scientific, Fair Lawn, NJ) eluted first with methanol: water (1:1, v/v) (fraction A) and then with chloroform: methanol: water (0.8:2:0.8, v/v/v) (fraction B). Fraction B was further separated by thin-layer chromatography (TLC) using chloroform: methanol: water (65:25:4, v/v/v) as the solvent system. Six bands were detected after iodide vapor exposure; and, they were scraped and extracted with chloroform: methanol: water (5:10:4, v/v/v). The  $R_f$  values of those fractions are: 0.31 for fraction I, 0.40 for fraction II, 0.53 for fraction III, 0.65 for fraction IV, 0.80 for fraction V and 0.99 for fraction VI (Figure 3.1). All six fractions were collected, evaporated to dryness under nitrogen, and stored at -20 °C before structure analysis.

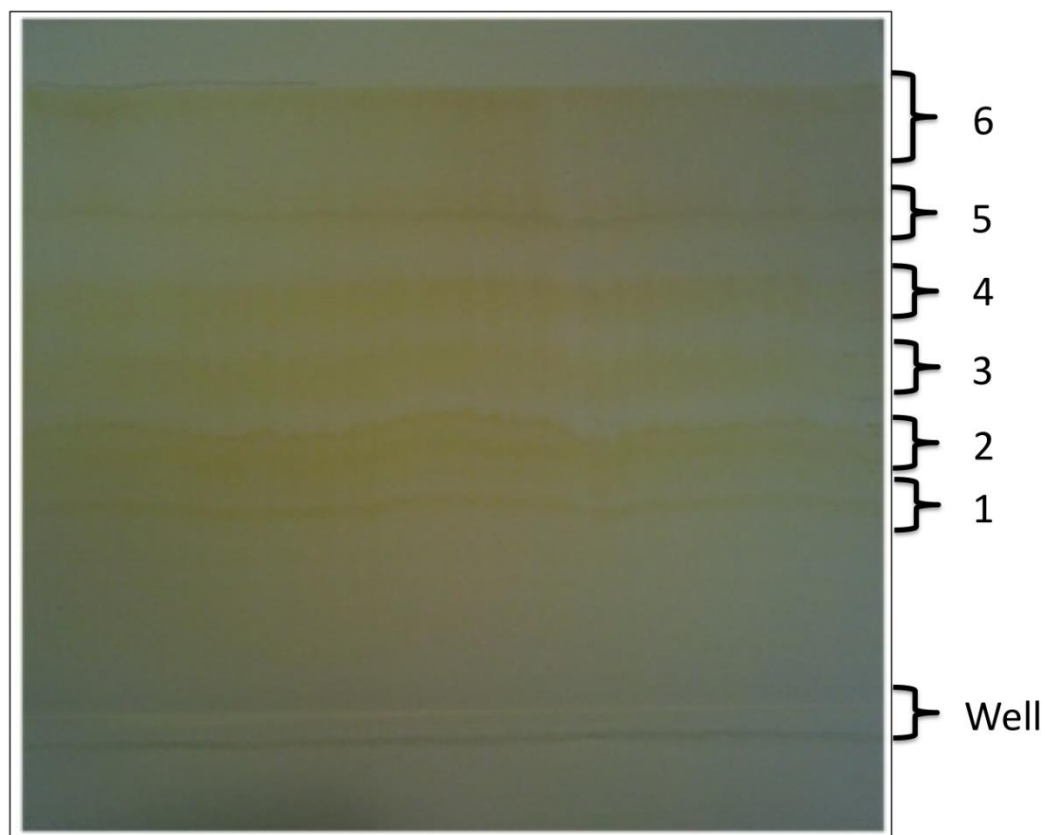


**Figure 3.1** Thin layer chromatography of lipids extracted from *GWE1* gave 6 different bands.

### **3.2.4 Attenuated total reflection- Fourier transform infrared (ATR-FTIR)**

#### **spectroscopy**

Isolated fractions were dissolved in chloroform and 10  $\mu\text{l}$  of sample was placed on diamond lens and allowed to evaporate to make a thin layer of the lipid. ATR-FTIR experiments were performed on a Germanium (Ge) multibounce ATR accessory mounted in a Nicolet Magna 750 FTIR spectrometer that was equipped with a mercury cadmium telluride A (MCTA) detector. Single beam spectra were recorded as an average of 50 scans with a resolution of  $2\text{ cm}^{-1}$ . Solvent spectrum was used as a reference spectrum.

### **3.2.5 NMR Spectroscopy**

About 6-8 mg of dried fraction was dissolved in 1 ml deuterated methanol and deuterated chloroform (2:1, v/v), mixed well and centrifuged at 12,000 rpm for 30 minutes. The supernatant was transferred to NMR tube for further experiments. All the NMR spectroscopy experiments were done on Bruker Avance- III 500 NMR Spectrometer with a 5 mm broadband probe equipped with Z gradient and  $^2\text{H}$  lock at room temperature. Decoupling was achieved using Waltz 16 pulse sequence.

$^1\text{H}$  NMR spectroscopy was performed at 500.13 MHz, with a pulse duration (P1) of 12.6  $\mu\text{s}$ , spectral width (SW) of 20 ppm, and a relaxation delay (D1) of 2 s, acquisition time (AQ) of 6.34 s and a  $30^\circ$  pulse angle. Number of scans (NS) was set to 256 scans. Probe was tuned at 500.13 MHz.

$^1\text{H}$  decoupled  $^{13}\text{C}$  NMR was performed at 125.75 MHz, with a pulse duration (P1) 9  $\mu\text{s}$ , spectral width (SW) of 236 ppm, relaxation delay (D1) of 2 s, acquisition time (AQ) of 1.10 s and a  $30^\circ$  pulse angle. Number of scans (NS) was set to 13.5 K. Shifts were

referenced based on d-methanol shift ( $\delta_{\text{H}}$ , 3.31 ppm;  $\delta_{\text{C}}$ , 49.30 ppm). Channel 1 (observe channel) was tuned at 125.75 MHz and Channel 2 (decoupler channel) was tuned at 500.13 MHz.

J modulated spin echo experiment (JMOD) was performed using standard JMOD pulse sequence (43), with spectral width (SW) of 236 ppm, acquisition time (AQ) 1.10 s, number of scans (NS) 11000, relaxation delay (D1) 2 s at 125.75 MHz.

$^1\text{H}$ - $^1\text{H}$  Correlation Spectroscopy (COSY) spectrum was acquired with standard Bruker pulse program cosygpqf, with spectral width (SW) of 11 ppm in F1 and F2 dimension, acquisition time (AQ) 0.18 s, relaxation delay (D1) 1.5 s, number of scans (NS) 12, and matrix size  $512 \times 2048$  (F1 X F2).

Heteronuclear Single Quantum Correlation (HSQC) spectrum was acquired with standard Bruker pulse program hsqcetgp, with spectral width (SW) of 180 ppm in F1 and 10 ppm in F2, acquisition time (AQ) 0.10 s, relaxation delay (D1) 2.5 s, number of scans (NS) 64 and matrix size  $256 \times 1024$  (F1 X F2).

### **3.2.6 Mass Spectrometry**

Samples from NMR tubes were transferred to Eppendorf tubes and were evaporated to dryness under nitrogen. About 1 mg fraction was dissolved in methanol and used for experiment. ESI/MS analyses were performed on Agilent 1200 LC-6520B Q-TOF high resolution Mass Spectrometer with Dual ESI as ion source in both positive and negative ionization mode. About 10  $\mu\text{l}$  sample was injected with Agilent 1200 G1376B HiP autosampler. Full scan spectra were obtained by scanning masses between 100-1000 m/z. Other parameters were set as follows: sheath gas temperature, 300  $^{\circ}\text{C}$ ; sheath gas flow, 5

l/min; nebulizer, 30 psi; and capillary entrance voltage, 3500 V. Fragmentor and skimmer1 were operated at 150 V and 65 V, respectively. The MS scan data were collected at a rate of 1 spectra/s in range of 100-1000 m/z. In the targeted MS/MS mode, the MS and the MS/MS information were collected in the 50-1000 m/z range at the same rate as the MS scan and the collision energy was 25-35 V. All the MS and MS/MS data were collected with MassHunter Data Acquisition (Agilent) and MassHunter Qualitative Analysis B.02.00 (Agilent) was applied to identify lipid species.

### **3.3 Results and Discussion**

#### **3.3.1 ATR-FTIR Spectroscopy**

Fig3.2 shows FTIR spectrum obtained for fraction I-IV. ATR-FTIR experiments were conducted to decide whether lipid contains ester linkage or ether linkage. The bands were assigned to specific molecular groups on the basis of biochemical standards and published studies, as described previously (14, 15). Spectra contained peak at about 1737  $\text{cm}^{-1}$  for  $-\text{C}=\text{O}$  vibration suggesting presence of ester type linkage in lipid. Methylene antisymmetric and symmetric C-H stretching bands at about 2920 and 2850  $\text{cm}^{-1}$ , respectively, as well as the asymmetric and symmetric terminal methyl C-H stretching bands at about 2956 and 2872  $\text{cm}^{-1}$  and a peak at 1460  $\text{cm}^{-1}$  from  $-\text{CH}_2$  scissoring vibration is observed, which confirms presence of long chain fatty acid like molecule and mainly, peaks at 1363 and 1371  $\text{cm}^{-1}$  from  $-\text{CH}_3$  deformation bands (so called split umbrella peaks), indicate the presence of isopropyl group. There were no sharp peaks around 1640  $\text{cm}^{-1}$  related to  $-\text{C}=\text{C}$  stretching vibration as well as absence of  $=\text{C}-\text{H}$  stretching band around 3083  $\text{cm}^{-1}$  suggesting absence or very small amount of

unsaturated fatty acids in lipid. In fractions II, III and IV, we also observed peaks around  $1236\text{ cm}^{-1}$  due to the asymmetric stretching and around  $1080\text{ cm}^{-1}$  for symmetric stretching vibration for  $\text{PO}_2^-$  group. Peaks related to  $\text{PO}_2^-$  were not observed for fraction V and Fraction VI.

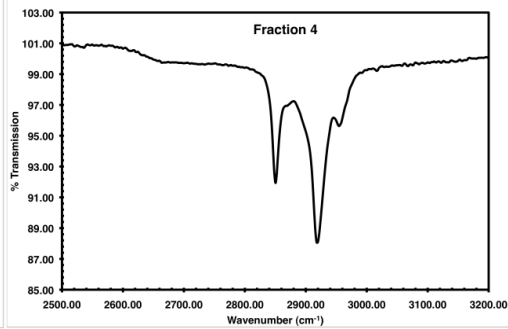
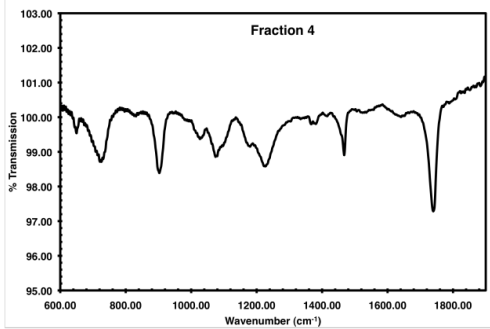
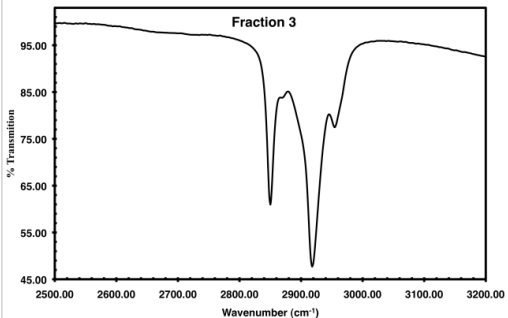
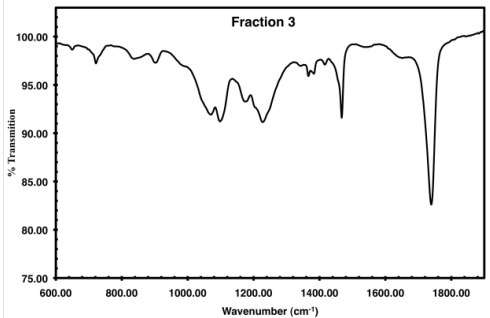
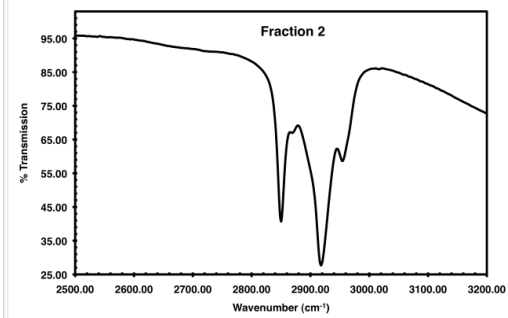
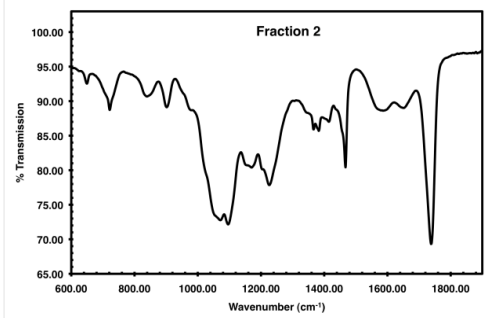
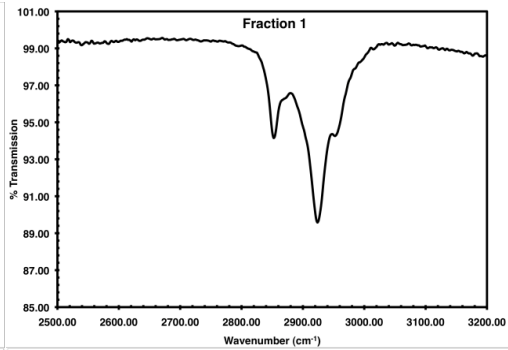
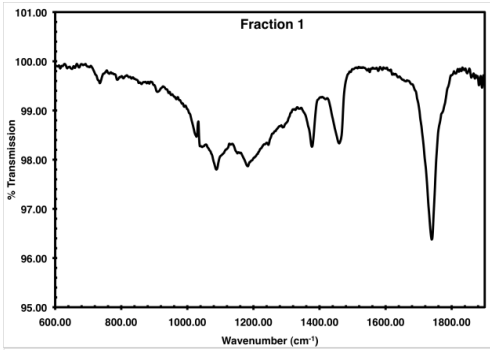


### Figure 3.2. ATR-FTIR spectra of fraction I-IV

Region between 600-1900  $\text{cm}^{-1}$  shows ester carbonyl peak at 1737  $\text{cm}^{-1}$  and  $-\text{CH}_3$  deformation bands at 1363 and 1371  $\text{cm}^{-1}$  (split umbrella peaks) for isopropyl group and 2500-3200  $\text{cm}^{-1}$  region showing  $-\text{CH}$  stretching bands. Single beam spectra were recorded as an average of 50 scans with a resolution of 2  $\text{cm}^{-1}$

### 3.3.2 NMR spectroscopy

The 1D proton NMR for fraction IV is shown in figure 3.3b. Proton resonances between 0.68 ppm and 6.0 ppm could be divided into three groups: a) fatty acid chain proton resonances between 0.69 to 2.9 ppm, b) phospholipid headgroup proton resonances 3.00 to 5.50 ppm, and c) glycerol backbone proton resonances between 3.00 to 5.5 ppm (16, 17, 18, 19). The NMR peak assignment is also based on the data from  $^{13}\text{C}$  NMR,  $^{31}\text{P}$  NMR, J-MOD and 2D NMR techniques (e.g., HSQC and COSY). We have described here complete NMR data analysis for fraction IV. Due to insufficient amounts of materials and lower sensitivity of NMR, we were unable to determine the lipid structures of other fractions by NMR.

#### 3.3.2.1 Phospholipid head group

Ethanolamine lipids were identified by their characteristic head group  $-\text{CH}_2\text{CH}_2\text{NH}_2$  methylene proton resonance at 3.12 ppm. Examination of COSY cross peaks (Figure 3.4) showed correlation cross peak (3.19 ppm, 4.07 ppm), which helped in identifying  $-\text{OCH}_2$  head group methylene protons at 4.07 ppm. Further analysis by HSQC (Figure 3.6) and J-MOD (Figure 3.5b) showed correlation of  $-\text{CH}_2\text{NH}_2$  methylene proton with methylene carbon at 40.18 ppm and  $-\text{OCH}_2$  methylene proton with methylene carbon at 63.04 ppm confirming the  $^1\text{H}$  NMR assignment. Also,  $^{13}\text{C}$  NMR spectrum (Figure 3.5a) showed  $^2J_{CP}$  value of 5.03 Hz for carbon at 63.04 ppm and  $^3J_{CP}$  value of 6.29 Hz for methylene

carbon at 40.18 ppm indicating attachment of phosphate group with ethanolamine head group (20).

### 3.3.2.2 Glycerol Backbone

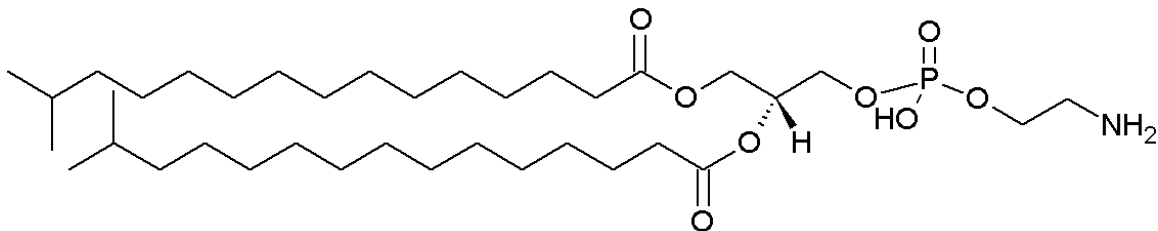
Features related to glycerol backbone are shown in table 1. The *sn1* methylene protons of PE lipids were chemical shift nonequivalent and appear at 4.47 and 4.22 ppm. Each peak appears as a doublet of doublets (Figure 3.3b), due to coupling with each other and with the *sn2* proton. Glycerol *sn2* proton at 5.25 ppm appears as complex multiplet due to coupling with both *sn1* and *sn3* nonequivalent protons and due to other lipids present in mixtures as observed in mass spectrum of fraction IV (Figure 3.7). Glycerol *sn3* protons appeared as a broad peak at 4.02 ppm with very small chemical shift differences due to nonequivalent chiral centre next to them. All three glycerol backbone protons showed clear cross peaks in COSY spectrum (Figure 3.4).  $^{13}\text{C}$  NMR shifts for *sn1*, *sn2* and *sn3* were at 63.78 ppm, 71.99 ppm, and 65.02 ppm respectively and *sn3* glycerol carbon and *sn2* also showed  $^{31}\text{P}$ - $^{13}\text{C}$  coupling constant 5.03 Hz ( $^2J_{CP}$ ) and 7.54 Hz ( $^3J_{CP}$ ) respectively with the absence of coupling to *sn1* carbon, suggesting phosphate group is attached with *sn3* glycerol carbon (21).

### 3.3.2.3 Acyl Chains

Ester linkages between glycerol carbon and acyl chains were identified from carbonyl carbon  $^{13}\text{C}$  NMR shift at 174.79 and 175.10 ppm (Table 3.1). Some noticeable peaks were methylene group  $\alpha$  to carbonyl groups showed a  $\delta^1\text{H}$  peak at 2.36 ppm, methylene protons  $\beta$  to carbonyl group at 1.62 ppm and bulk methylene protons at 1.31 ppm. Main feature of the acyl chain was terminal methyl group at 0.90 ppm that appeared as doublet

and methine group multiplet at 1.54 ppm, indicating presence of isopropyl group at the end of the acyl chain (22), in agreement with FTIR data. All these assignments were further confirmed with help of 2D NMR methods. Relevant data is summarized in Table 1. There were no peaks at 5.35-5.45 ppm for alkene protons, indicating presence of only saturated fatty acid chains in lipid fraction IV.

a)



b)

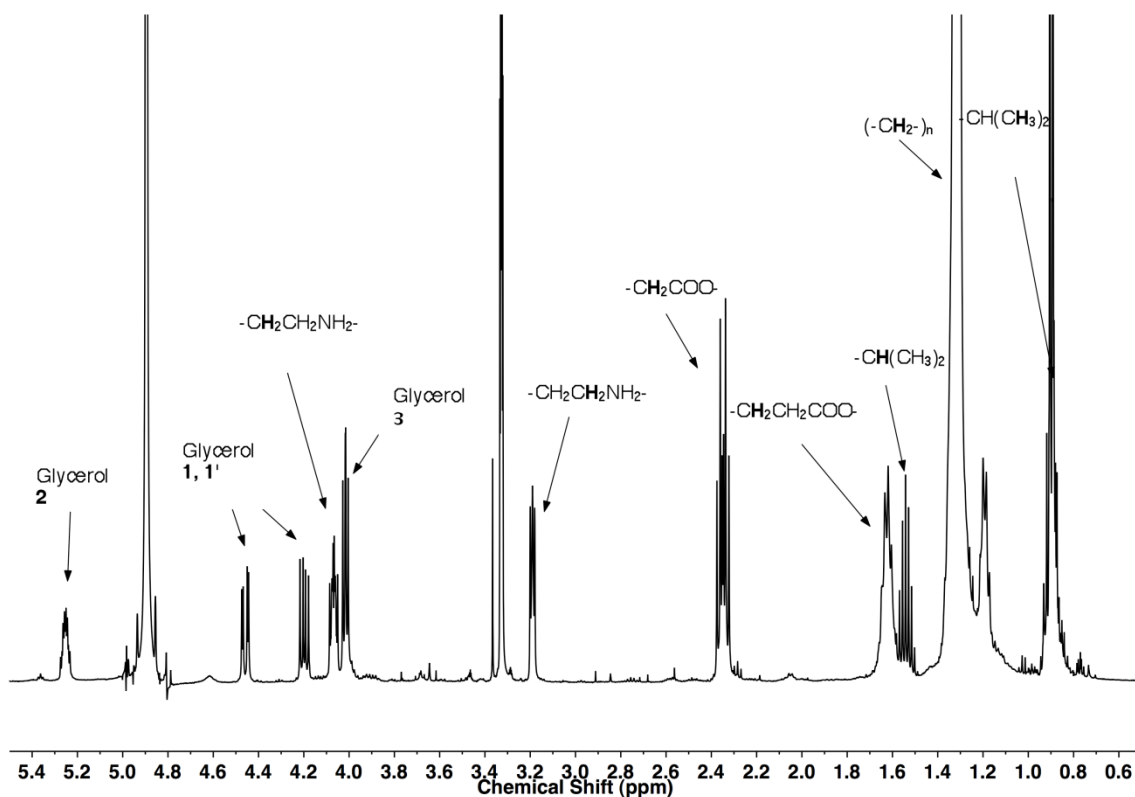
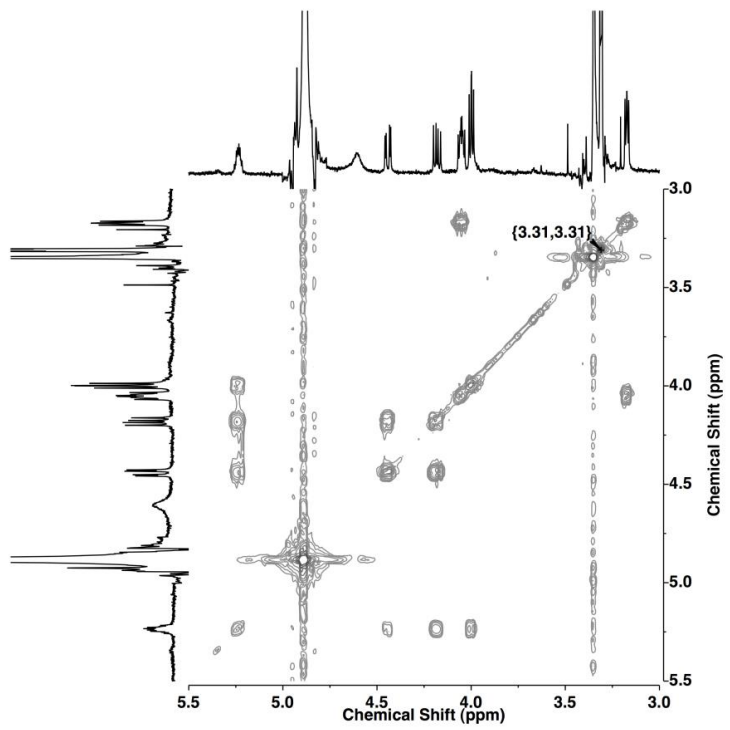


**Figure 3.3 a) Structure of phosphatidyl ethanolamine lipid b) Proton NMR spectrum of fraction IV lipids.**

The spectrum was obtained on 6-8 mg/ml of lipid extract in  $\text{CD}_3\text{OD-CDCl}_3$  2:1 at a temperature of 298 K; 256 scans were obtained for Fourier transformation and the residual methanol peak at 3.31 ppm was used as the reference chemical shift.

a)



b)

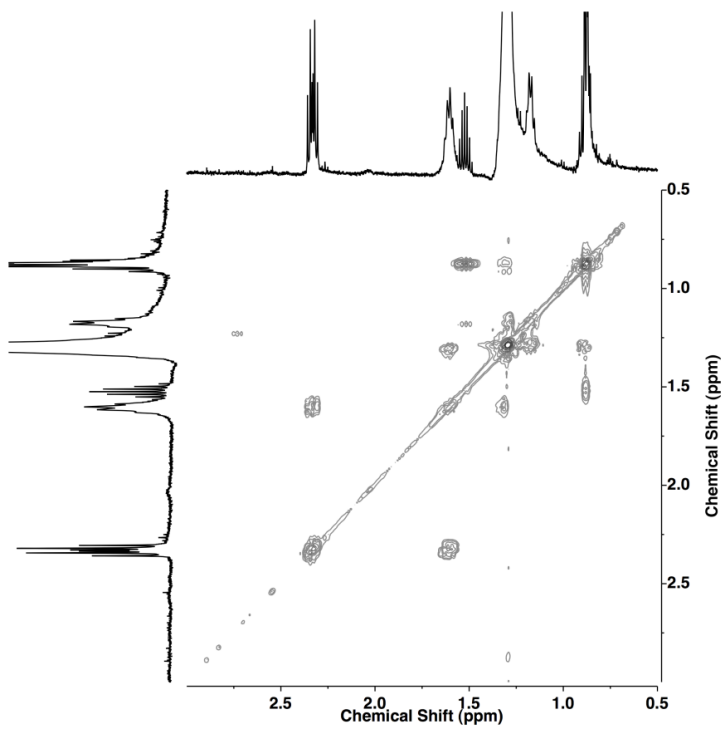
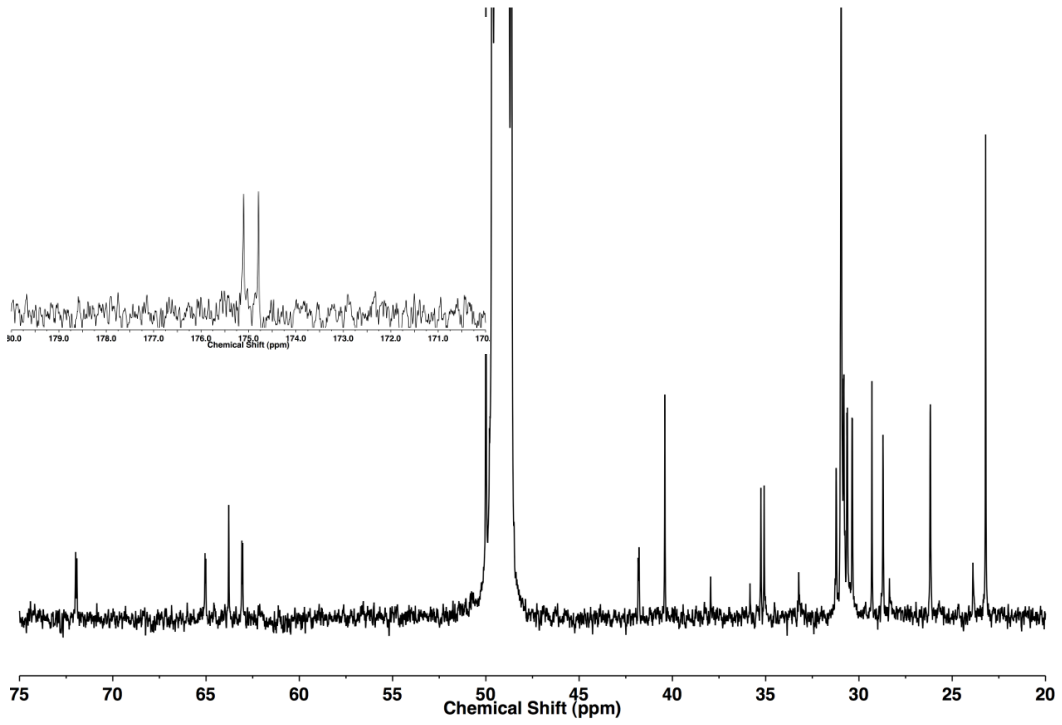


**Figure 3.4 2-D COSY spectrum of fraction IV lipids.**

a) 2-D COSY cross peaks for glycerol backbone and headgroup protons indicated presence of ethanolamine headgroup containing lipid and b) 2-D COSY cross peaks for FA chain links, confirmed  $^1\text{H}$  NMR assignment and showed cross peak between -CH multiplet at 1.54 ppm with  $-\text{CH}_3$  protons doublet at 0.90 ppm. Residual methanol peak at 3.31 ppm was used as reference chemical shift

a)



b)

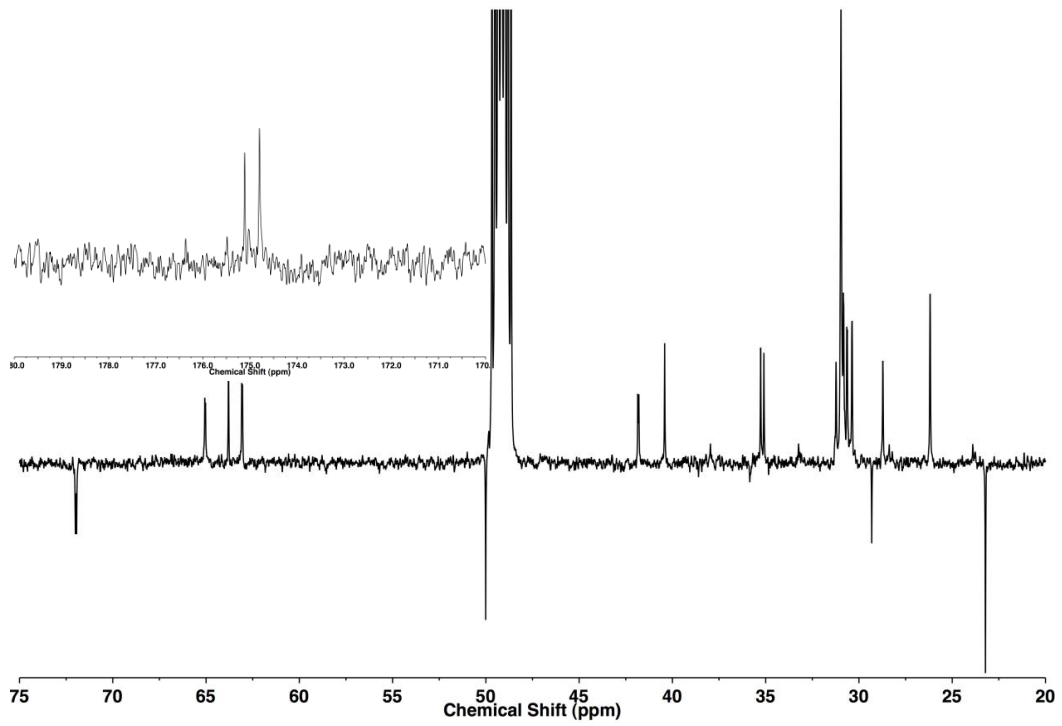
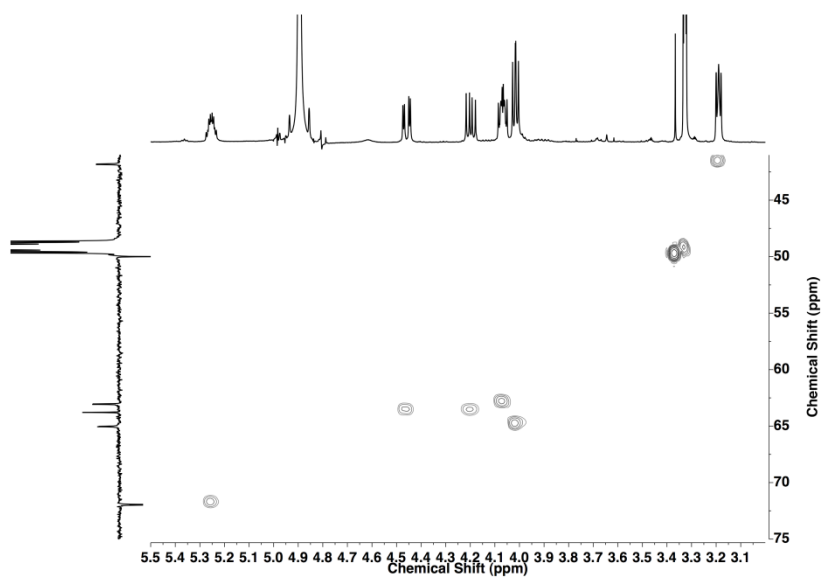


**Figure 3.5 a) Proton decoupled  $^{13}\text{C}$  NMR spectrum of fraction IV. b) J-Modulated spin echo  $^{13}\text{C}$  NMR spectrum**

$^{13}\text{C}$  NMR spectrum showing glycerol *sn1*, *sn2*, *sn3* carbon peaks at 63.79, 71.99, and 65.02 ppm respectively, headgroup carbon at 63.04 and 40.18 ppm respectively and FA chain carbons in 20-40 ppm region. Inset shows ester carbonyl carbon peaks at 173.5 and 173.18 ppm. b) J-Modulated spin echo  $^{13}\text{C}$  NMR spectrum confirms the multiplicity of assigned carbons, showing  $-\text{CH}_2$  and  $-\text{C}$  carbons upwards and  $-\text{CH}$  and  $-\text{CH}_3$  carbon downwards.  $^{13}\text{C}$  NMR and J-MOD spectra were referenced at residual solvent peak (49.15 ppm).

a)



b)

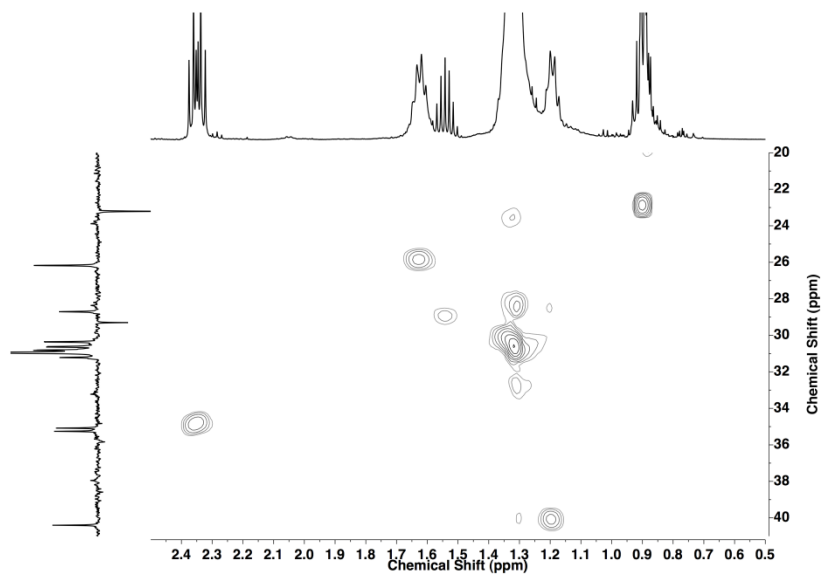


**Figure 3.6**  $^1\text{H}$ - $^{13}\text{C}$  heteronuclear single quantum coherence (HSQC) lipid profile of *GWE1* strain fraction IV.

a)  $^1\text{H}$ - $^{13}\text{C}$  correlation for glycerol backbone and head group b)  $^1\text{H}$ - $^{13}\text{C}$  correlation for FA chain.

Group	Position	$\delta^{13}\text{C}$	J-MOD		$\delta^1\text{H}$	$^1\text{H}$ - $^1\text{H}$ COSY
Glycerol Backbone	<i>sn1</i>	63.78	-CH <sub>2</sub>	1, 1'	4.47, 4.22	<i>1-1', sn2</i>
	<i>sn2</i>	71.99	-CH		5.25	<i>sn1, sn3</i>
	<i>sn3</i>	65.06	-CH <sub>2</sub>		4.02	<i>sn2</i>
Head group	-CH <sub>2</sub> CH <sub>2</sub> NH <sub>2</sub> (a)	63.08	-CH <sub>2</sub>		4.07	(b)
	-CH <sub>2</sub> CH <sub>2</sub> NH <sub>2</sub> (b)	41.79	-CH <sub>2</sub>		3.19	(a)
Fatty acid chain	-C=O (1)	174.79, 175.10	-C			
	-CH <sub>2</sub> COO (2)	35.26	-CH <sub>2</sub>		2.36	
	-CH <sub>2</sub> CH <sub>2</sub> COO- (3)	26.17	-CH <sub>2</sub>		1.62	(2)
	(-CH <sub>2</sub> ) <sub>n</sub> (4)	30.95	-CH <sub>2</sub>		1.31	(3)
	-CH(CH <sub>3</sub> ) <sub>2</sub> (5)	29.29	-CH		1.54	(4)
	-CH(CH <sub>3</sub> ) <sub>2</sub> (6)	23.21	-CH <sub>3</sub>		0.90	(5)

**Table 3.1:  $^1\text{H}$  and  $^{13}\text{C}$  NMR spectral data and 2D NMR correlations for fraction IV.**

### 3.3.3 Mass Spectrometry

We performed ESI-MS and ESI MS-MS to further identify lipids present in fractions I-IV. Positive and negative ion mode ESI-MS spectra (Figure 3.7) and fragmentation pattern analysis of fraction IV (Figure 3.8), indicated presence of PE as a major fraction of polar lipids, with major  $[M+H]^+$  and  $[M-H]^-$  ions at  $m/z$  692.5 and 690.5 respectively. Fraction IV also contained other  $[M+H]^+$  ions for PE lipids like  $m/z$  664.5, 678.5, 706.5, 720.5 and other sodiated adduct  $[M+Na]^+$  ions at  $m/z$  700.5 and 714.5. Negative ESI spectrum also revealed  $[M-H]^-$  ions for lipids at  $m/z$  662.5, 676.5, 704.5 (PE) and 647.5 (PA). Lipid molecules found from fraction I-IV are listed in Table 3.

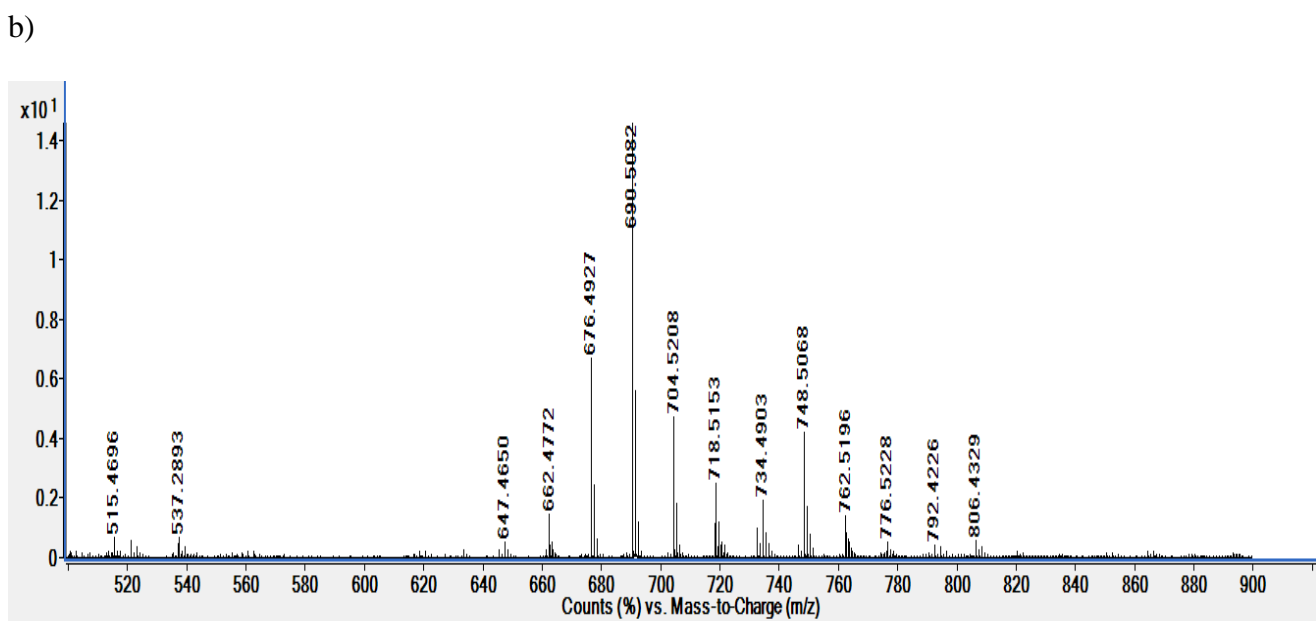
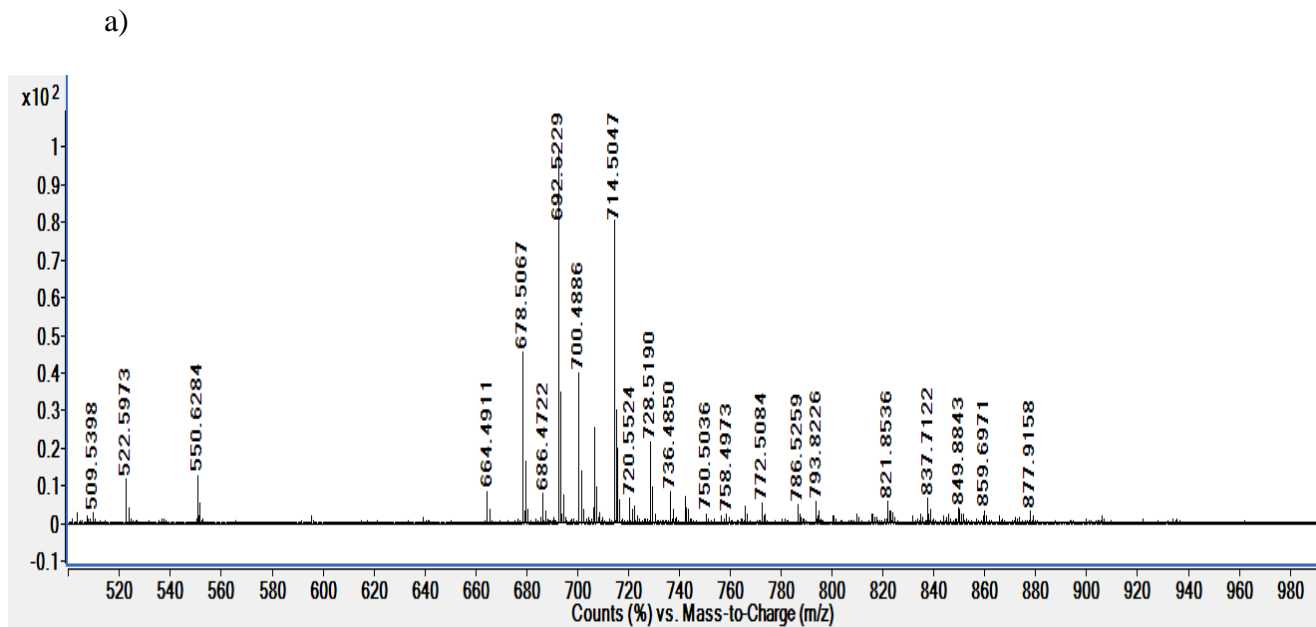
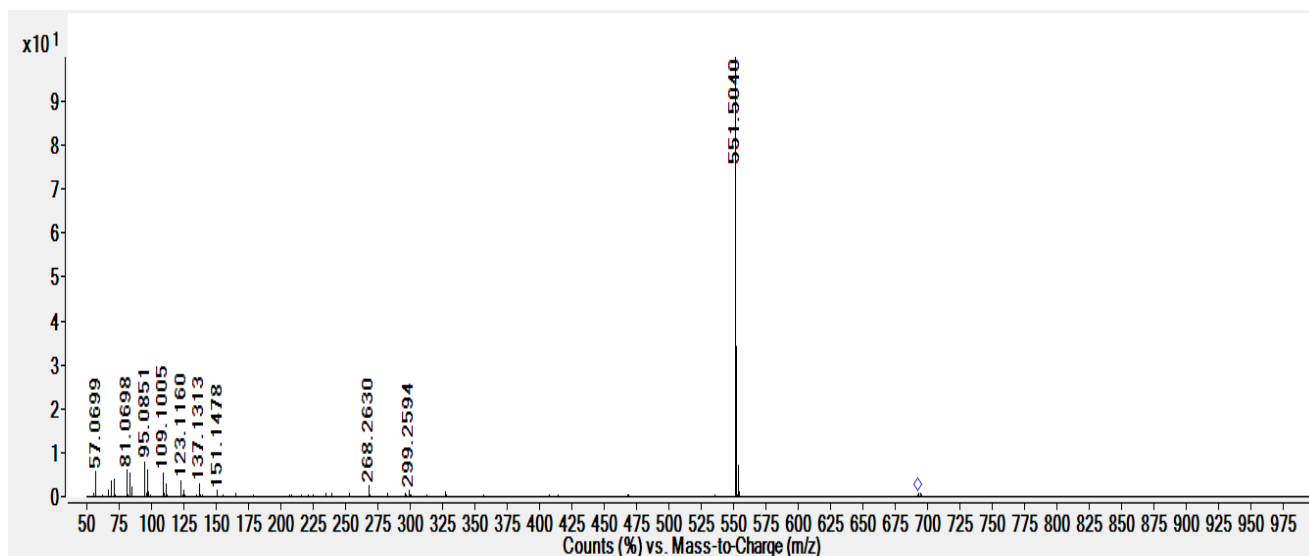


**Figure 3.7 a) Positive ion ESI-MS spectrum for fraction IV b) Negative ion ESI-MS spectrum for fraction IV**

a)



b)

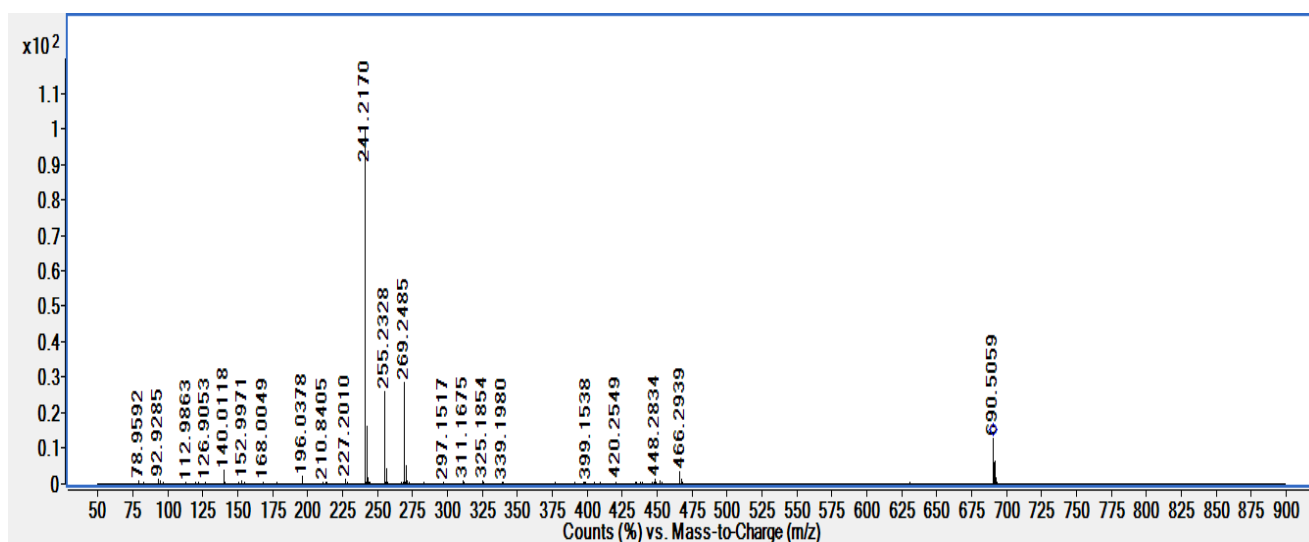


**Figure 3.8 Positive (a) and negative (b) ESI-MS-MS spectra for m/z 692.5**

a) Positive ion ESI-MS/MS spectrum for m/z 692.5, showing neutral loss of 141 for ethanolamine head group in PE lipid b) Negative ion ESI MS/MS spectrum for m/z 690.5, showing presence of isobaric PE lipid with C16:0/C16:0 and C15:0/C17:0.

	[M+H] <sup>+</sup>	[M-H] <sup>-</sup>	[M+Na] <sup>+</sup>	Lipid	Proposed structure <i>sn1/sn2</i>
Fraction IV	664.5	662.5		PE	C15:0/C15:0 C14:0/C16:0
	678.5	676.5	700.5	PE	C15:0/C16:0
	692.5	690.5	714.5	PE	C16:0/C16:0 C15:0/C17:0
	706.5	704.5	-	PE	C16:0/C17:0
	720.5	718.5	-	PE	C17:0/C17:0
	678.5			PC	C14:0/C14:0
		647.5	-	PA	C16:0/C16:0
Fraction III	-	693.5	-	PG	C15:0/C15:0 C14:0/C16:0
	-	707.5	-	PG	C15:0/C16:0
	-	721.5	-	PG	C16:0/C16:0 C15:0/C17:0
	-	735.5	-	PG	C16:0/C17:0 C18:0/C15:0
	-	749.5	-	PG	C17:0/C17:0 C16:0/C18:0
	-	769.5	-	CL*	C15:0/C15:0
	-	783.5	-	CL*	C16:0/C16:0
	-	797.5	-	CL*	C17:0/C17:0
	-	1351.9		CL	-
	-	1323.9		CL	-

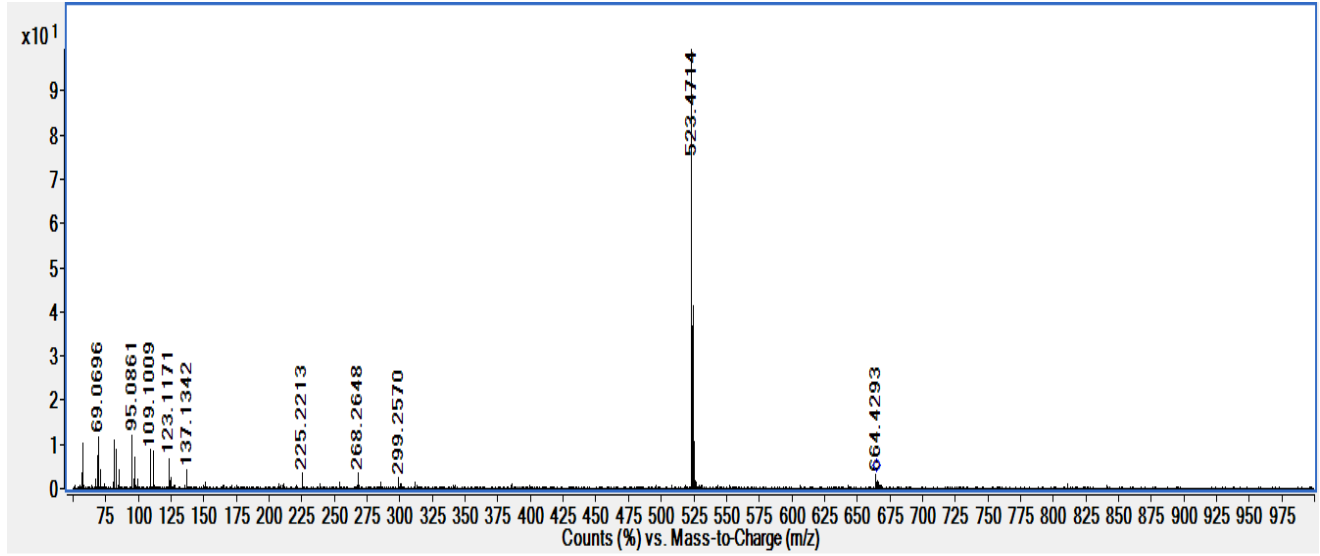
**Table 3 2 lipid analysis and lipid composition of major phospholipids from *GWE1* strain fraction I-IV.**

(\* indicates daughter ions of cardiolipins, which were detected in addition to the CL in ESI-MS spectrum. Neutral loss of 136 and comparison with theoretical m/z confirmed the structure. )

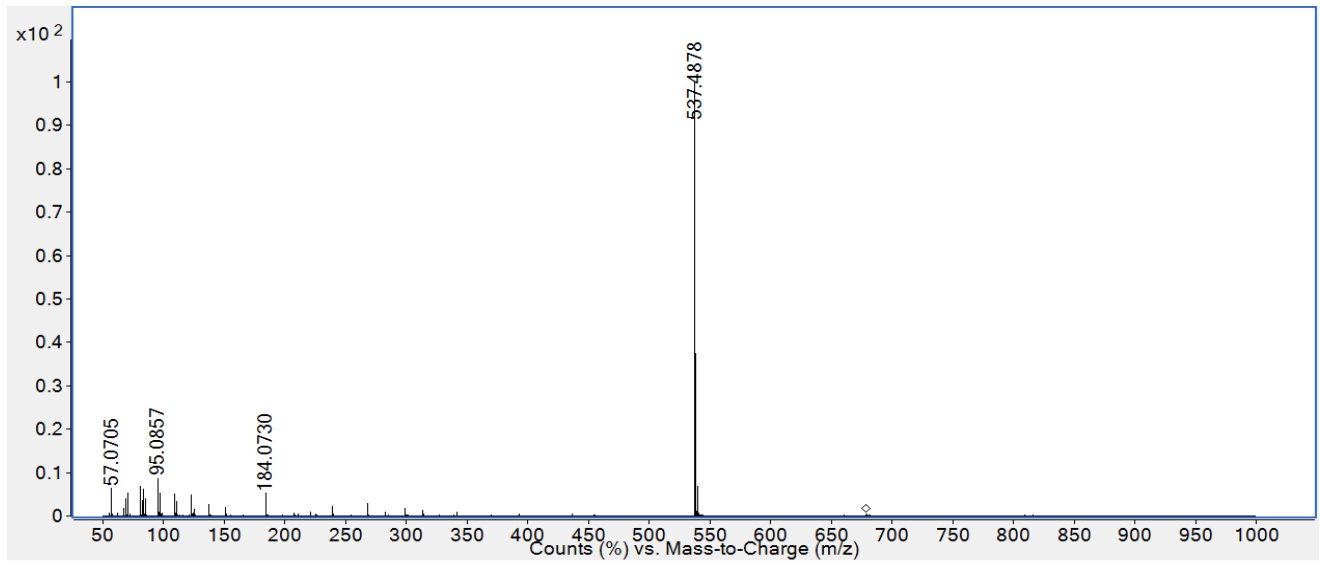
Positive ion MS/MS analysis provides valuable information about headgroup present in the lipid through a neutral loss of headgroup from  $[M+H]^+$  ion (23, 24). Positive ion ESI MS/MS analysis of individual ions (figure 3.9) indicated neutral headgroup  $[(HO)_2POOCH_2CH_2NH_2]$  loss of  $m/z$  141 confirming presence of PE lipids (23, 24). Fragmentation spectrum (figure 3.9d, 3.9e) of sodiated adducts also yielded characteristic sodium adduct daughter ions at  $m/z$  164 ( $[(HO)_2POOCH_2CH_2NH_2 Na]^+$ ) and  $[M+Na-141]^+$ .

Fraction IV also has shown presence of phosphatidylcholine lipid group in trace amount. We have detected daughter ion at 184 (phosphocholine group) (figure 3.9b), which is indication of phosphatidylcholine group lipid class (25). We have also seen presence of phosphatidic acid (PA) ( $m/z$  647.5) C14:0/C14:0-PA lipid in trace quantity in fraction IV. However due to low amount of ion 647.5 in this fraction, we were unable to obtain ms/ms spectrum for that ion. We have confirmed that observed mass matches well with exact mass of lipid, which confirms the identity of molecule (Table 3).

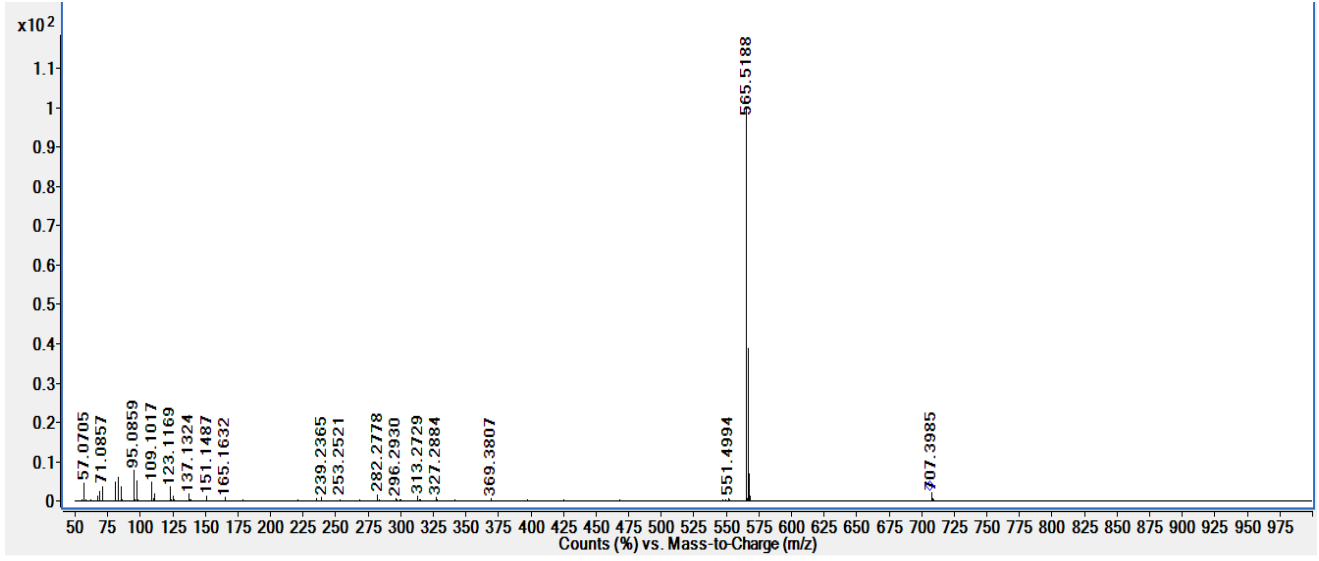
a)



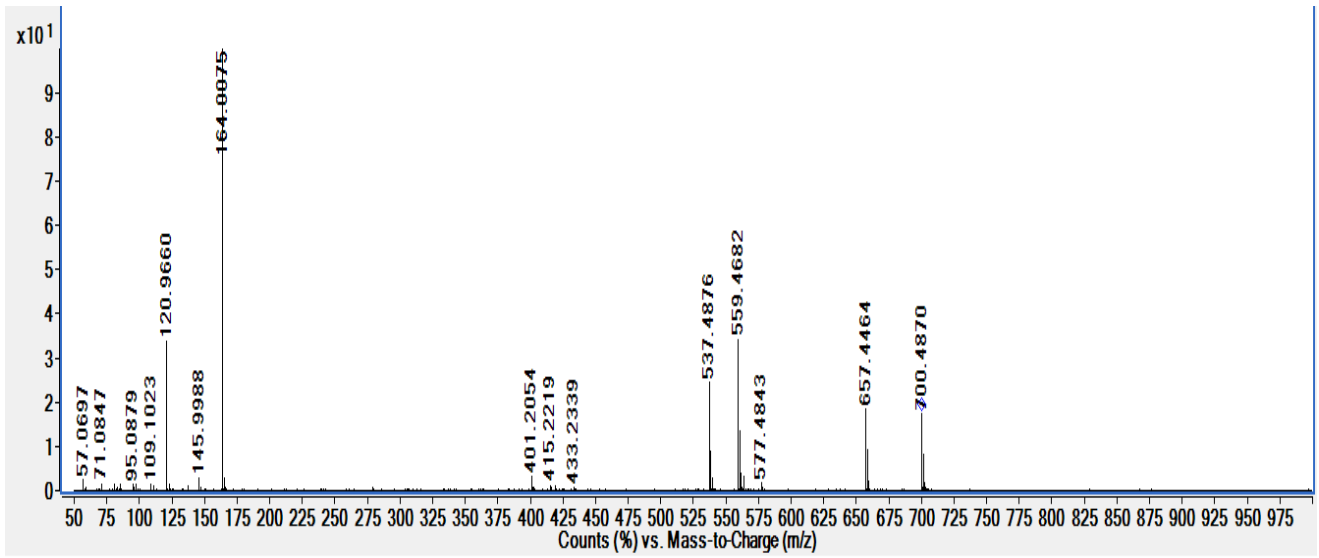
b)



c)



d)



e)

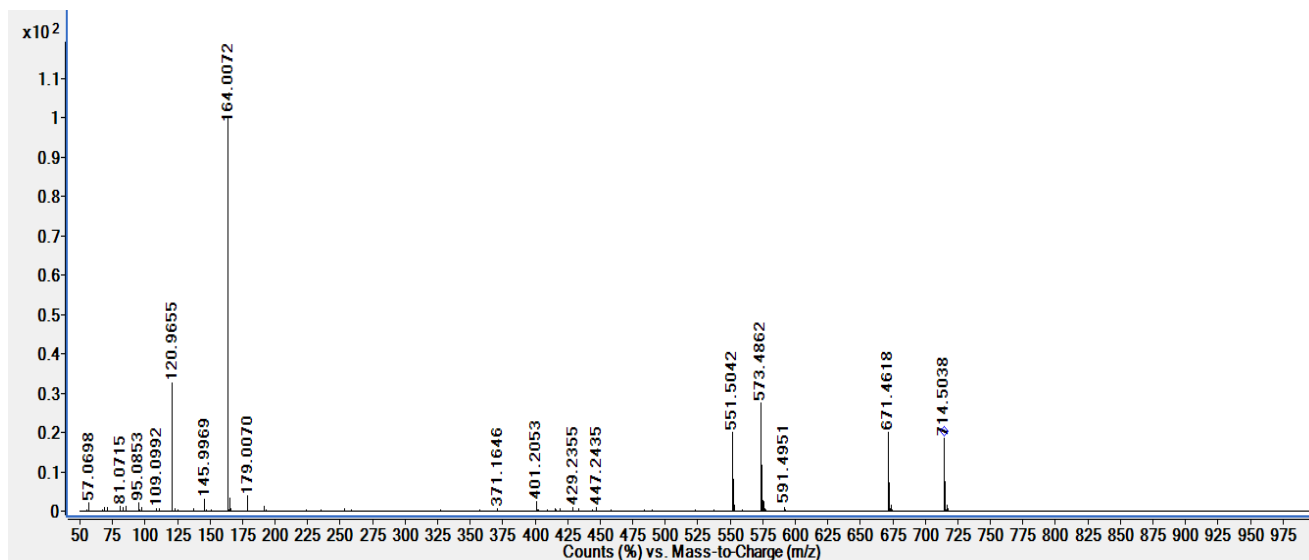


**Figure 3.9 ESI-MS-MS (+ve) Fragmentation spectra of lipids in fraction IV**  
a) m/z 664.5 b) m/z 678.5 c) m/z 706.5 d) m/z 700.5 e) m/z 714.5

Type	(M-H) <sup>-</sup>			(M+H) <sup>+</sup>		
	Observed m/z	Exact m/z	Error (ppm)	Observed m/z	Exact m/z	Error (ppm)
PE	662.4772	662.4766	0.90	664.4911	664.4912	0.15
	676.4927	676.4923	0.59	678.5067	678.5068	0.15
	690.5082	690.5079	0.43	692.5229	692.5225	0.58
	704.5208	704.5236	3.97	706.5390	706.5381	1.27
	-			720.5524	720.5538	1.94
PA	647.4650	647.4656	0.93			
PG	693.4712	693.4712	0			
	707.4872	707.4869	0.42			
	721.5028	721.5025	0.42			
	735.5184	735.5182	0.27			
	749.5334	749.5338	0.53			
CL & Daughter ions CL	769.4428	769.4426	0.26			
	783.4582	783.4584	0.26			
	797.4740	797.4739	0.12			
	1351.9625	1351.9650	1.84			
	1323.9322	1323.9337	1.13			

**Table 3.3: Comparison of observed mass with exact mass of the predicted molecule. All the lipids were predicted with sub ppm level accuracy**

PG and cardiolipins were also found in fraction III negative ESI-MS spectrum (Figure 3.10). Negative ESI-MS spectrum revealed presence of several PG lipids at  $m/z$  693.5, 707.5, 721.5, 735.5 and 749.5 (supplementary figure 3.10) and we observed in minor quantity daughter ions of cardiolipins at 769.5, 783.5, 797.5 and some cardiolipins at 1323.9, and 1351.9. Daughter ions of cardiolipins after loss of dehydrated phosphatidyl glycerol (136 amu) undergo same fragmentation pattern as PA lipids and made structure assignment possible (26). We were unable to obtain ms/ms spectra for cardiolipins due to excessive fragmentation in ESI-MS spectrum and limited amount of cardiolipin in fraction III and assignment of fatty acid chain position was not possible for intact cardiolipin molecules. Negative ion ESI MS/MS (figure 3.11) also provided valuable information regarding fatty acyl chain length and relative position of fatty acyl chains on *sn2* and *sn1* based on relative abundance of  $R_1COO^-$  compare to  $R_2COO^-$  (23-24), By comparing relative abundance of individual fatty acid daughter ions *sn2* and *sn1* position have been assigned in table 3.2. All the fractions showed absence of unsaturation in acyl chains and ATR-FTIR spectra and NMR spectra confirmed presence of iso-branched FA chains in all lipid fractions. Based on this information we proposed structure of intact lipids PE, PA, PG and cardiolipins with saturated iso-branched fatty acids in table 2. All the predicted lipid structures were also confirmed by comparing them with exact mass of predicted molecule with sub ppm level accuracy (table 3.3).

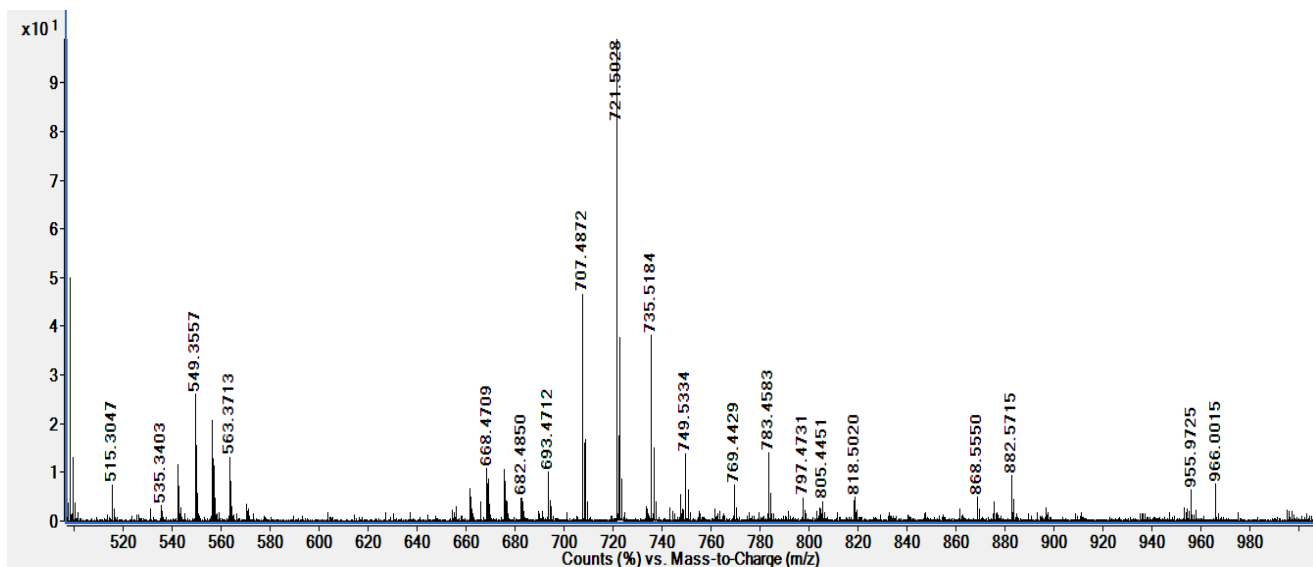
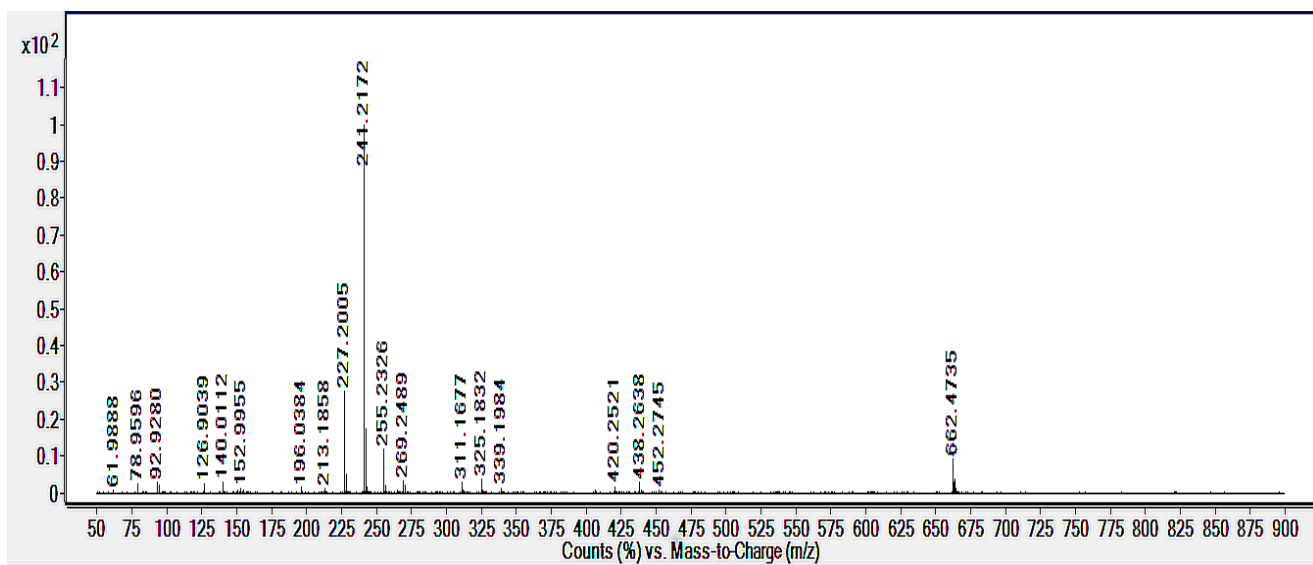
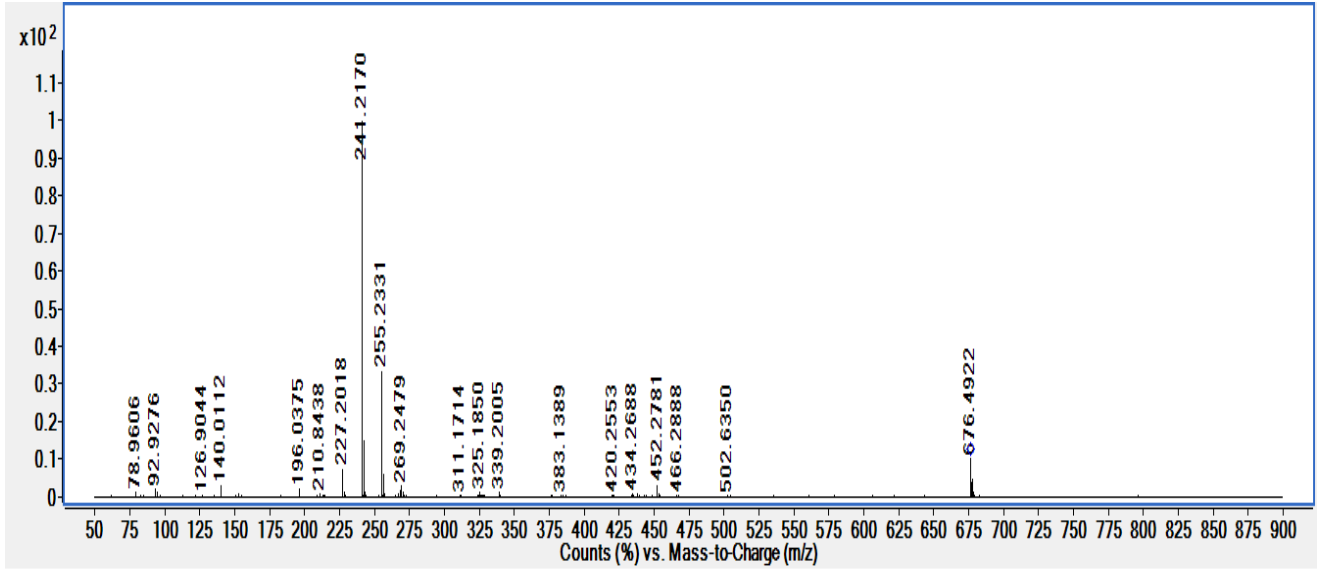


Figure 3.10 ESI-MS (-ve) spectrum for fraction III

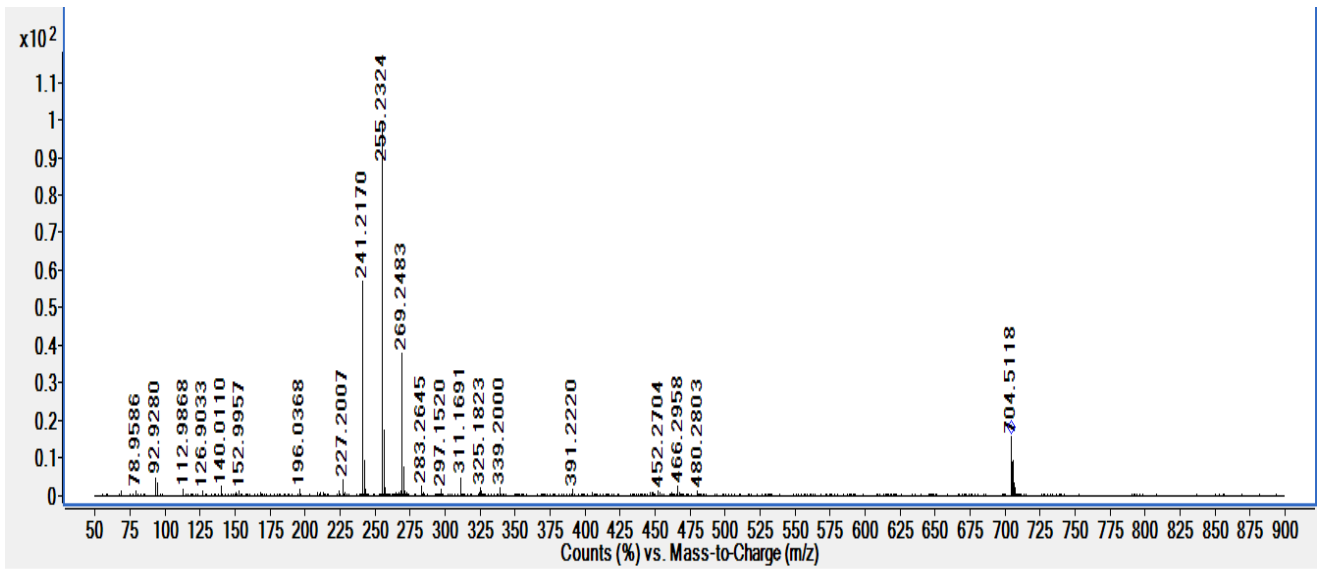
a)



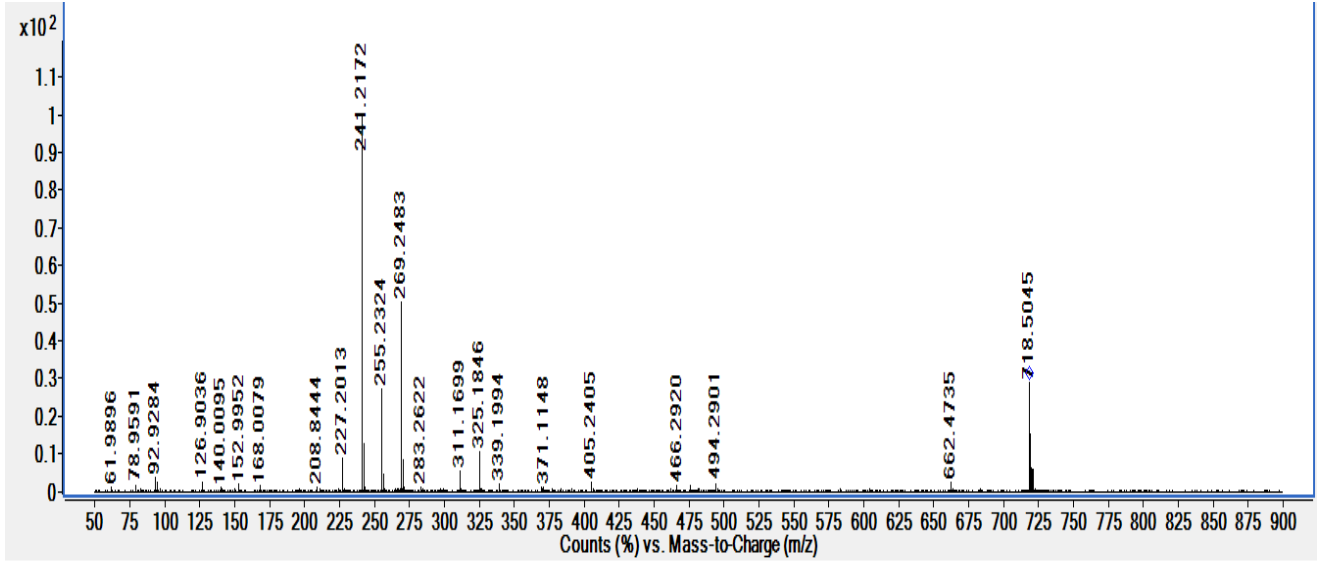
b)



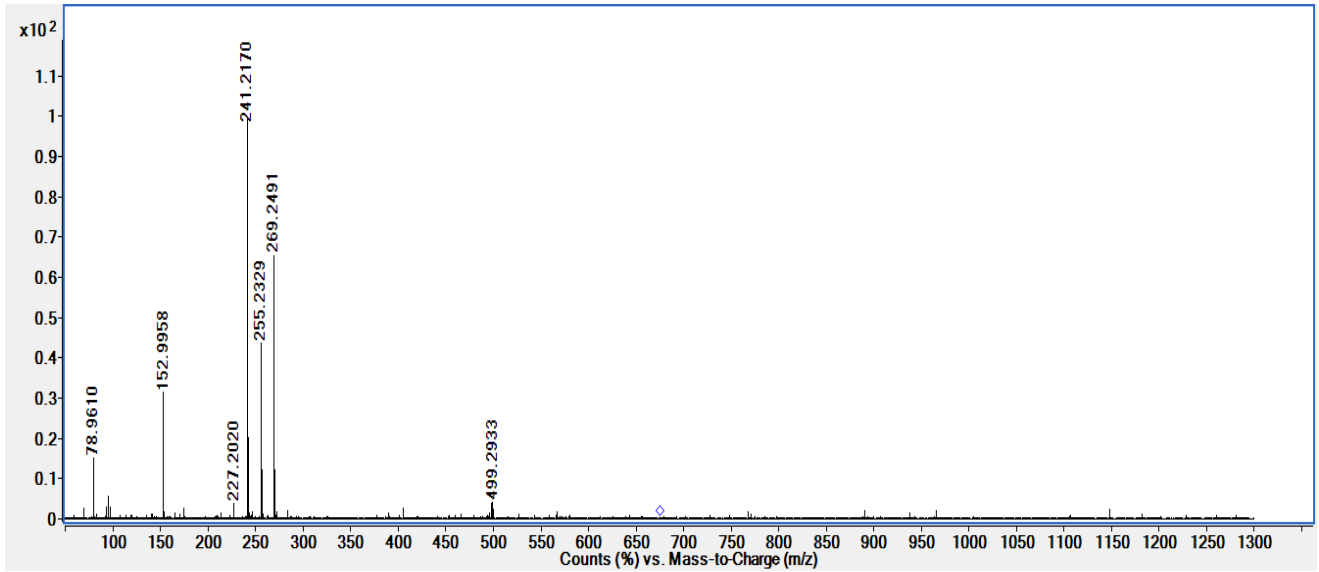
c)



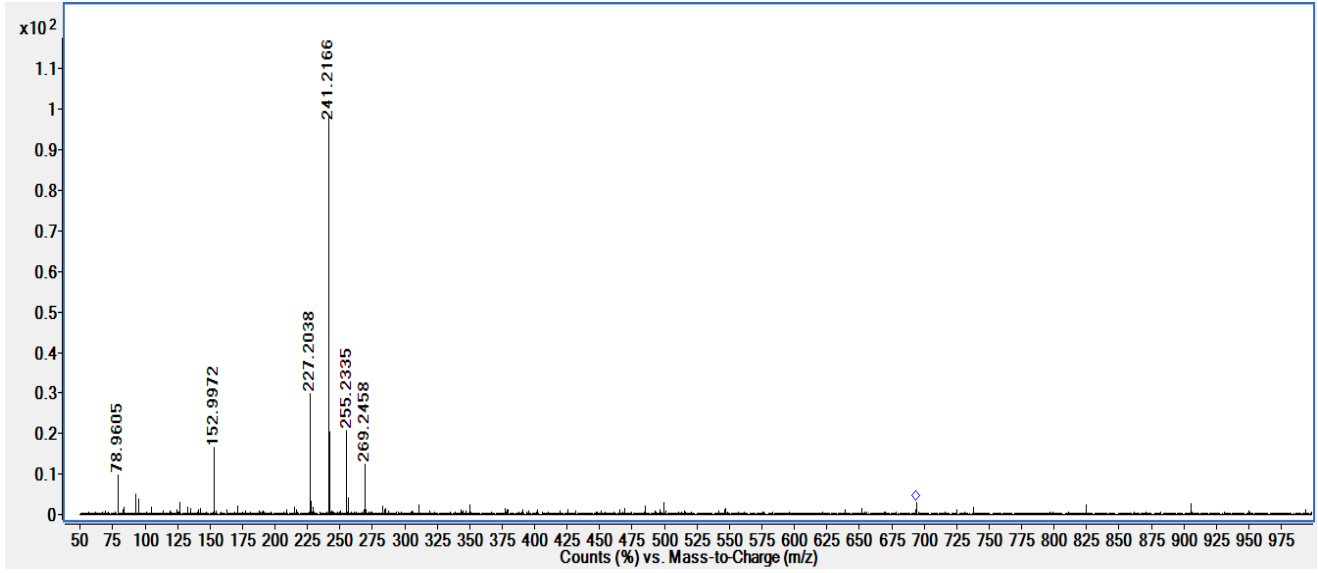
d)



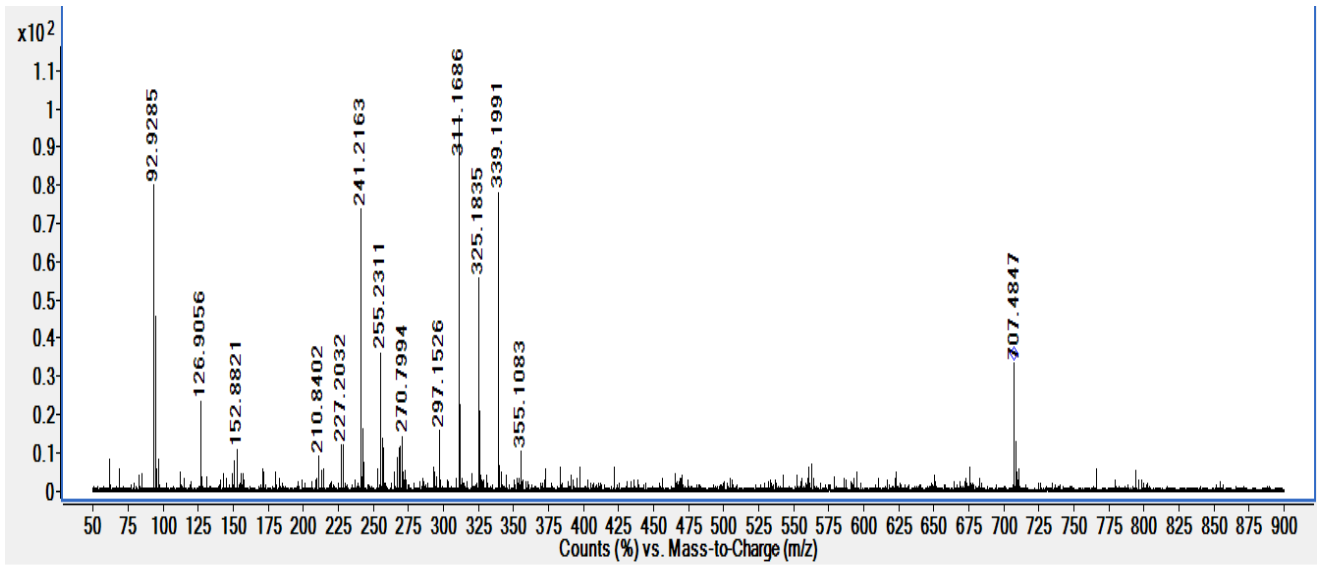
e)



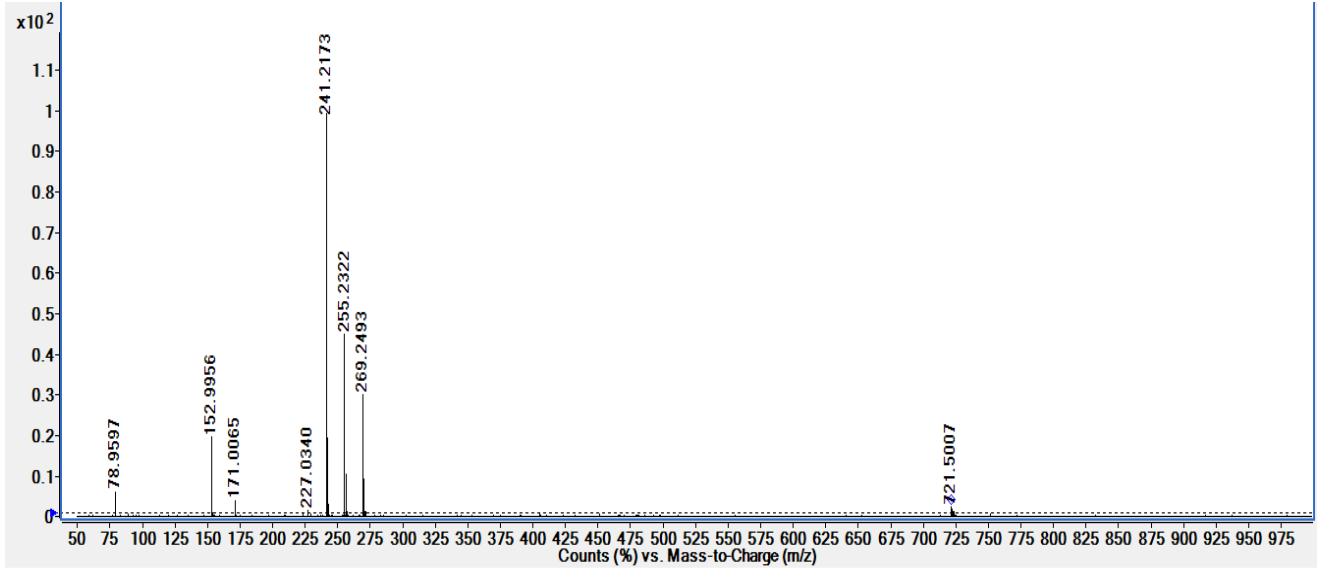
f)



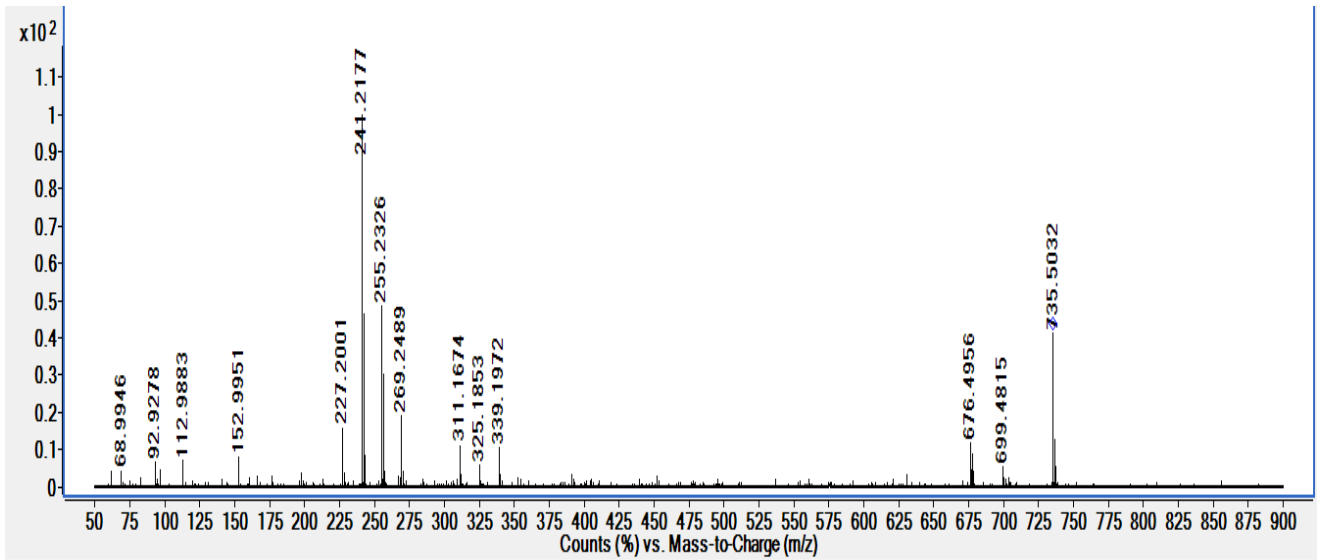
g)



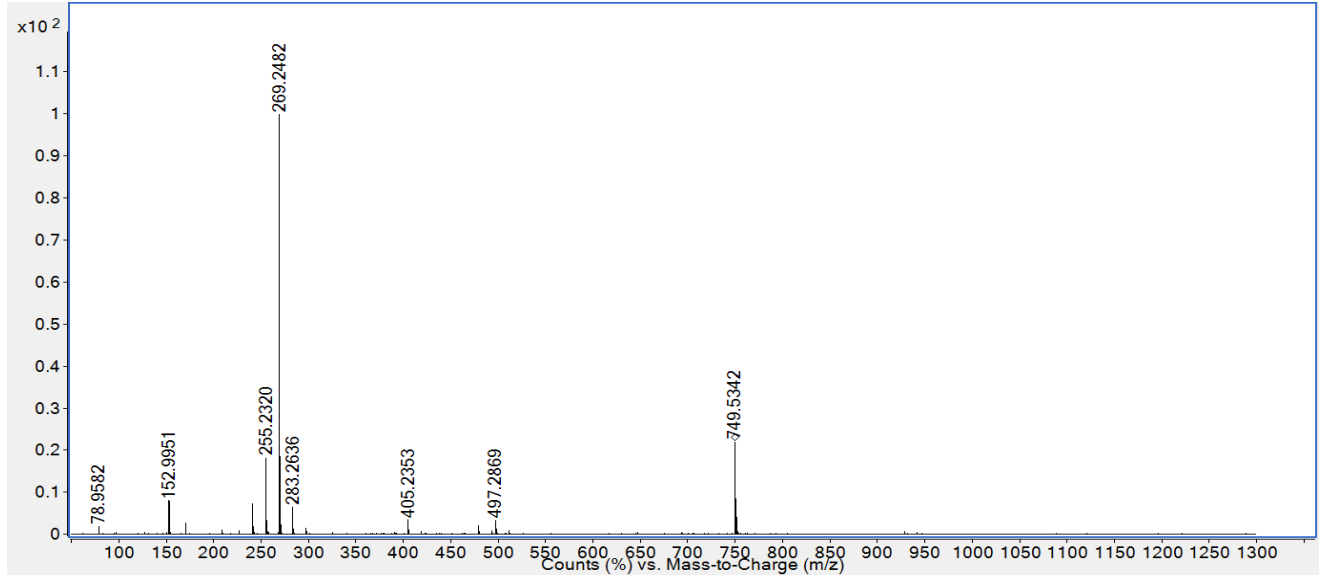
h)



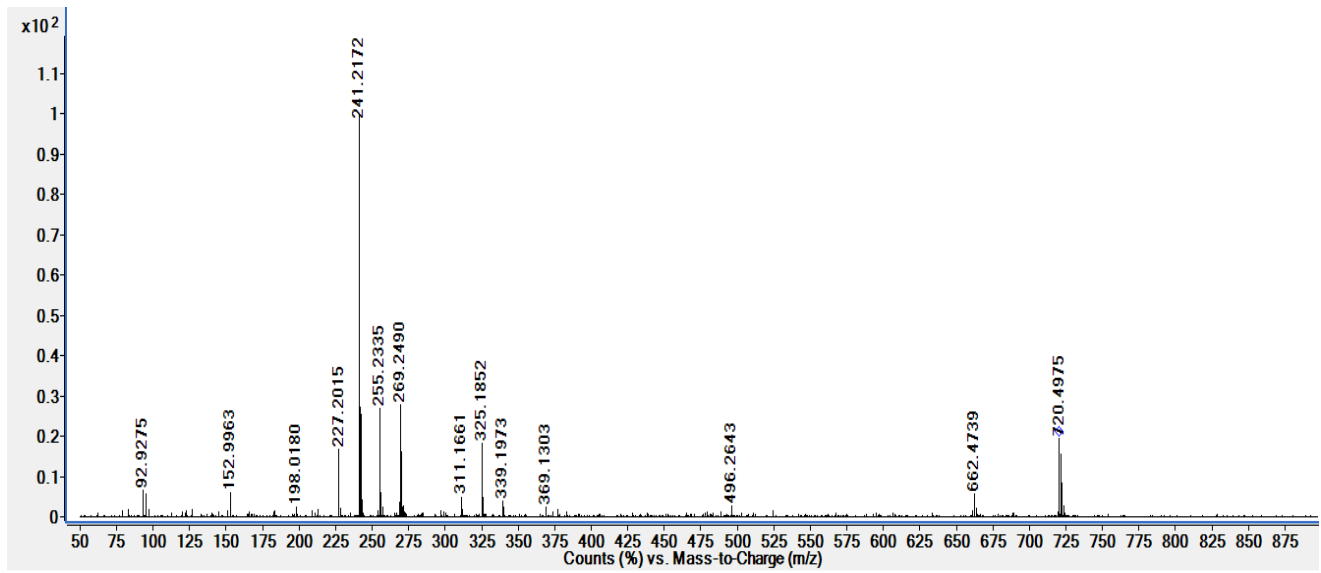
i)



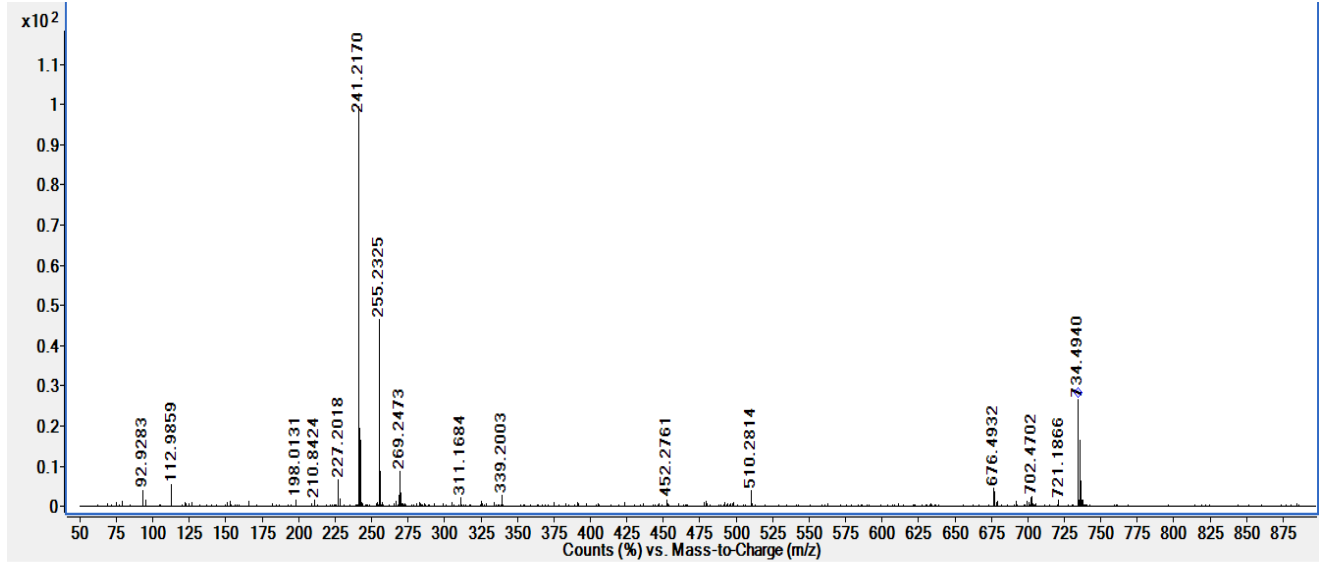
j)



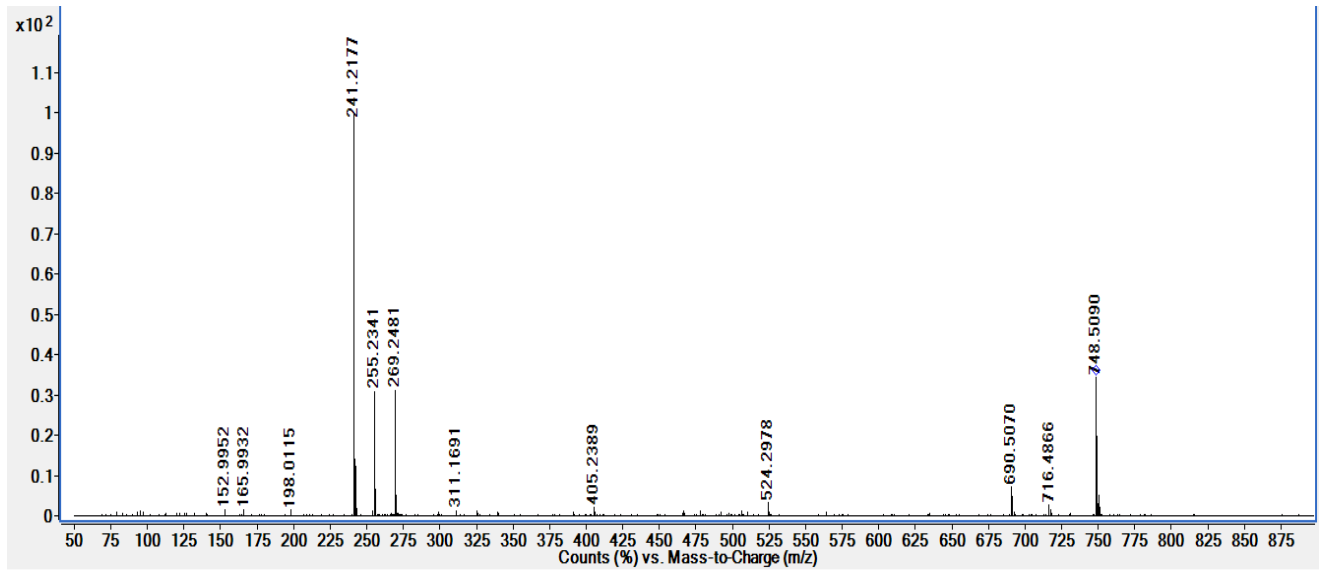
k)



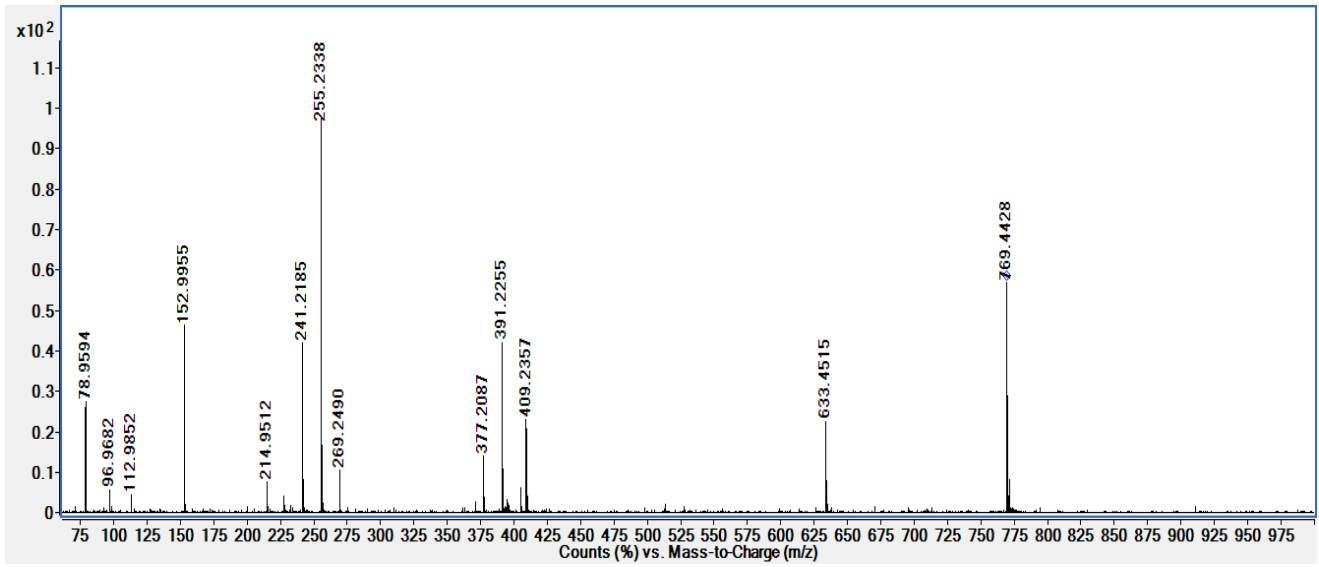
l)



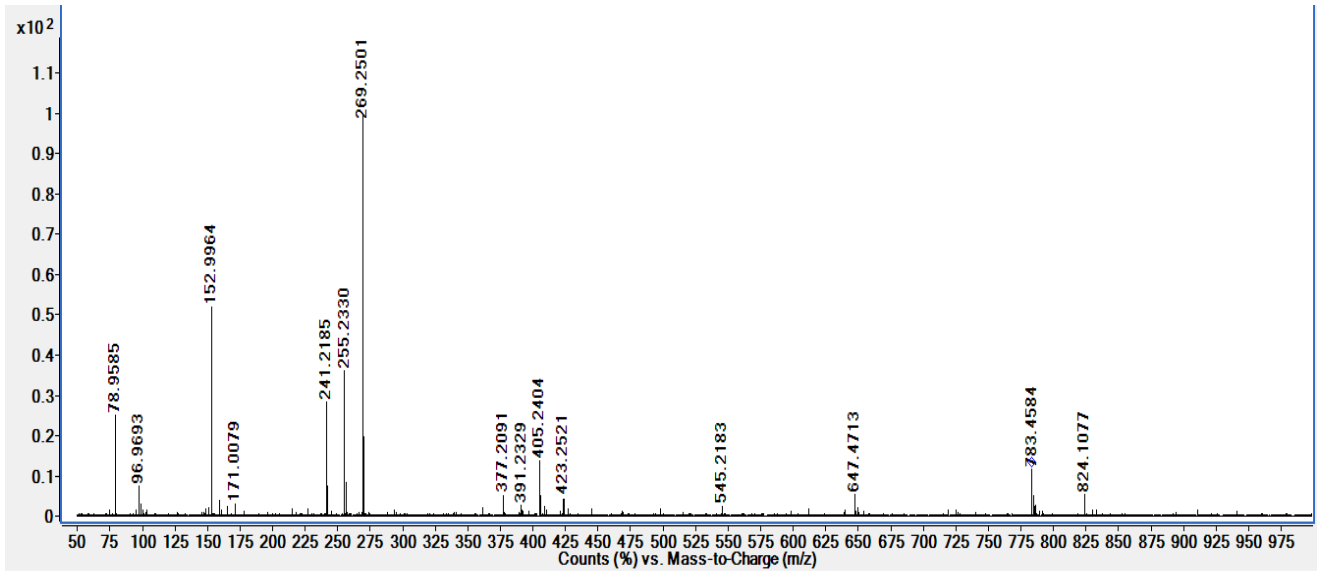
m)



n)



o)



p)

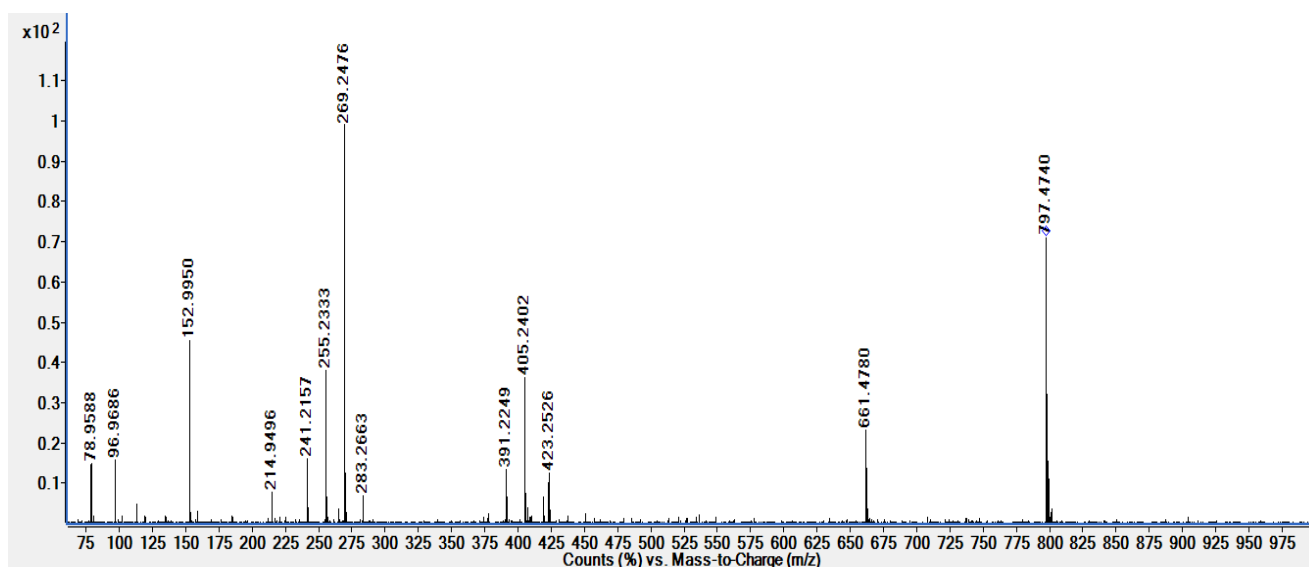


**Figure 3.11 ESI MS-MS (-ve) fragmentation spectra of lipid molecules from fraction III and IV.**

a) m/z 662.5 b) m/z 676.5 c) m/z 704.5 d) m/z 718.5 e) m/z 675.5 f) m/z 693.5 g) m/z 707.5 h) m/z 721.5 i) m/z 735.5 j) m/z 749.5 k) m/z 720.5 l) m/z 734.5 m) m/z 748.5 n) m/z 769.5 o) m/z 783.5 p) m/z 797.5

We have also observed interesting fragmentation pattern in MS/MS spectrum of fraction II with m/z of 807.3, 821.3 and 835.3 in negative ESI mode (Figure 3.12, Figure 3.13). Each parent ion shows neutral loss of -176 amu, which, to our knowledge, has not been reported yet in literature for any known lipid class. However, increasing chain length by 14 amu indicates presence of fatty acyl chains with increasing number of  $-\text{CH}_2$  group, and MS/MS spectra on those individual parent ions detected presence of fragment ion at 153 m/z indicating presence of glycerophosphate group. However due to trace amount of sample with mixture of other lipids present proper identification of structure is beyond the limit of mass spectrometry analysis. We were unable to find other lipid class in ESI-MS spectrum of fraction I, V, and VI (Data not shown).

In a previous study of *GWEI*, GC-MS analysis revealed that major cellular fatty acids were iso-15:0 (13.6 %), iso-16:0 (28.5 %) and iso-17:0 (13.5 %) (1). In the present study, we have observed similar results by using multiple chemical instrumentation analyses. Also Amenabar et al. (2) recently isolated exceptionally thermostable glutamate dehydrogenase from *GWEI* strain, which maintains its activity up to 70 % after incubating for 5 hours at 100 °C, which makes it most thermostable enzyme being reported in the family of dehydrogenases (2). Having stable enzymes with thermophilic lipid components (iso branched saturated fatty acids) in the cell of *GWEI* strain may be the reasons for exceptional thermostability compare to other mesophilic bacteria.

The absolute quantitation of lipids and identification of unknown peaks in mass spectrum remains future objective of this work and more efforts are required in this area. This is the first attempt to identify and isolate *GWEI* strain polar lipids with shotgun lipidomics, NMR spectroscopy and FTIR methods.

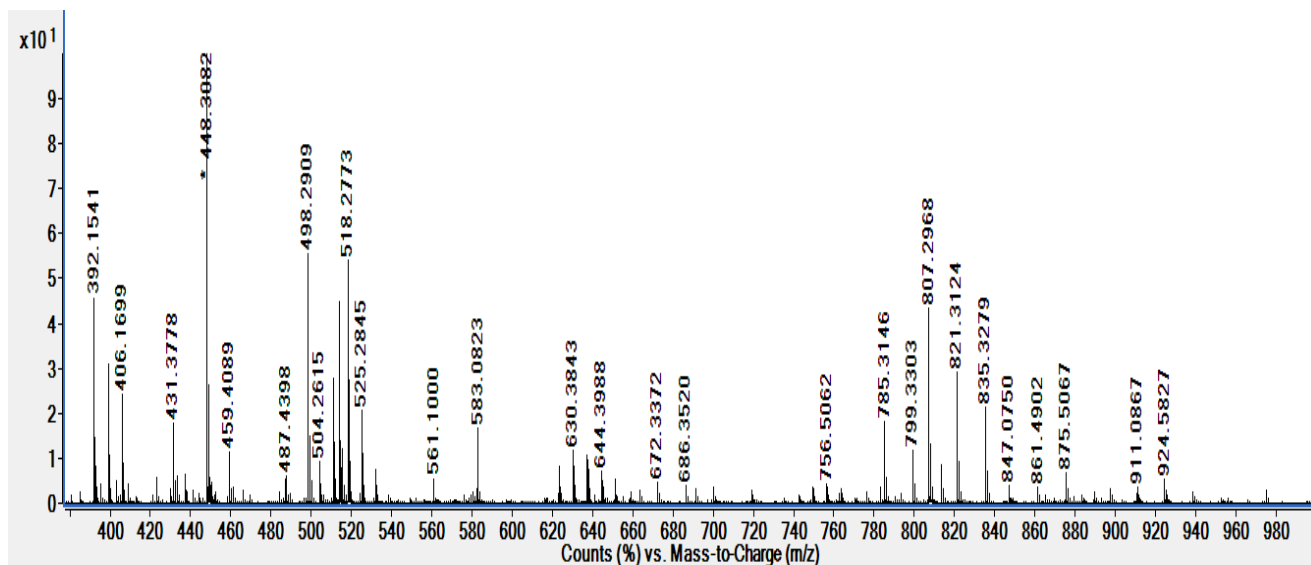
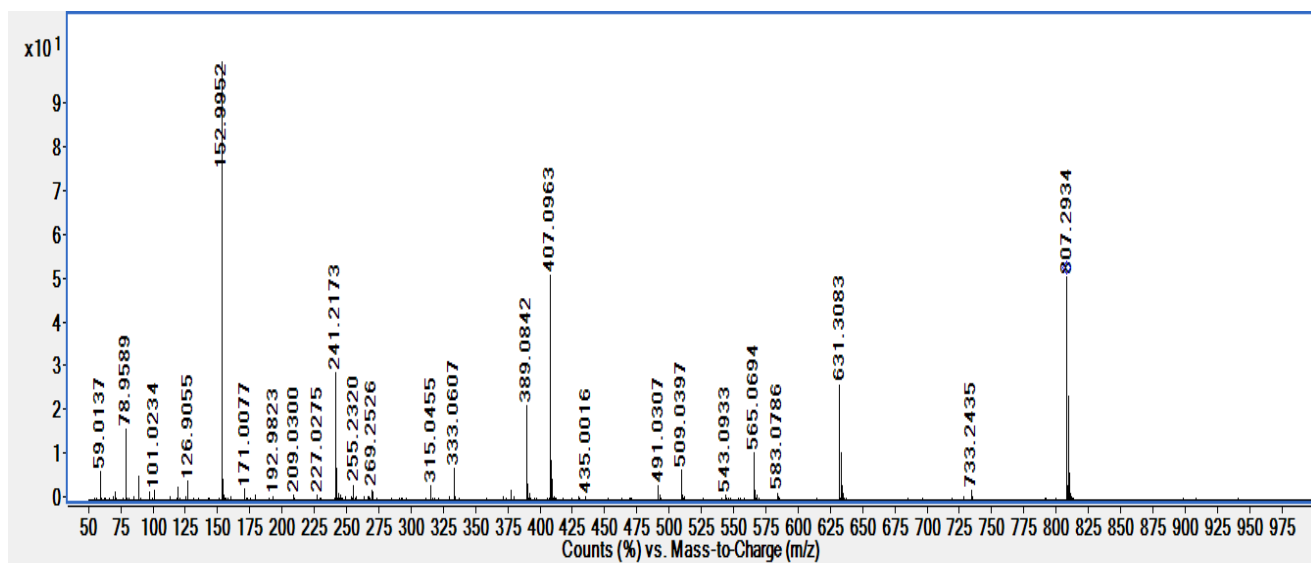
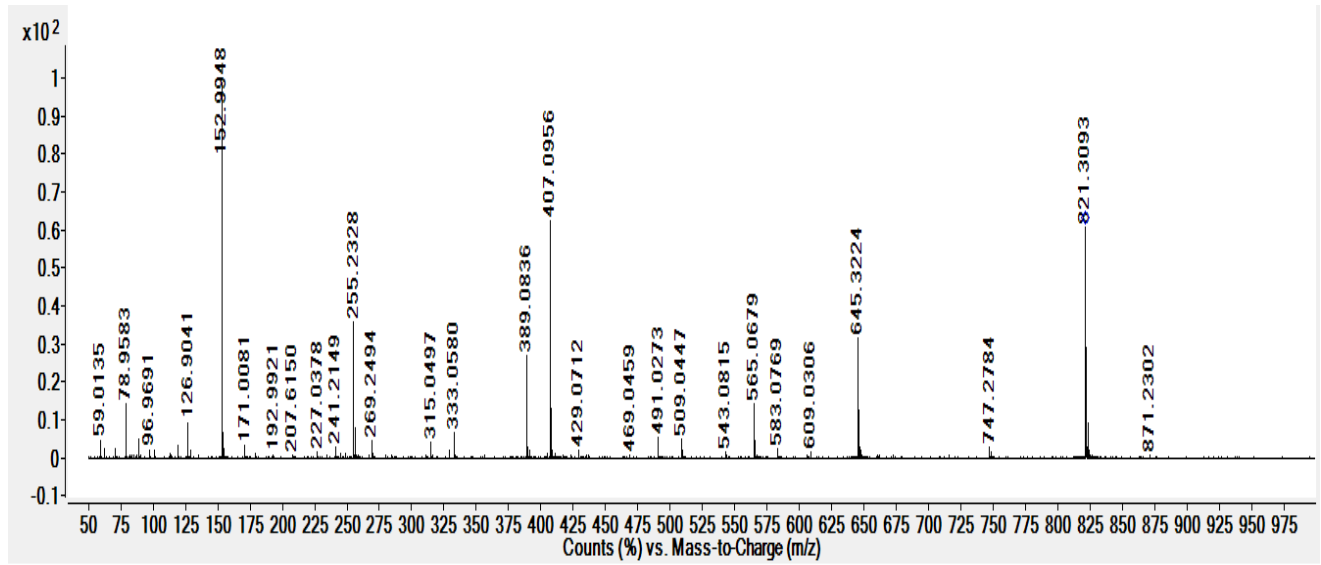


Figure 3.12: ESI-MS (-ve) spectrum for fraction II.

a)



b)



c)

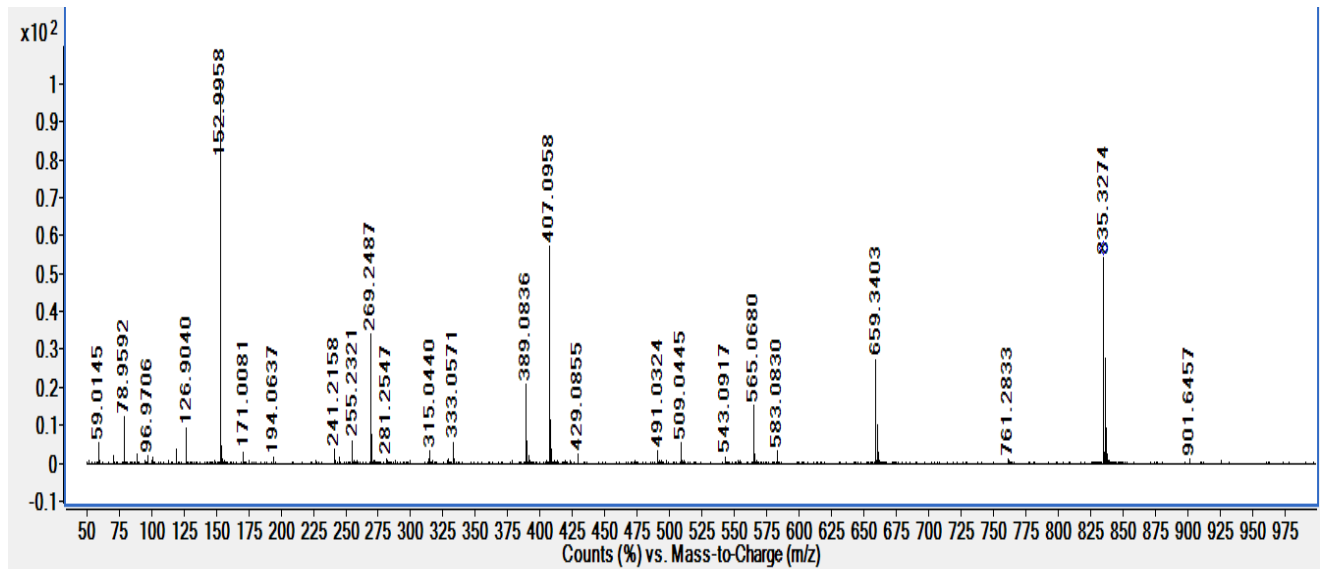


**Figure 3.13 ESI MS-MS spectra of unknown lipid like molecule from fraction II a) m/z 807.3 b) m/z 821.3 c) m/z 835.3**

### 3.4 Conclusion

Bacteria adapt to increased growth temperature by increasing the acyl chain length of fatty acid, increasing the iso/anteiso ratio to survive and decreasing permeability to solute molecules from outside environment by increasing phase transition temperature except some ether linkage lipid containing bacteria discussed earlier (11). We were able to detect straight chain saturated iso branched fatty acid containing lipids in *GWE1* strain fractions. We detected PE and PG lipids as major constituents of cell membrane and PA, PC and cardiolipins in minor amount in *GWE1* cell membrane (Table 2). We were unable to observe any ether lipids in current analysis. The presence of iso branched C14-C17 fatty acids and absence of unsaturated fatty acids in all the fractions could be a partial reason for *GWE1* being thermophilic.

### 3.5 Reference

- 1) Correa-Llantén, D., Larraín-Linton, J., Muñoz, P.A., Castro M., Boehmwald, F. & Blamey, J.M. Characterization of the thermophilic bacterium *Geobacillus* sp. strain *GWE1* isolated from a sterilization oven. *Kor. J. Microb. Biotech.* **41(3)**, 278-283 (2013).
- 2) Amenabar, M.J. & Blamey, J.M. Purification and characterization of a thermostable glutamate dehydrogenase from a thermophilic bacterium isolated from a sterilization drying oven. *BMB reports* **45**, 91-95 (2012).
- 3) Pack, S.P. & Yoo, Y.J. Protein thermostability: structure-based difference of amino acid between thermophilic and mesophilic proteins. *Journal of Biotechnology* **111**, 269-277 (2004).
- 4) Rothschild, L.J. & Mancinelli, R.L. Life in extreme environments. *Nature* **409**, 1092-1101 (2001).
- 5) Daniel, R.M. & Cowan, D.A. Biomolecular stability and life at higher temperatures. *Cell Mol. Life Sci.* **57**, 250-264 (2000).
- 6) Konings, W.N., Albers, S.V., Koning, S. & Driessen, A.J.M.,. The cell membrane plays a crucial role in survival of bacteria and archaea in extreme environments. *Antonie van Leeuwenhoek* **81**, 61-72 (2002).
- 7) Rilfors, L., Wieslander, A. & Stahl, S. Lipid and protein composition of membranes of *Bacillus megaterium* variants in the temperature range 5 to 70°C. *Journal of Bacteriology* **135**, 1043-1052 (1978).
- 8) Lai, D., Springstead, J.R. & Monbouquette. H.G. Effect of growth temperature on ether lipid biochemistry in *Archaeoglobus fulgidus*. *Extremophiles* **12**, 271-278 (2008).

- 9) Shimada, H., Nemoto, N., Shida, Y., Oshima, T. & Yamagishi, A. Effects of pH and temperature on the composition of polar lipids in *Thermoplasma acidophilum* HO-62. *J. Bacteriol.* **190**, 5404-5411 (2008).
- 10) Chong, P.L. Archaeobacterial bipolar tetraether lipids: Physico-chemical and membrane properties. *Chem. Phys. Lipids.* **163**, 253-265 (2010).
- 11) Koga, Y. Thermal adaptation of bacterial and archaeal lipid membranes. *Archaea* **2012**, 1-6 (2012).
- 12) Leone, S., Molinaro, A., Lindner, B., Romano, I., Nicolaus, B., Parrilli, M., Lanzetta, R. & Holst, O. The structures of glycolipids isolated from the highly thermophilic bacterium *Thermus thermophilus* Samu-SA1. *Glycobiology* **16**, 766-775 (2006).
- 13) Lo, S.L. & Chang, E.L. Purification and characterization of a liposomal forming tetraether lipid fraction. *Biochem. Biophys. Res. Commun.* **167**, 238-243 (1990).
- 14) Lewis, R.N.A.H., Mantsch, H.H. & McElhaney, R.N. Thermotropic phase behavior of phosphatidylcholines with  $\omega$ -tertiary-butyl fatty acyl chains. *Biophys. J.* **56**, 183-193 (1989).
- 15) Nzai, J.M. & Proctor, A. Soy lecithin phospholipid determination by Fourier transform infrared spectroscopy and the acid digest/Aarseno-molybdate method: A comparative study. *JAOCS* **76**, 61-66 (1999).
- 16) Sparling, M.L., Zidovetzki, R., Muller, L. & Chant, S.I. Analysis of membrane lipids by 500 MHz NMR  $^1\text{H}$  NMR. *Analytical Biochemistry* **178**, 67-76 (1989).

- 17) Casu, M., Anderson, G.J., Choi, G. & Gibbons, W.A. NMR lipid profiles of cells, tissues and body fluids-1D and 2D proton NMR of lipids from rat liver. *Magnet. Reson. Chem.* **29**, 594-602 (1991).
- 18) Adoskaru, K.R., Choi, G., Kokotos, V.C., Anderson, M.M. & Gibbons, W.A. NMR lipid profiles of cells, tissues, and body fluids: proton NMR analysis of human erythrocyte lipids. *J. Lipid Res.* **35**, 1925-1931 (1994).
- 19) Adosraku, R.K., Anderson, M.M., Anderson, G.J., Choi, G., Croft, S.L., Yardley, V., Phillipson, J.D. & Gibbons, W.A. Proton NMR lipid profile of *Leishmania donouani promastigotes*. *Mol. Biochem. Parasitol.* **62**, 251-262 (1993).
- 20) Murari, R., Abd El-Rahman, M.A., Wedmid, Y., Parthasarathy, S. & Baumann, W.J. Carbon-13 nuclear magnetic resonance spectroscopy of phospholipids in solution. Spectral and stereochemical assignments based on  $^{13}\text{C}$ - $^{31}\text{P}$  and  $^{13}\text{C}$ - $^{14}\text{N}$  couplings. *J. Org.Chem.* **47**, 2158-2163 (1982).
- 21) Birdsall, N.J., Feeney, J., Lee, A.G., Levine, K. & Metcalfe, J.C. Dipalmitoyl-lecithin: assignment of the  $^1\text{H}$  and  $^{13}\text{C}$  nuclear magnetic resonance spectra, and conformational studies. *J. Chem. Soc., Perkin Trans.* **2**, 1441-1445 (1972).
- 22) Nichols, F. C., Riep, B., Mun, J., Morton, M. D., Kawai, T., Dewhirst, F. E. & Smith, M. B. Structures and biological activities of novel phosphatidylethanolamine lipids of *Porphyromonas gingivalis*. *J. Lipid Res.* **47**, 844-853 (2006).
- 23) Hsu, F.F. & Turk, J. Characterization of phosphatidylethanolamine as a lithiated adduct by triple quadrupole tandem mass spectrometry with electrospray ionization. *J. Mass Spectrom.* **35**, 595-606 (2000).

- 24) Hsu, F.F. & Turk, J. Electrospray ionization/tandem quadrupole mass spectrometric studies on phosphatidylcholines: the fragmentation processes. *J. Am. Soc. Mass Spectrom.* **14**, 352-363 (2003).
- 25) Hsu, F.F. & Turk, J. Studies on phosphatidylglycerol with triple quadrupole tandem mass spectrometry with electrospray ionization: fragmentation processes and structural characterization. *J. Am. Soc. Mass Spectrom.* **12**, 1036-1043 (2001).
- 26) Hsu, F.F. & Turk, J. Structural characterization of cardiolipin by tandem quadrupole and multiple-stage quadrupole ion-trap mass spectrometry with electrospray ionization. *J. Am. Soc. Mass Spectrom.* **16**, 491-504 (2004).

## CHAPTER

### 4. EFFORTS TO IDENTIFY UNKNOWN LIPID MOLECULE FROM *GWEI* STRAIN

Focus of this chapter is to discuss efforts to solve unknown lipid structure found in *GWEI* strain. As discussed in chapter 3 we have noticed few unknown lipids at  $m/z$  807.3, 821.3 and 835.3 and we have made an effort to solve these unknown lipid structure using tandem mass spectrometry.

#### 4.1 Introduction

High resolution mass spectrometry of *GWEI* strain fraction 2 revealed three lipid like molecule with mass difference of 14 amu. Further analysis of these ions by using MS-MS showed the unique fragmentation pattern with neutral loss of 176 amu. We have not observed any other lipid class that follows this fragmentation pattern and we tried to identify these molecules using MS<sup>3</sup> technique.

#### 4.2 Materials and methods

##### 4.2.1 Materials

HPLC grade acetonitrile, water, methanol and formic acid were obtained from either Sigma(St. Louis, MO, USA) or Fisher Scientific (Waltham, MA, USA).

##### 4.2.2 Cell Growth and Extraction of polar lipids

Refer to chapter 3 for Cell growth and extraction of polar lipids

##### 4.2.3 Methods

###### 4.2.3.1 Sample Preparation

We have transferred about 2 mg of fraction II sample in 2 ml Eppendorf tube and added 1ml of methanol with 0.1 % formic acid. Prepared sample was directly injected by flow injection analysis (FIA) at 0.25 ml/min rate into Ion trap mass spectrometer for tandem mass analysis.

#### **4.2.3.2 Mass Spectrometry**

ESI/MS analyses were performed on Agilent 1200 LC-6520B Q-TOF high resolution Mass Spectrometer with Dual ESI as ion source in negative ionization mode. Detailed parameters for ESI-MS analysis and ESI-MS/MS analysis is discussed in chapter 3.

ESI-MS<sup>3</sup> analysis was performed using using a U3000 (Dionex) on line with linear trap quadrupole (ThermoFisher). In general, the sample was injected in full loop mode directly in to the mass spectrometer. Mass spectroscopy data was acquired with full MS from 100 to 1000 (negative mode) followed by MS-MS of 821.3 (unknown lipid like molecule) and MS-MS-MS of other individual daughter ions. Detailed parameters include: isolation width 7Da; normalized collision energy 35%; activation Q 0.15, activation time 16 milliseconds. Data was acquired in centroid mode.

#### **4.3 Results and Discussion**

Fraction 2 mass spectrum in negative mode using linear trap quadrupole mass gave us same pattern as earlier discussed in chapter 3. We observed three lipid like molecules (m/z 807, 821 and 835) from full ms scan of fraction II. After obtaining mass scan, fragmentation analysis was performed on m/z 821.4 ion, which is shown in figure 4.1. Fragmentation pattern for m/z 821.4 ion matches with fragmentation pattern reported earlier in Figure 3.13b using qTOF mass analyzer.

### 4.3.1 MS-MS Scan

As shown in figure 4.1, MS-MS scan of m/z 821.4 ion gave fragment ions at 152.99 which is due to glycerol phosphate molecule (1). However these ions show unique fragmentation pattern (loss of 176 amu), which is not reported yet. There are three different ways m/z 821.3 fragmentation occurs,

- 1) First loss observed in m/z 821.31 is loss of 74 amu. which gives daughter ion at 747. 28. It has been reported that loss of 74 amu is due to loss of glycerol as  $-C_3H_6O_2$  (2, 3, 4).
- 2) It also generates daughter ion at 645.32 after neutral loss of 176 amu, which we believe is headgroup of the molecule.
- 3) Another pattern observed is loss of fatty acyl chain as ketene (238 amu) and acid (256 amu) molecule to generate 583 and 565 daughter ions respectively (2, 3, 4).

Higher abundance of 565 daughter ions confirm glycerophosphate ( PA) like fragmentation (3). PA molecules showed that fatty acyl chain cleaves as acid rather than ketene, in contrast to glycerophosphoethanolamine (PE). Similar pattern was observed for m/z 835 and 807 (data not shown).

Daughter ions' fragmentation patterns were also useful in identifying part of molecule.

Daughter ion 747 fragments further to generate 491 (loss of 256) and 509 (loss of 238).

We do not observe loss of 176 from 747, which indicates that loss of 74 comes from head group and only part of headgroup is remaining in 747 ion. We were unable to obtain MS-MS-MS scan for 747 m/z because of low abundance.

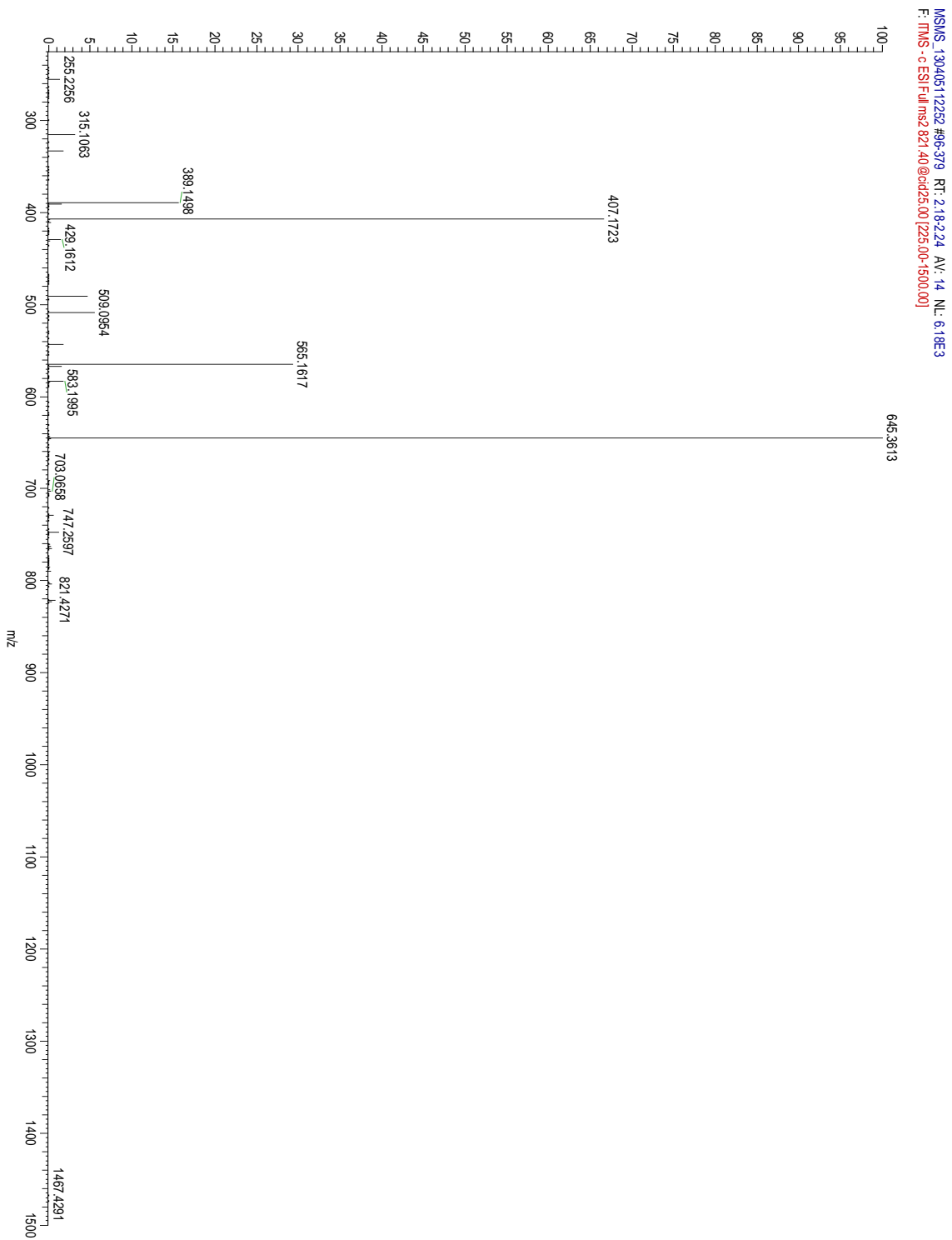


**Figure 4.1 MSMS scan of m/z 821.4 molecule using linear trap quadrupole mass analyzer**

### 4.3.2 MS-MS-MS Scan

Daughter ion 645 (loss of 176 amu from parent ion) also goes through loss of 256 and 238 amu to generate 389 and 407 ions (Figure 4.2). Daughter ion 565 (loss of acyl chain 256 amu from parent ion) also loses headgroup (176 amu) and gives m/z 389 (Figure 4.3).

Based on knowledge we gained, we can confirm that compound contains head group (176 amu), fatty acid  $R_2COO^-$  (255 amu) and compound contains anhydrous glycerol phosphate (m/z 153). We could not confirm about second fatty acyl chain and headgroup.

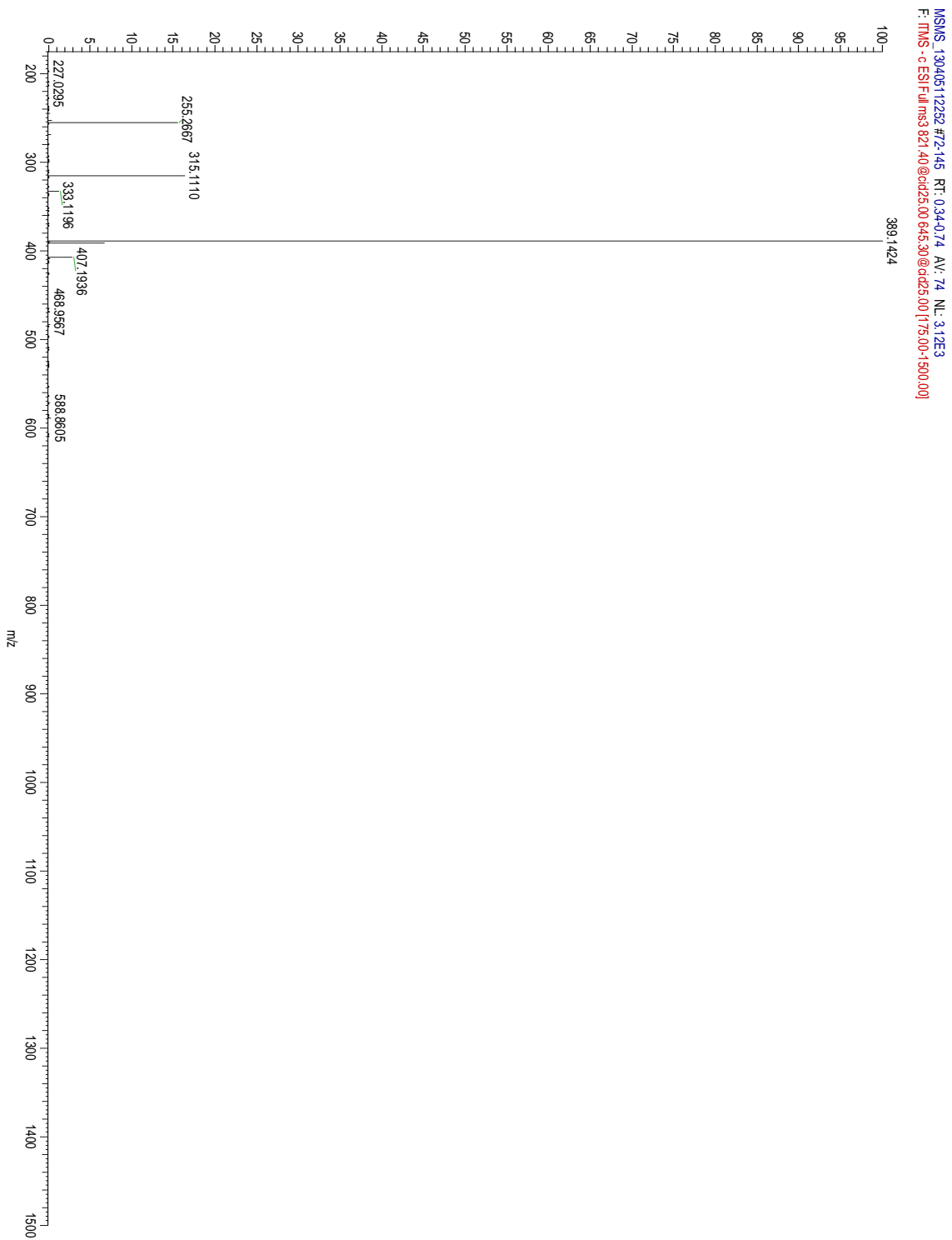


**Figure 4.2 MS-MS-MS Scan for daughter ion m/z 645**

MSMS: 13040511252 #718-768 RT: 3.99-4.26 AV: 50 NL: 8.87E2  
F: TMS - c ESI Full ms3 821.50@cid25.00 565.00@cid20.00 [155.00-1500.00]

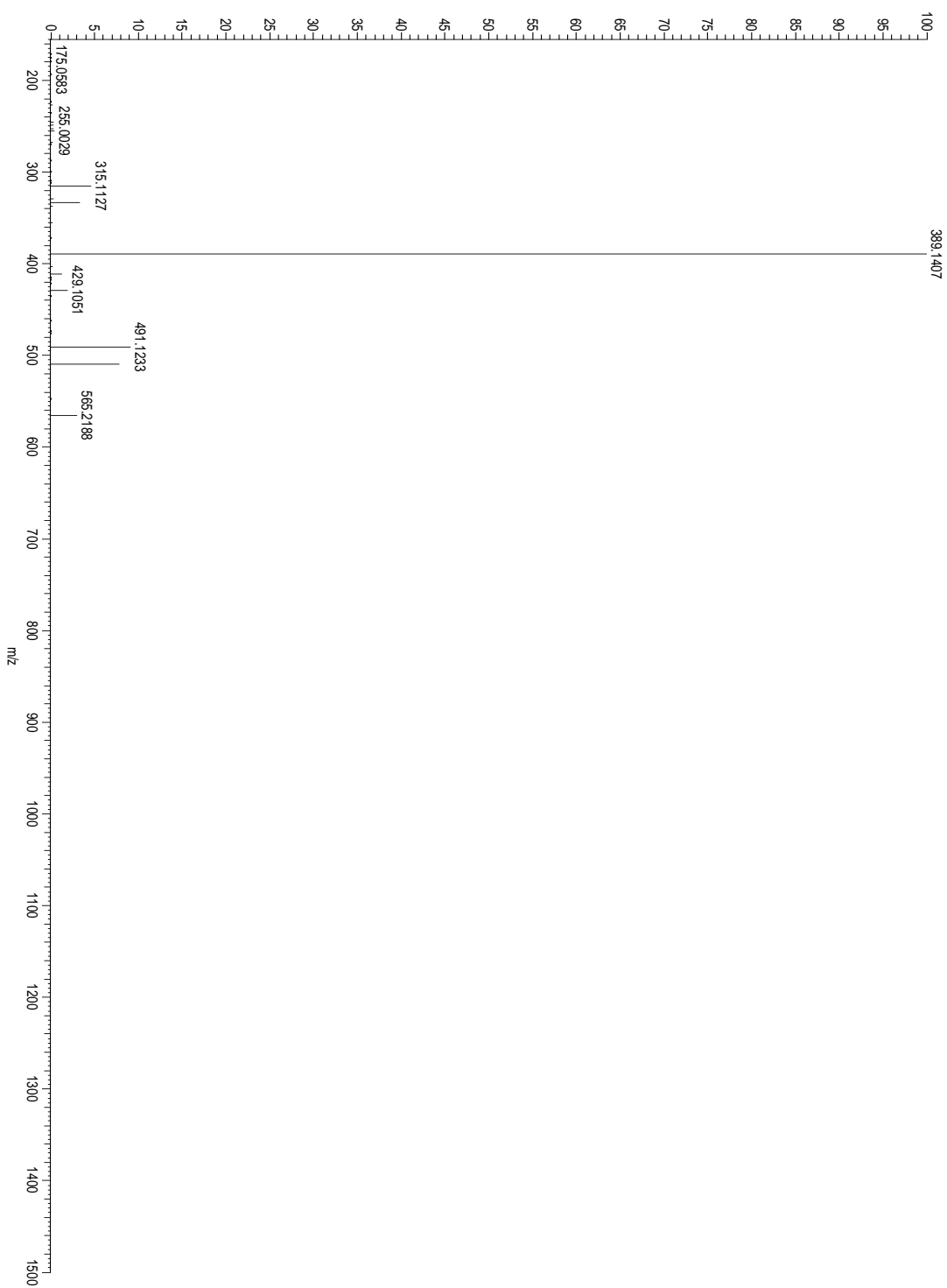


Figure 4.3 MS-MS-MS Scan for daughter ion m/z 565

#### **4.3.2.1 Structure of second fatty acyl chain like molecule**

Daughter ion  $m/z$  407 is formed after loss of ketene from  $m/z$  645, so  $m/z$  407 contains important information about second chain. We performed  $MS^3$  analysis on 407 ion that gave us daughter ions at  $m/z$  333 and  $m/z$  153 (Figure 4.4). Daughter ion at 153  $m/z$  was confirmed as anhydrous glycerol phosphate earlier and subtraction of that part of molecule gave the exact mass for second fatty acyl chain which was 253.0945. Searching molecular formula based on exact mass did not give any structure that correlates with observation of mass spectrometer analysis to confirm our results. Possible options are given in table 4.1.

MSMS\_130405112252\_#144-1180 RT: 6.34652 AV: 35 NL: 6.63E4  
F: TMS - c ESI Full ms3 583.30@cid20.00 407.20@cid5.00 [1+10.00-1500.00]

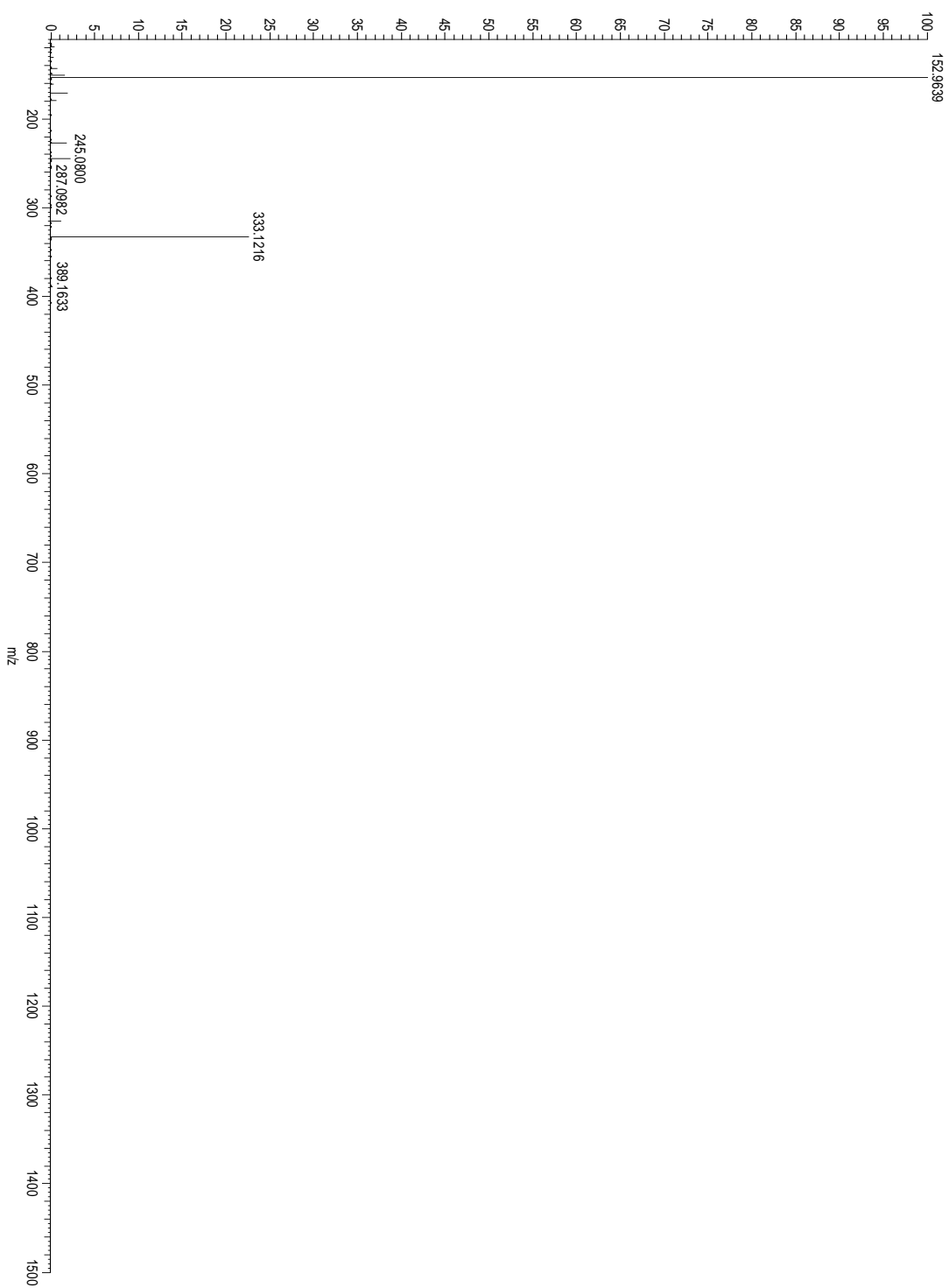


Figure 4.4 MS-MS-MS Scan for daughter ion m/z 407

	<b>MF</b>	<b>Monoisotopic mass</b>	<b>PPM</b>	<b>Unaturation</b>
1	C <sub>16</sub> H <sub>15</sub> NS	253.0925201786	0.08	10
2	C <sub>4</sub> H <sub>14</sub> N <sub>8</sub> O <sub>3</sub> P	253.0926478706	0.584	2.5
3	C <sub>9</sub> H <sub>17</sub> O <sub>8</sub>	253.0923425233	0.622	1.5
4	C <sub>8</sub> H <sub>11</sub> N <sub>7</sub> O <sub>3</sub>	253.0923372569	0.643	7
5	C <sub>12</sub> H <sub>18</sub> N <sub>2</sub> PS	253.0928307923	1.307	5.5
6	C <sub>8</sub> H <sub>19</sub> N <sub>3</sub> O <sub>2</sub> S <sub>2</sub>	253.0918682532	2.496	1
7	C <sub>10</sub> H <sub>21</sub> O <sub>3</sub> S <sub>2</sub>	253.0932109237	2.809	0.5
8	C <sub>10</sub> H <sub>13</sub> N <sub>4</sub> O <sub>4</sub>	253.0936799274	4.662	6.5
9	C <sub>6</sub> H <sub>16</sub> N <sub>5</sub> O <sub>4</sub> P	253.0939905412	5.889	2
10	C <sub>7</sub> H <sub>15</sub> N <sub>3</sub> O <sub>7</sub>	253.0909998528	5.927	2

**Table 4.1 Possible chemical formulas for fatty acyl like molecule at 253.0945.**

#### 4.3.2.2 Analysis for head group structure

We confirmed from the observation that difference in parent ion 821.3093 and daughter ion 645.3224 from qTOF mass spectrum ( 175.9869 amu) belongs to headgroup of molecule. We were unable to find possible chemical structure for possible formula. Possible chemical formulas are displayed in table 2.

	<b>MF</b>	<b>Monoisotopic mass</b>	<b>PPM</b>	<b>mDa</b>	<b>unsaturation</b>
1	C <sub>5</sub> H <sub>6</sub> NO <sub>2</sub> S <sub>2</sub>	175.9839948248	1.734	-0.305	3.5
2	CHN <sub>6</sub> O <sub>3</sub> P	175.9847744422	2.696	0.474	5
3	C <sub>9</sub> H <sub>5</sub> PS	175.9849573639	3.735	0.657	8
4	H <sub>5</sub> N <sub>2</sub> O <sub>7</sub> P	175.9834370381	4.904	-0.863	0
5	C <sub>4</sub> H <sub>2</sub> NO <sub>7</sub>	175.9831264244	6.669	-1.174	4.5
6	C <sub>7</sub> N <sub>2</sub> O <sub>4</sub>	175.985806499	8.56	1.506	9
7	C <sub>3</sub> H <sub>4</sub> N <sub>4</sub> OS <sub>2</sub>	175.9826521542	9.364	-1.648	4
8	C <sub>3</sub> H <sub>3</sub> N <sub>3</sub> O <sub>4</sub> P	175.9861171127	10.325	1.817	4.5
9	N <sub>8</sub> O <sub>2</sub> S	175.9864919778	12.455	2.192	5
10	C <sub>2</sub> N <sub>4</sub> O <sub>6</sub>	175.9817837538	14.298	-2.516	5

**Table 4.2: Possible Chemical formula generated for head group.**

#### **4.4 Conclusion**

We were unable to obtain the structure of compound based on information available.

Compound could be complex multicharged molecule or it could be intermediate structure of some other lipid molecule. Due to trace amount of compound it was impossible to isolate and obtain more data using NMR spectroscopy.

#### 4.5 References

- 1) Shah, S.P., Jansen S.A., Taylor, L.J., Chong P.L., Correa-Llantén D.N. & Blamey J.M. Lipid composition of thermophilic *Geobacillus* sp. strain *GWE1*, isolated from sterilization oven. *Chemistry and Physics of Lipids* **180**, 61-71 (2014).
- 2) Hsu, F.F. & Turk, J. Studies on phosphatidylglycerol with triple quadrupole tandem mass spectrometry with electrospray ionization: fragmentation processes and structural characterization. *J. Am. Soc. Mass Spectrom.* **12**, 1036-1043 (2001).
- 3) Hsu, F.F. & Turk, J. Structural characterization of cardiolipin by tandem quadrupole and multiple-stage quadrupole ion-trap mass spectrometry with electrospray ionization. *J. Am. Soc. Mass Spectrom.* **16**, 491-504 (2004).
- 4) Hsu, F.F. & Turk, J. Characterization of phosphatidylethanolamine as a lithiated adduct by triple quadrupole tandem mass spectrometry with electrospray ionization. *J. Mass Spectrom.* **35**, 595-606 (2000).

## CHAPTER

### 5. LIPID COMPOSITION OF PSYCHROTOLERANT *SERRATIA* SP. STRAIN *IIP*, ISOLATED FROM ANTARCTICA.

(Note: Content of this Chapter is adapted from the submitted manuscript “Siddharth P. Shah, Susan A. Jansen , Sean P. Lawrence, Parkson Lee-Gau Chong, Daniela N. Correa-Llantén, Jairo Pereira, Jenny M. Blamey, Lipid composition of psychrotolerant *Serratia* sp. strain *IIP*, isolated from Antarctica.)

#### 5.1 Introduction

Psychrotolerant organisms are able to grow at low temperatures with much lower rates, and they have growth optima in the range of mesophilic organisms (20-40°C) (1).

Psychrotolerants, successfully colonize in permanently cold ecosystems on the earth, such as deep oceans, glaciers, and polar areas. They constitute an important part of cold-adapted biodiversity by performing an essential role as nutrient cyclers and waste mineralizers (2). In this paper, we have reported the lipid composition and fatty acid profile of the psychrotolerant strain *IIP* and the implication for survival strategy at lower temperatures. *IIP* is a rod shaped psychrotolerant bacterium isolated from Antarctica (3). *IIP* was phylogenetically evaluated through nucleotide sequencing of the 16S rRNA, with results indicating that this microorganism belongs to the genus *Serratia* spp. (3). *IIP* is a non-spore forming bacterium capable of generating a large amount of a thick exopolysaccharide (EPS) under conditions of environmental stress. It grows in a wide range of temperatures from 8 to 35 °C and at an optimal pH of 7. It has proved to be

catalase positive and can grow on NaCl in a range between 2% and 8% (3), which is consistent with the description of other microorganisms of the genus *Serratia* (4). *Serratia* is a genus comprising mobile bacilli, facultative anaerobes of the family *Enterobacteriaceae*, which are found in many environments (5). Focus of this paper is to identify lipid composition and fatty acid profile of organism and to understand the ability of organism to survive at lower temperature by looking at the lipid composition. To survive in cold environments, psychrophiles need to adapt to two main challenges: firstly, low temperatures as a decrease in temperature decrease the rates of biochemical reactions and secondly, the viscosity of aqueous surroundings increases by about a factor of 2 between 37 °C and 0 °C (6). Membrane fluidity at lower temperatures is maintained by an adaptation in the lipid composition of its cell membrane. Lipid composition governs physical properties of the membrane and affects cell membrane functionality (7). As a response to cold environment, microorganism produces lipids with shorter, unsaturated, or methyl branched fatty acids (6). Chintalapati et al. reported a high proportion of *cis* double bonds and anteiso branched fatty acids when they compared fatty acid content of psychrophiles *Halomonas glacei* and *Pseudomonas antarctica* with closely related mesophiles *Halomonas variabilis* and *Pseudomonas orientalis* respectively (8). *Bacillus megaterium* has 25% iso-C15 and nearly 50% anteiso-C15 fatty acids at 20°C growth temperature and 35% iso-C15 and 15% anteiso-C15 at the growth temperature 60°C (9). This suggests that the iso-C15 fatty acid is thermophilic and the anteiso-C15 fatty acid is psychrophilic in this bacterial species (9). These changes increase membrane fluidity at lower temperatures by introducing steric constraints in the lipid packing and/or by

reducing the number of interactions between the headgroups in the membrane (7,8). Chintalapati et al. found a relationship between an increased content of large head groups with a decrease in growth temperature (9).

Psychrophilic microorganisms express cold-acclimation proteins (CAPs), which act as a chaperone to maintain transcription, translation protein folding and other functions within the cell at lower temperature (4). Psychrophiles also express antifreeze proteins (AFPs) that bind to ice crystals through a large complementary surface creating thermal hysteresis and lowering the minimum temperature at which the microorganism can grow (10). At lower temperature psychrophiles over express enzymes that retain activity at low temperatures. One hypothesis for this cold adaptation is the activity–stability–flexibility relationship, which suggests that psychrophilic enzymes increase the flexibility of their structure to compensate for the decrease in temperature (11). Common adaptive trends include: the reduction of the number of ion pairs, hydrogen bonds and hydrophobic interactions; decreased intersubunit interactions; increased interaction with the solvent; a reduced apolar fraction in the core; higher accessibility to the active site; increased exposure of apolar residues to the solvent; decreased cofactor binding; clustering of glycine residues; and a lower proline and arginine content (12). Saunders et al. showed that working from psychrophilic to thermophilic Archaea, there is a trend in increasing leucine content and decreasing glutamine and threonine content (13). Khachane et al. found a significant inverse correlation between the uracil content of 16S rRNA and the optimum growth temperature ( $T_{opt}$ ) of cultured organisms (14).

In this paper we have focused on the lipid composition and fatty acid profile of the *IIP* bacterium to predict the effects of its composition on membrane fluidity. Through shotgun lipidomics we have identified PE and PG lipids with unsaturated fatty acids. GC fatty acid profile analysis showed the following results for fatty acid percentage 16:0 34.20%, 16:1 $\omega$ 7c 29.34%, 18:1 $\omega$ 7c 10.10 %, 17:0 cyclopropane 7.61%, 16:1 iso 6.72%, 14:0 5.39%.

## **5.2 Materials and Methods**

### **5.2.1 Cell growth**

*IIP* cells were isolated from Antarctica (1). The microorganism was grown at 22°C and pH 7.0. The growth medium contains tryptone 1% (w/v), yeast extract 0.5% (w/v) and NaCl 6% (w/v).

### **5.2.2 Materials**

HPLC grade acetonitrile, water, chloroform, methanol, and formic acid were obtained from either Sigma (St. Louis, MO, USA) or Fisher Scientific (Waltham, MA, USA).

### **5.2.3 Extraction of polar lipids**

Total polar lipids were extracted by the method of Lo and Chang (15). In brief, dried cells were soxhlet-extracted with chloroform/methanol (1:1, v/v) for 24 h. The crude lipids were fractionated by reversed-phase column chromatography using C-18 PrepSep columns (Fisher Scientific, Fair Lawn, NJ) eluted first with methanol: water (1:1, v/v) (fraction A), then with chloroform:methanol:water (2:5:2, v/v/v) (fraction B) and then with chloroform:methanol:water (65:25:4, v/v/v) (fraction C). All three fractions were

collected, evaporated to dryness under nitrogen, and stored at -20 °C before structural analysis.

#### **5.2.4 Gas Chromatography**

Fatty acid methyl ester (FAME) analysis was performed by following instructions of Microbial Identification System (MIDI, Microbial ID Inc.) (16). In brief, 1 ml of reagent 1 (45 g sodium hydroxide, 150 ml methanol, and 150 ml distilled water) was added to freeze dried bacterial cells containing tube to cleave fatty acids from lipids. Addition of 2 ml of reagent 2 (325 ml certified 6.0 N hydrochloric acid and 275 ml methyl alcohol) caused methylation of cleaved fatty acids. FAMEs were extracted using 1.25 ml of reagent 3 (200 ml hexane and 200 ml methyl tert-butyl ether). Obtained sample was further cleaned with reagent 4 (10.8 g NaOH dissolved in 900 ml distilled water). About 2/3 of the organic phase was pipetted and injected into Agilent 6890 Gas Chromatography system coupled with flame ionization detector (FID). A 25m × 0.2mm phenyl methyl silicone fused capillary column was used for separation by using temperature program, which increases from 170 °C to 270 °C at 5 °C per minute. Sherlock MIS data analysis software was used to qualify and quantify FAME peaks.

#### **5.2.5 Mass Spectrometry**

Portion of each sample was transferred to Eppendorf tube and was evaporated to dryness under nitrogen. About 1 mg fraction was dissolved in methanol and used for experiment. ESI/MS analyses were performed on Agilent 1200 LC-6520B Q-TOF high resolution Mass Spectrometer with Dual ESI as ion source in both positive and negative ionization mode. About 10 µl sample was injected with Agilent 1200 G1376B HiP autosampler.

Full scan spectra were obtained by scanning masses between 50-1700 m/z. Other parameters were set as follows: sheath gas temperature, 300 °C; sheath gas flow, 5 l/min; nebulizer, 30 psi; and capillary entrance voltage, 3500 V. Fragmentor and skimmer1 were operated at 150 V and 65 V, respectively. The MS scan data were collected at a rate of 1 spectrum/s in range of 50-1700 m/z. In the targeted MS/MS mode, the MS and the MS/MS information were collected in the 50-1000 m/z range at the same rate as the MS scan and the collision energy was 45 V. All the MS and MS/MS data were collected with MassHunter Data Acquisition (Agilent) and MassHunter Qualitative Analysis B.02.00 (Agilent) was applied to identify lipid species.

## **5.3 Results and Discussion**

### **5.3.1 Gas Chromatography**

FAME analysis was performed to obtain information about fatty acid profile in *IIP* strain. The fatty acid profile for *IIP* strain is described in table 5.1. FAME analysis revealed that major fatty acids were 16:0 and 16:1( $\omega$ 7/6) with a fatty acid % composition value of 34.2% and 29.7% respectively. It also contained 6.72% of 14:0 3OH fatty acid, which is a characteristic of this bacterial family (5). Other major fatty acids in this strain were 18:1 (10.10%), 17:0 cyclopropane (7.61%), 14:0 (5.39%), and 12:0 (1.80%), 18:0 (1.68%), 17:0 (0.50%) and 15:0 (0.41%). Total percentage of unsaturated fatty acids comprised about 40% of the total fatty acids in the strain. Comparison of fatty acid profiles with those of known bacteria in the MIDI database revealed similarity(SIM) index value of 0.64 and 0.59 with *S. fonticola* and *S. grimesii* respectively.

<b>Fatty Acid</b>	<b>% Composition</b>
12:0	1.80
14:0	5.39
14:0 3OH	6.72
15:0	0.41
16:1( $\omega$ 7/6)	29.34
16:1( $\omega$ 5)	0.25
16:0	34.20
17:0 Cyclopropane	7.61
17:0	0.50
18:2( $\omega$ 6)	0.22
18:1( $\omega$ 7)	10.10
18:0	1.68
19:0 (cyclo $\omega$ 8)	0.23
19:0	0.13

**Table 5.1: Whole cell fatty acid Profile for *Iip* strain**

### 5.3.2 Mass Spectrometry

ESI-MS negative scan (Figure 5.1) was performed with LC-6520B Q-TOF high resolution Mass Spectrometer. We have detected glycerophosphoglycerol (PG), glycerophosphate (PA), glycerophosphoethanolamine (PE) and acyl glycerophosphoglycerol (acyl PG) lipids which are described in Table 2. We were unable to observe any lipid structures in fraction A or B (data not shown). The major lipid found in *IIP* strain is PG, followed by PA, PE and minor amounts of acyl PG lipids. [M-H]<sup>-</sup> ions for PG lipids include 719.48, 733.50, 745.50, 747.51, 759.51 and 773.57 as shown in figure 5.3. We have confirmed this assignment using fragmentation characterization of individual molecules. PG molecule (m/z 719.48) fragmentation analysis (Figure 5.2) showed fragments at m/z 253.2 (C16:1) and m/z 255.2 (C16:0) which are fatty acid molecules R<sub>2</sub>-COO<sup>-</sup> and R<sub>1</sub>COO<sup>-</sup> ions, respectively. Higher abundance of one fatty acid over another indicates sterically favorable elimination of one over another and this helps us to identify their relative position in individual lipids (17), which indicates lipid structure for m/z 719.48 as PG C16:0/16:1. We have also detected PA lipids in negative ESI-MS spectrum, which includes m/z 645.44 and 659.46 and minor amount of PE lipids at m/z 688.48 (figure 5.3). We have identified these PLs by using mechanism reported by Hsu et al (18, 19, 20).

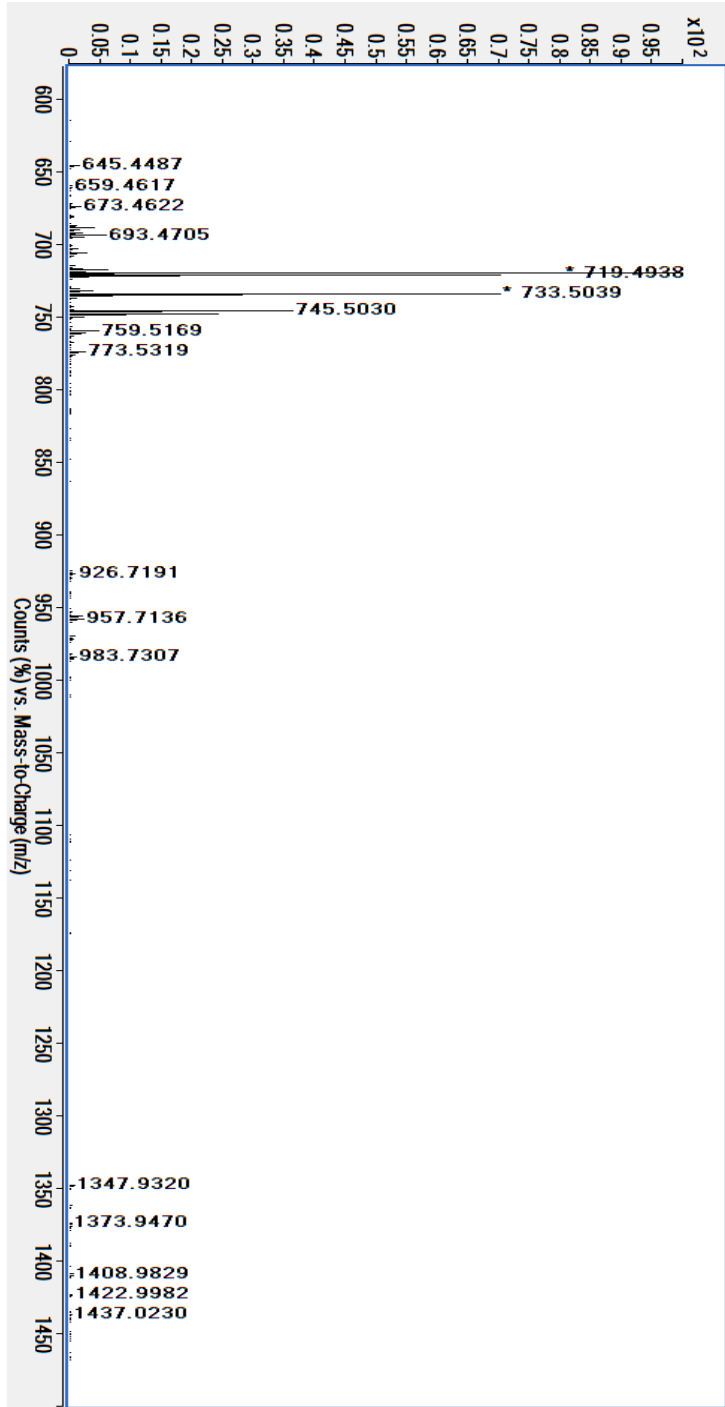


**Figure 5.1: ESI-MS scan of fraction C, obtained by LC-6520B Q-TOF high resolution Mass Spectrometer**

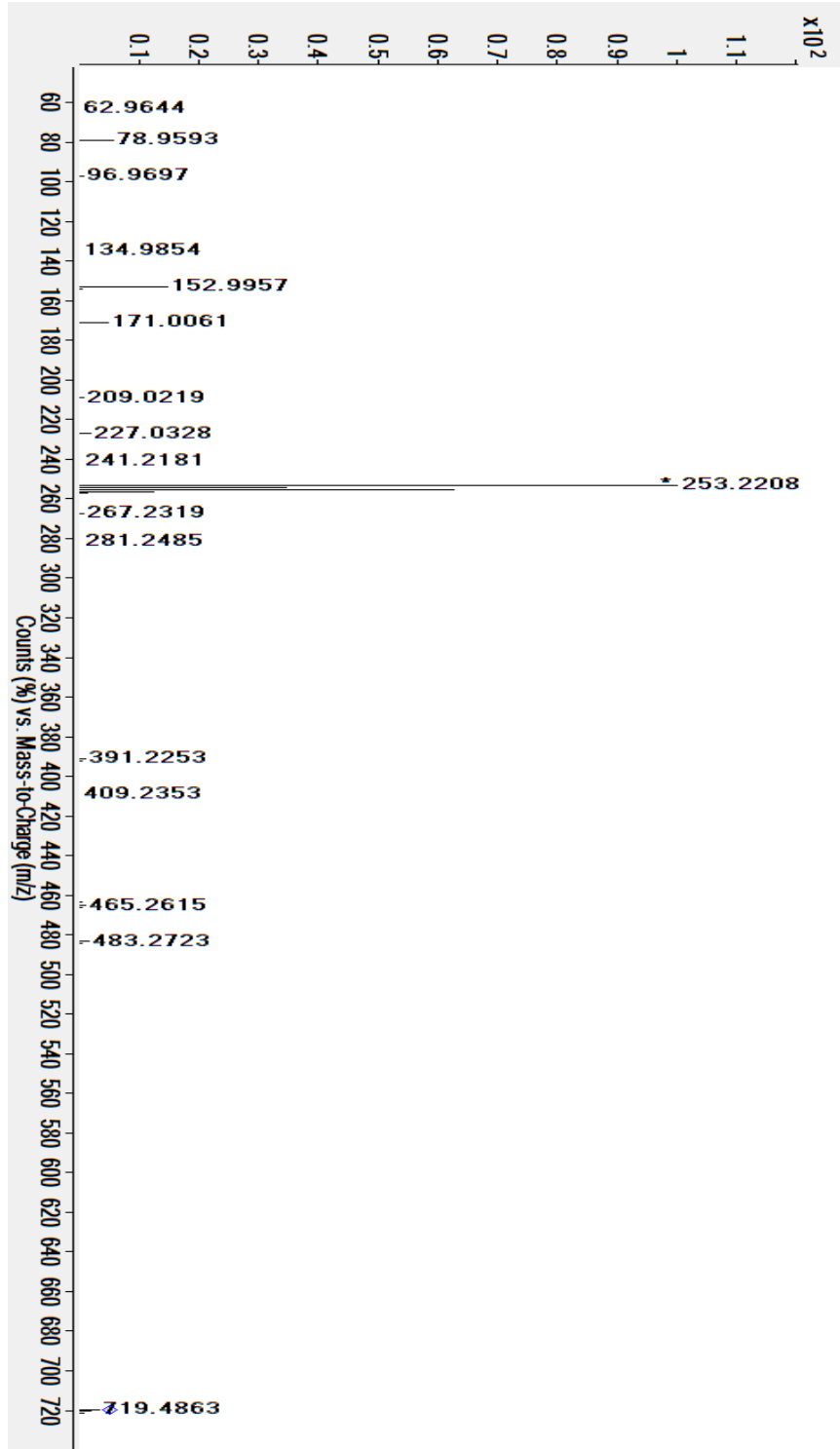
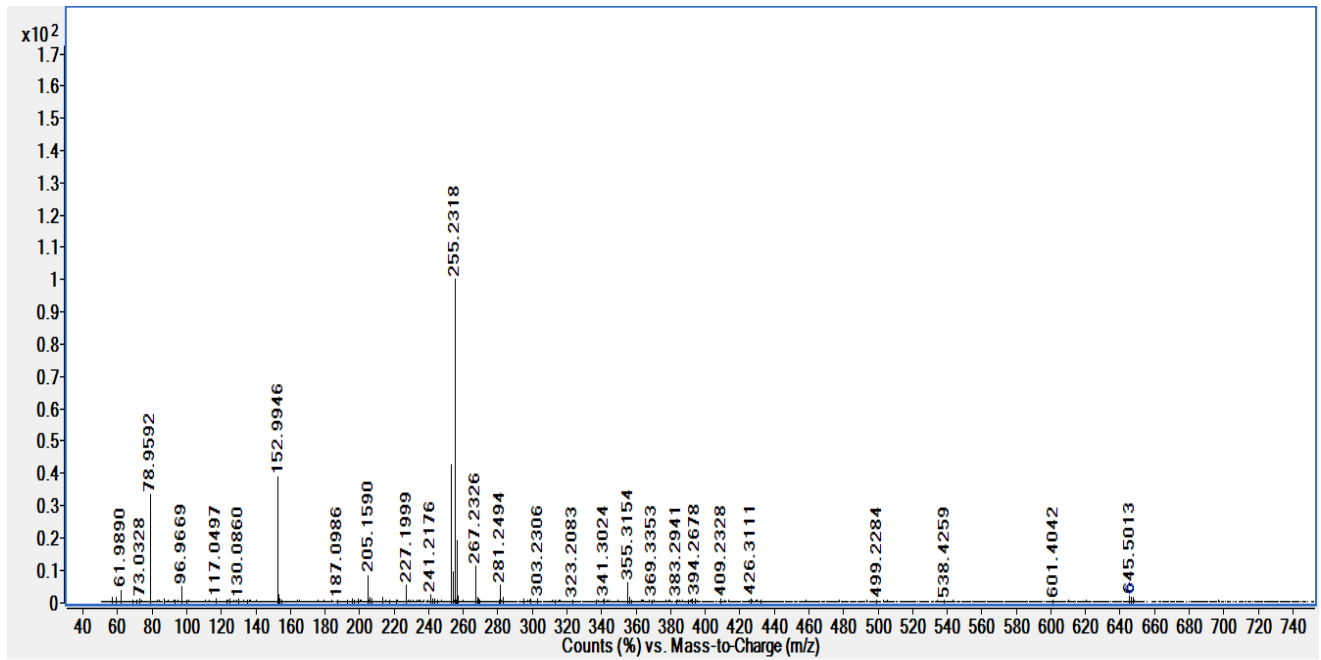
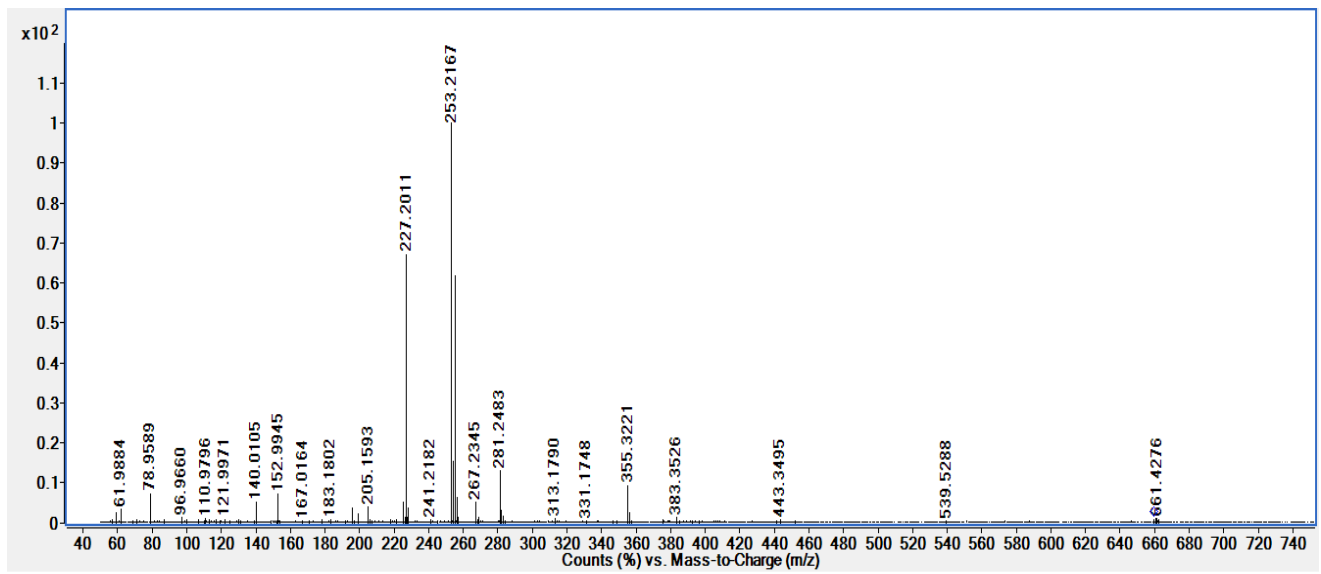


Figure 5.2: Negative ESI- MS/MS analysis of PG lipid at m/z 719.48

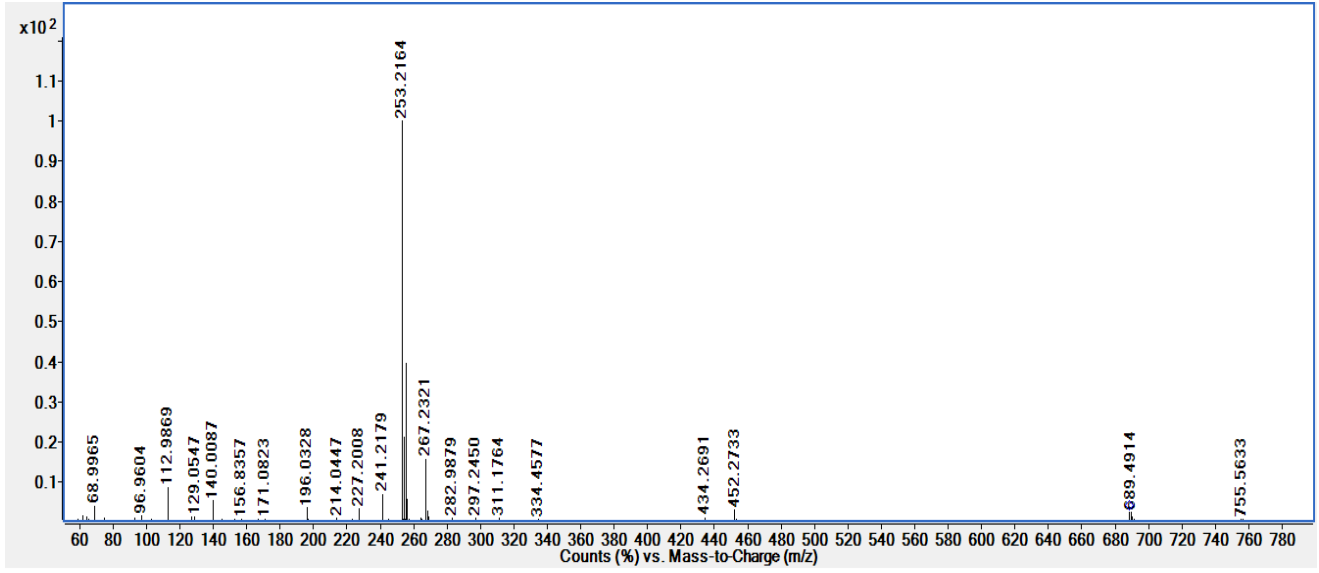
a)



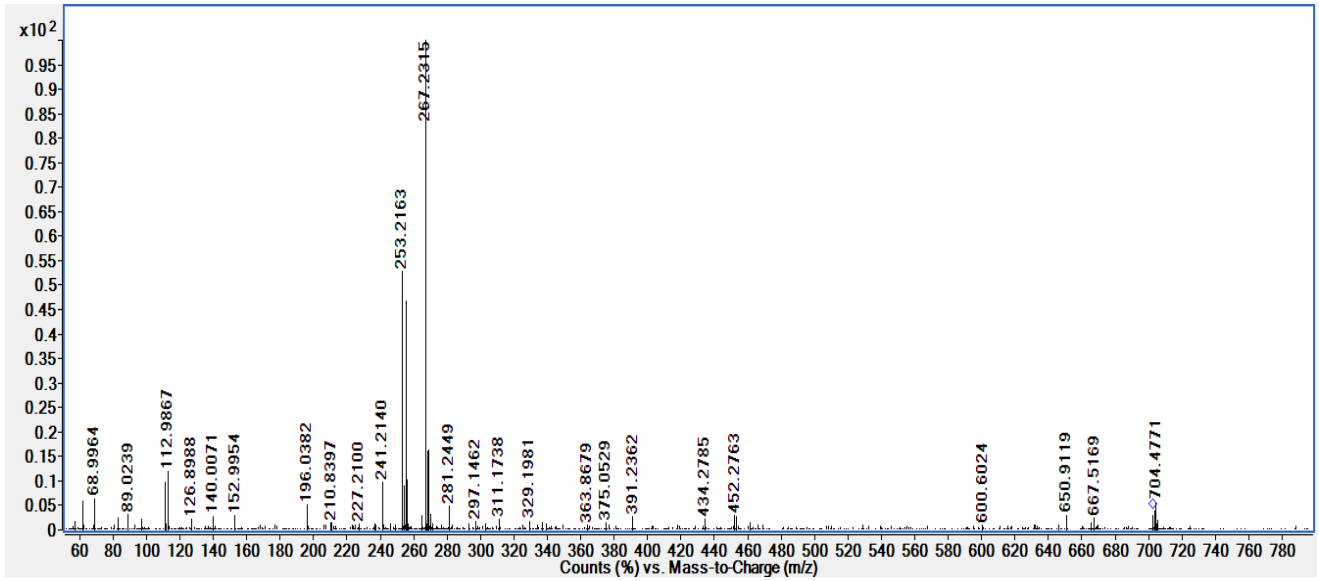
b)



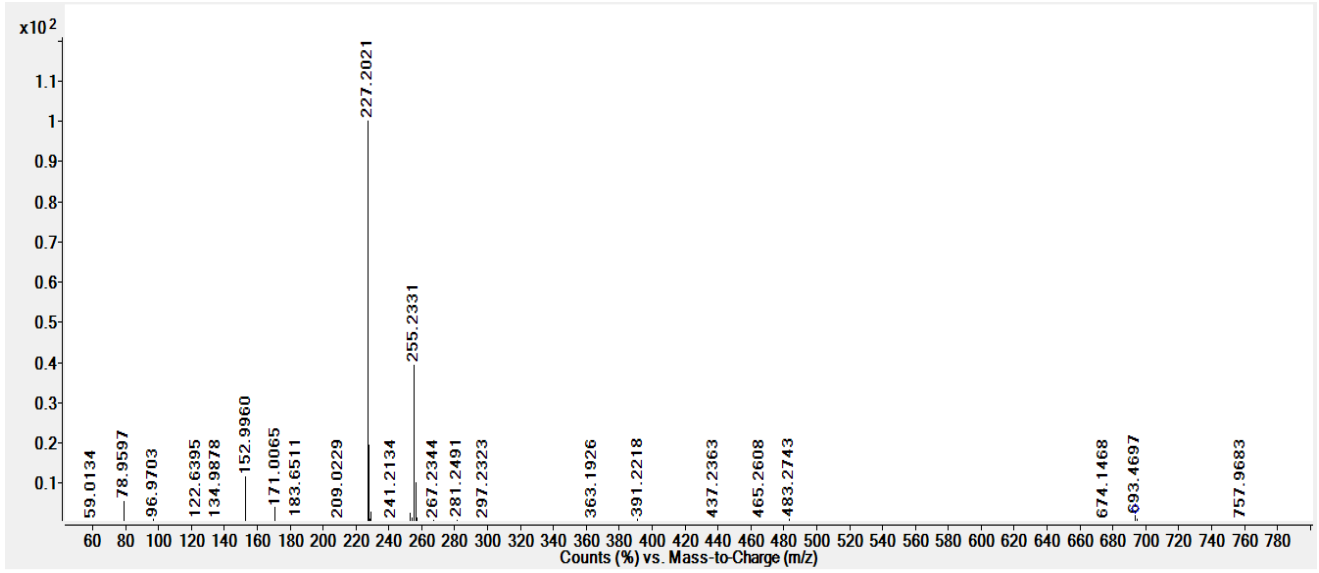
c)



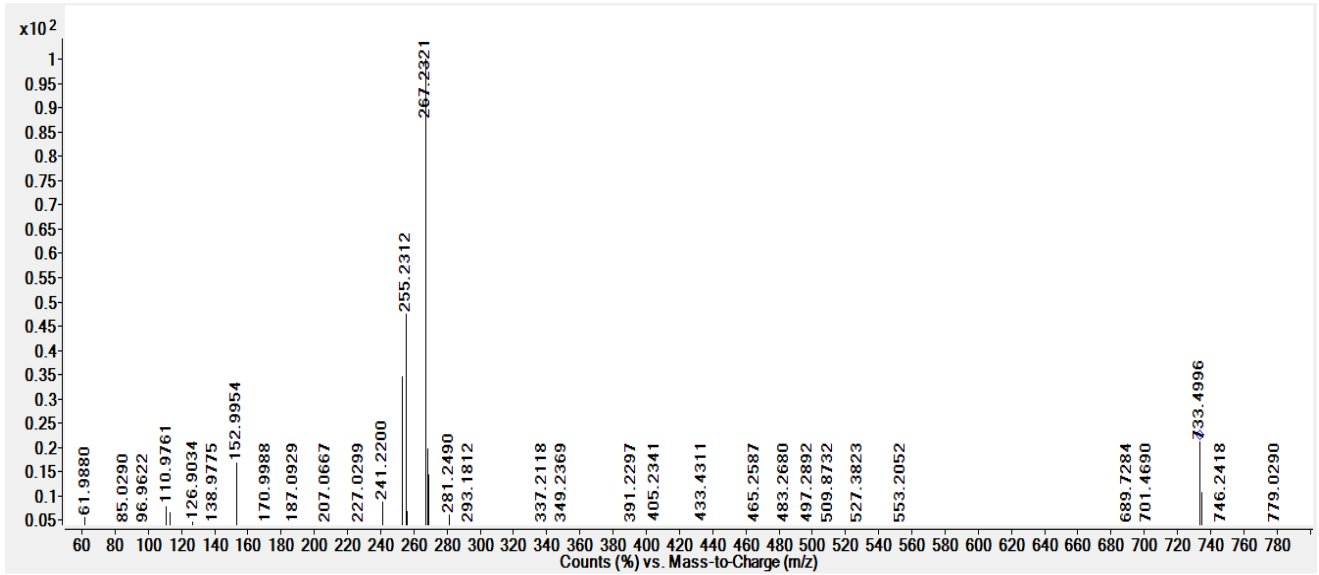
d)



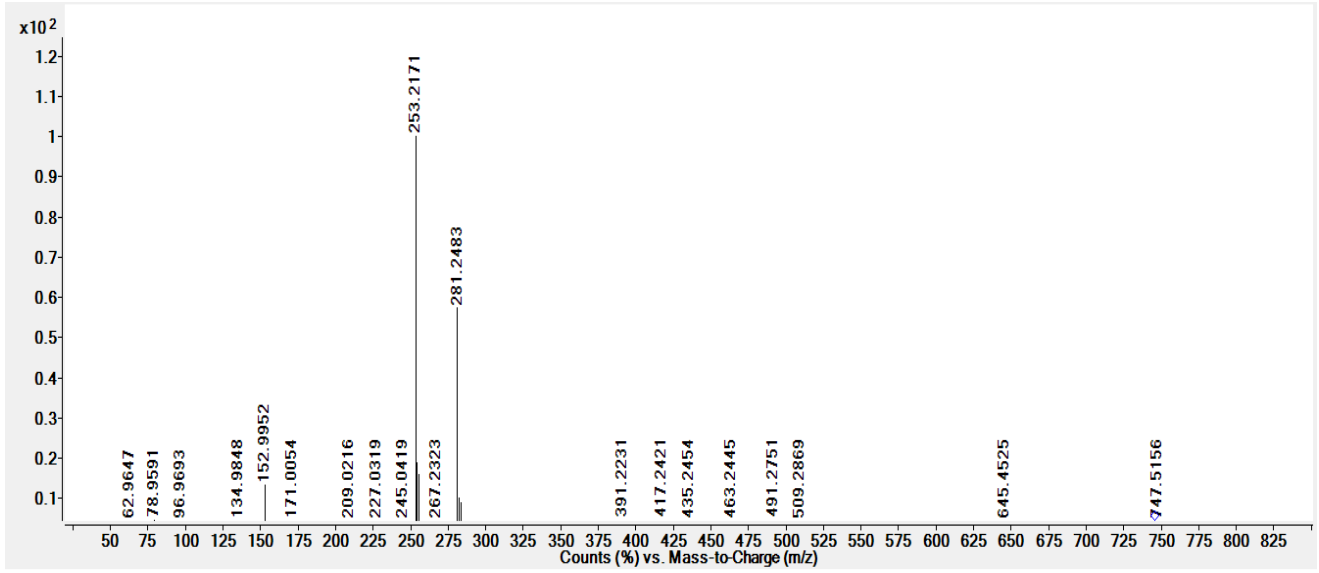
e)



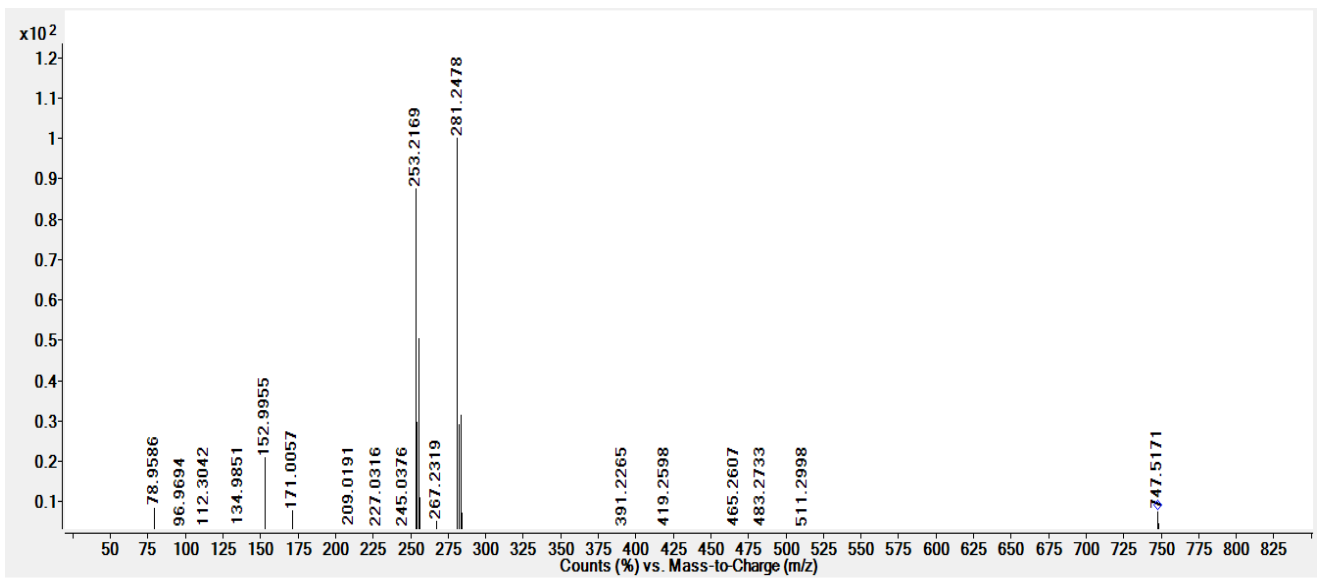
f)



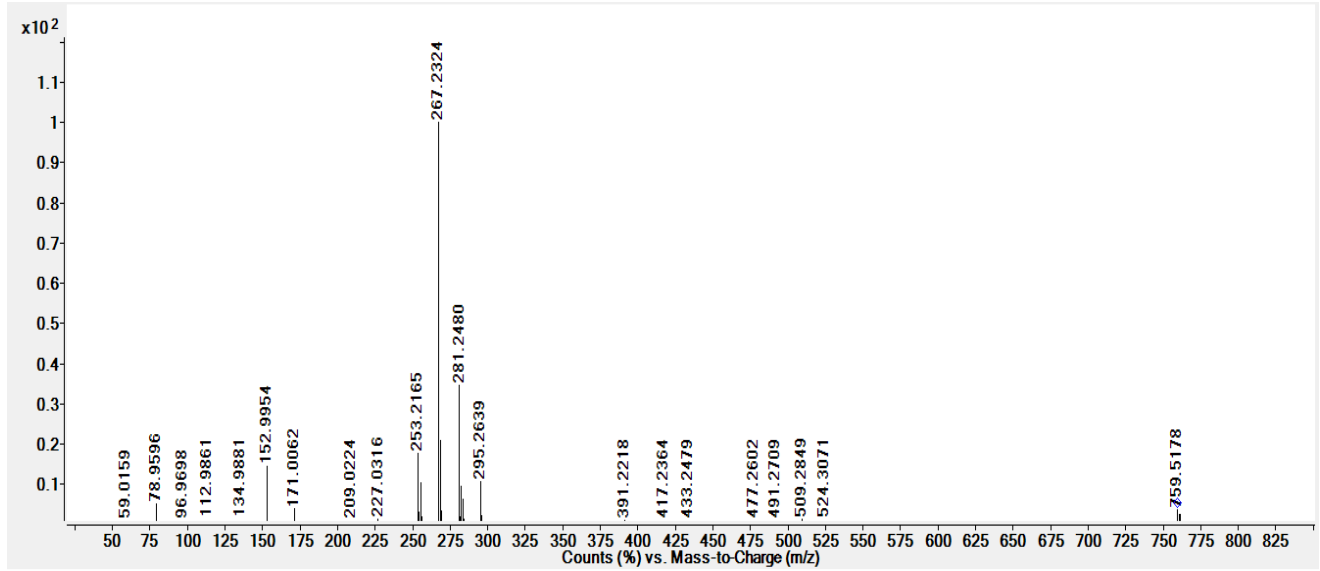
g)



h)



i)



j)

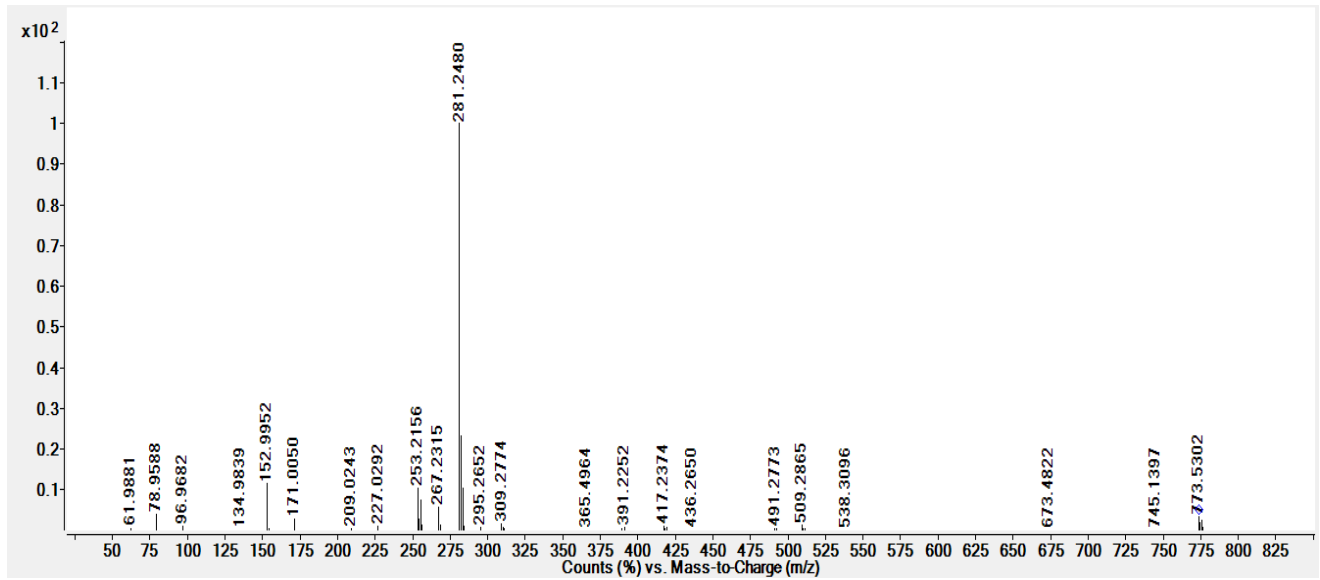
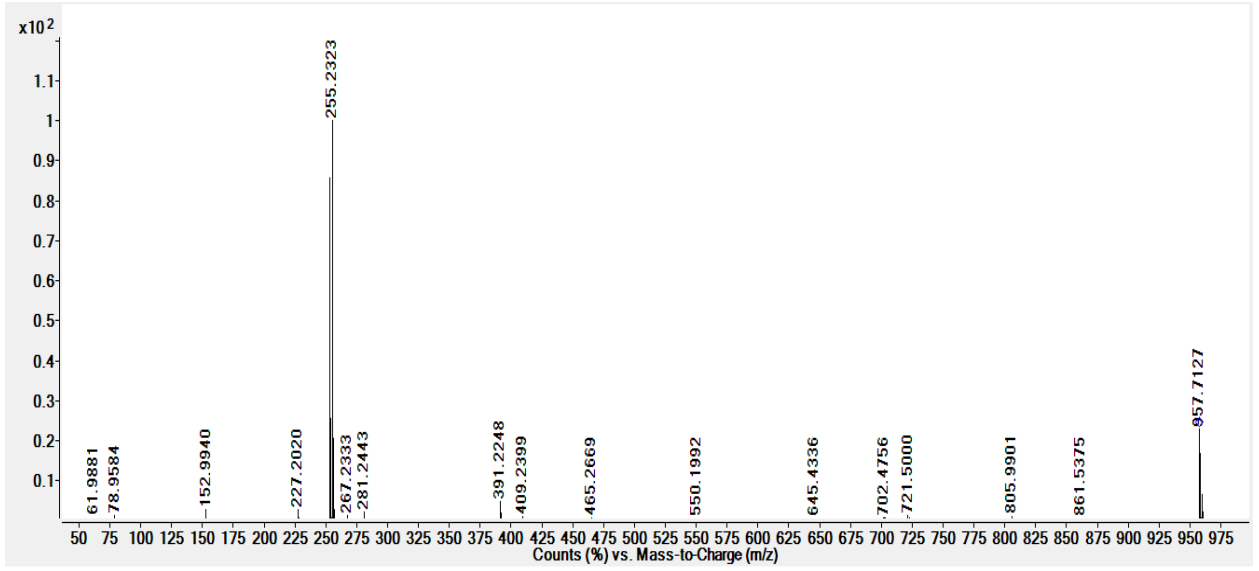


**Figure 5.3 ESI MS-MS (-ve) fragmentation spectra of lipids in fraction C**

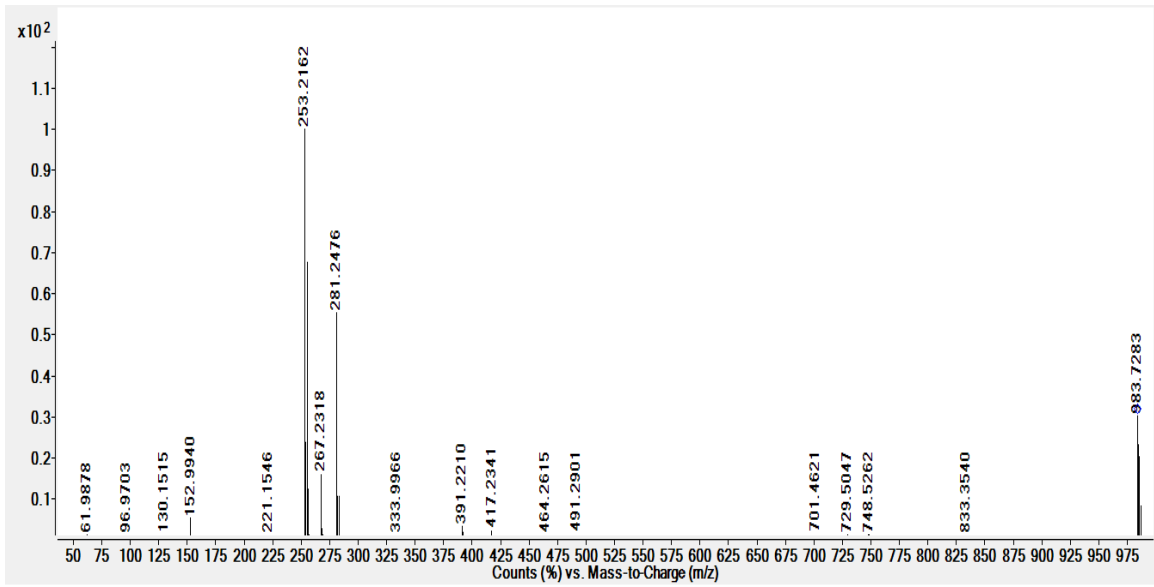
a) m/z 645.4 b) m/z 659.4 c) m/z 688.49 d) m/z 702.50 e) m/z 693.5 f) m/z 733.5 g) m/z 745.5 h) m/z 747.5 i) m/z 759.5 j) m/z 773.5

We have also observed a trace amount of acyl PG ( $m/z$  957.71, 983.72), which has not been identified for any *Serratia* spp. strain before. Hsu et al. (20) reported these lipids in *Salmonella typhimurium*. ESI-MS-MS scan in negative mode for  $m/z$  957.71 and 983.72 is shown in Figure 5.4a and 5.4b. Acyl PG lipids have a unique structure (Figure 5.4c), in which glycerol headgroup contains third fatty acid chain. Hsu et al. reported that the relative abundance of each fatty acid chain has a preference for elimination based on their position similar to PG lipids (20). They reported that the relative abundance of each fatty acyl position in fragmentation analysis in the order  $sn2 > sn3 \gg sn1$ . Using this knowledge, we reported the structure in Table 5.2. However, isobaric interferences (Different lipid structure with same nominal masses) due to presence of other fatty acid chain combinations and trace amount of acyl PG lipid make this assignment difficult and we have tentatively reported acyl PG lipid structures in Table 5.2. We have also confirmed the predicted lipid structures by comparing them with exact mass of predicted molecule (Table 5.3). This is the first attempt to identify fatty acid profile and polar lipids of *IIP* strain using GC-FID and shotgun lipidomics, respectively.

a)



b)



c)

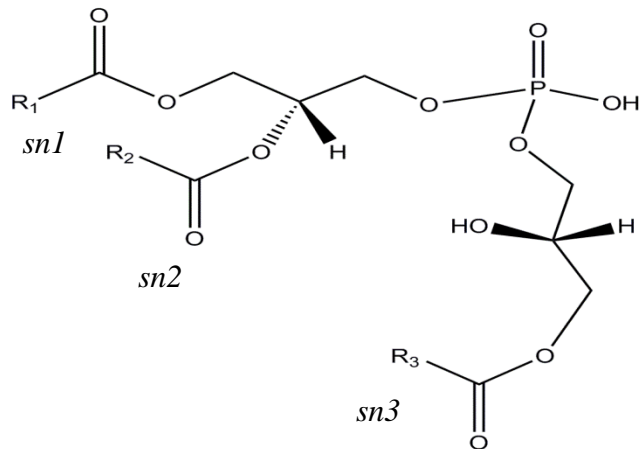


**Figure 5.4 Negative ESI- MS/MS analysis of acyl PG lipid at a)  $m/z$  957.71 b)  $m/z$  983.72 c) Structure of acyl PG lipid.**

[M-H] <sup>-</sup>	Lipid	<i>sn1/sn2/sn3</i>
645.44	PA	C16:1/16:0 C15:0/17:1 C14:0/18:1
659.46	PA	C17:0/16:1 C17:1/16:0 C19:0/14:0 C18:1/15:0
688.49	PE	C16:0/16:1 C15:0/17:1
693.47	PG	C14:0/16:0 C15:0/15:0
702.50	PE	C16:0/17:1 C17:0/16:1
719.48	PG	C16:0/16:1 C15:0/17:1 C18:1/14:0
733.50	PG	C16:0/17:1 C17:0/16:1
745.50	PG	C17:1/17:1 C18:1/16:1
747.51	PG	C17:0/17:1 C16:0/18:1 C18:0/16:1
759.51	PG	C17:1/17:1 C16:1/18:1 C15:1/19:1
773.53	PG	C18:1/18:1 C19:1/17:1 C20:1/16:1
957.71	Acyl PG	C16:1/16:0/16:1
983.72	Acyl PG	C18:1/16:1/16:0

**Table 5.2 lipid composition of major polar lipids from *IIP* strain fraction C**

Type	(M-H) <sup>-</sup>		
	Observed m/z	Exact m/z	Error (ppm)
PG	719.4863	719.4869	0.8
	733.5025	733.5065	5.4
	745.5030	745.5025	0.67
	747.5171	747.5182	1.4
	759.5178	759.5182	0.5
	773.5302	773.5338	4.6
PA	645.4491	645.4487	0.6
	659.4617	659.4657	6.0
Acyl PG	957.7136	957.7160	2.5
	983.7307	983.7316	0.91
PE	688.4893	688.4923	4.35
	702.5067	702.5079	1.70

**Table 5.3: Comparison of observed mass with exact mass of the predicted molecule.**

#### 5.4. Conclusion

We have successfully identified composition of fatty acids and lipids for psychrotolerant *Serratia* spp. strain IIP. Major cellular fatty acids identified from whole cell fatty acid analysis were 16:0 and 16:1. Unsaturated fatty acid contents made up 40% of total fatty acids. Moreover we observed a higher amount of short chain fatty acids (C14-C16) with combined percentage of about 70 % compared to long chain fatty acids (C17-C19). We have identified several PL classes in IIP strain. The major lipid found in the membrane of the IIP strain was PG followed by PA, PE and acyl PG. Most of the polar lipids (PLs) found contained at least one unsaturated fatty acid chain in their structure. While, other strains from *Serratia* spp. *S. liquefaciens* and *S. marcescens* contain PE as major phospholipid and PG as minor lipid with unsaturated fatty acid chains (21). *IIP* strain survived at lower temperatures by producing lipids with unsaturated fatty acids as an adaptation to cold environments. This trend is also observed in other psychrophiles/psychrotolerants. *Asticcacaulis benevestitus* sp. nov., a psychrotolerant contained unsaturated PG as major phospholipid and minor amount of other phospholipids and glycolipids with unsaturated fatty acid molecule (22). Guan et al. reported polar lipids of *C. psychrophilum*, an anaerobic psychrophile. *C. psychrophilum*, contains PG, PE, glycerophosphatidylserine (PS) and cardiolipins with unsaturated fatty acid molecule (23). These adaptations in cell membrane structure lead to steric constraints in lipid bilayer packing, decreasing interactions between headgroups. These changes allow cell membrane to function at lower temperatures by maintaining

membrane fluidity (6, 7, 8), which could be one factor in *IIP* survival at lower temperature.

## 5.5 References

- 1) Correa-Llantén, D. & Blamey, J.M. Isolation and characterization of a *Serratia* sp. strain *IIP*. (Manuscript in progress)
- 2) Morita, R.Y. Psychrophilic Bacteria. *Bacteriol Rev* **39**, 144-167 (1975).
- 3) Russi, M., Buzzini, P., Cordisco, L., Amaretti, A., Sala, M., Raimondi, S., Ponzoni, C., Pagnoni, U.M. & Matteuzzi, D. Growth, lipid accumulation, and fatty acid composition in obligate psychrophilic, facultative psychrophilic, and mesophilic yeasts. *FEMS Microbiol. Ecol.* **69**, 363-372 (2009).
- 4) Grimont, P.A.D., Grimont, F. & Dulong de Rosnay, H.L.C. 1976. Taxonomy of the Genus *Serratia*. *Journal of General Microbiology* **98**, 39-46 (1976).
- 5) Rascoe, J., Berg, M., Melcher, U., Mitchell, F. L., Bruton, B. D., Pair, S. D. & Fletcher, J. Identification, phylogenetic analysis, and biological characterization of *Serratia marcescens* strains causing cucurbit yellow vine disease. *Phytopathology* **93**, 1233-1239 (2003).
- 6) D'Amico, S., Collins, T., Marx, J.C., Feller, G. & Gerday, C. Psychrophilic microorganisms: challenges for life. *EMBO reports* **7**, 385-389 (2006).
- 7) Konings, W.N., Albers, S.V., Koning, S. & Driessen, A.J.M.,. The cell membrane plays a crucial role in survival of bacteria and archaea in extreme environments. *Antonie van Leeuwenhoek* **81**, 61-72 (2002).
- 8) Chintalapati, S., Kiran, M.D. & Shivaji, S. (2004). Role of membrane lipid fatty acids in cold adaptation. *Cell Mol Biol (Noisy-le-grand)* **50**, 631-642 (2004).
- 9) Rilfors, L., Wieslander, A. & Stahl, S. Lipid and protein composition of membranes of

*Bacillus megaterium* variants in the temperature range 5 to 70°C. *Journal of Bacteriology* **135**, 1043-1052 (1978).

10) Gilbert, J.A., Hill, P.J., Dodd, C.E. & Laybourn-Parry, J. Demonstration of antifreeze protein activity in Antarctic lake bacteria. *Microbiology* **150**, 171-180 (2004).

11) Johns, G.C. & Somero, G.N. (2004). Evolutionary convergence in adaptation of proteins to temperature: A4-lactate dehydrogenases of Pacific damselfishes (*Chromis* spp.). *Mol Biol Evol* **21**, 314-320 (2004).

12) Violot, S., Aghajari, N., Czjzek, M., Feller, G., Sonan, G.K., Gouet, P., Gerday, C., Haser, R. & Receveur-Brechot, V. Structure of a full length psychrophilic cellulase from *Pseudoalteromonas haloplanktis* revealed by X-ray diffraction and small angle X-ray scattering. *J Mol Biol* **348**, 1211-1224 (2005).

13) Saunders, N.F *et al.* Mechanisms of thermal adaptation revealed from the genomes of the Antarctic Archaea *Methanogenium frigidum* and *Methanococoides burtonii*. *Genome Res* **13**, 1580–1588 (2003).

14) Khachane, A.N., Timmis, K.N. & dos Santos, V.A. Uracil content of 16S rRNA of thermophilic and psychrophilic prokaryotes correlates inversely with their optimal growth temperatures. *Nucleic Acids Res* **33**, 4016-4022 (2005).

15) Lo, S.L. & Chang, E.L. Purification and characterization of a liposomal forming tetraether lipid fraction. *Biochem. Biophys. Res. Commun.* **167**, 238–243 (1990).

16) Sasser, M., *Bacterial identification by gas chromatographic analysis of fatty acids methyl esters (GC-FAME)*. (Technical note for MIDI, Microbial ID Inc., 2006)

- 17) Oursel, D., Loutelier-Bourhis, C., Orange, N., Chevalier, S., Norris, V. & Lange, C.M. Lipid composition of membranes of *Escherichia coli* by liquid chromatography/tandem mass spectrometry using negative electrospray ionization. *Rapid Commun. Mass Spectrom.* **21**, 1721-1728 (2007).
- 18) Hsu, F.F. & Turk, J. Studies on phosphatidylglycerol with triple quadrupole tandem mass spectrometry with electrospray ionization: fragmentation processes and structural characterization. *J. Am. Soc. Mass Spectrom.* **12**, 1036-1043 (2001).
- 19) Hsu, F.F. & Turk, J. Characterization of phosphatidylethanolamine as a lithiated adduct by triple quadrupole tandem mass spectrometry with electrospray ionization. *J. Mass Spectrom.* **35**, 595-606 (2000).
- 20) Hsu, F.F., Turk, J., Shi, Y. & Groisman, E.A. Characterization of acylphosphatidylglycerols from *Salmonella typhimurium* by tandem mass spectrometry with electrospray ionization. *J. Am. Soc. Mass Spectrom.* **15(1)**, 1-11 (2004).
- 21) Aluyi, H.S., Boote, V., Drucker, D.B., Wilson, J.M. & Ling, Y.H., Analysis of polar lipids from some representative enterobacteria, *Plesiomonas* and *Acinetobacter* by fast atom bombardment-mass spectrometry. *Journal of Applied Bacteriology* **73(5)**, 1365-2672 (1992).
- 22) Vasilyeva, L., Omelchenko, M., Berestovskaya, Y., Lysenko, A., Abraham, W., Dedysh, S. & Zavarzin, G., 2006. *Asticcacaulis benevestitus* sp. nov., a psychrotolerant, dimorphic, prosthecate bacterium from tundra wetland soil. *Int J Syst Evol Microbiol* **56(9)**, 2083-2088 (2006).

23) Guan, Z., Tian, B., Perfumo, A., & Goldfine, H. 2013. The polar lipids of *Clostridium psychrophilum*, an anaerobic psychrophile. *Biochimica et Biophysica Acta* **1831(6)**, 1108-1112 (2013).

## CHAPTER

# 6. LIPID COMPOSITION OF THERMOPHILIC *ANOXYBACILLUS* SP. STRAIN 7L, ISOLATED FROM CHILEAN COPAHUE VOLCANO

*(Note: Content of this Chapter is adapted from the submitted manuscript “Siddharth P. Shah, Susan A. Jansen , Sean P. Lawrence, Parkson Lee-Gau Chong, Daniela N. Correa-Llantén, Francisca Contreras, Jenny M. Blamey. Lipid Composition of Thermophilic Anoxybacillus sp. Strain 7L, Isolated from Chilean Copahue Volcano )*

### 6.1 Introduction

Active Copahue Volcano is located in the northwest corner of Neuquén province in Argentina, in the northern Patagonian Cordillera bordering Chile. It is an excellent source to study biodiversity because of varying temperature conditions (6-87°C) and acidic environment (pH 1.0-4.8) (1). A few interesting microbes have been isolated from Copahue geothermal area. As an example, a novel species ALE1 in the genus *Acidianus* was found to be able to use both iron and sulfur compounds with different oxidation states. This organism can grow both hetero and auto-trophically, dependent and independent of oxygen. Such growth flexibility may be related to the biogeochemical sulfur and iron cycling in Copahue geothermal area (2).

In the present study, we focus on the microorganism 7L, which is a strain recently isolated from a hot spring in Copahue Volcano, Chile (3). The analysis of the 16S ribosomal RNA indicates that this microorganism belongs to the genus *Anoxybacillus* (3)

belonging to the *Bacillaceae* family (4). The cells of *Anoxybacillus* sp. 7L are Gram-positive, rod-shaped, motile, facultative anaerobe, and they form endospores. The 7L strain is moderately thermophilic and alkalitolerant; and it grows at the temperature range from 40 to 60°C and at pH 5.0 to 8.0. Optimum growth was observed at 58°C and pH 7.0 (3).

In this paper we have reported, for the first time, the lipid and fatty acid content of *Anoxybacillus* sp. strain 7L. Using GC-FAME analysis, we found that the major fatty acid content of the 7L strain includes 15:0 iso 52.3%, 17:0 iso 18.7 %, 16:0 7%, 17:0 anteiso 5.3%, 15:0 anteiso 4.2%, and 16:0 iso 4%. Through shotgun lipidomics we have mainly observed CL, PG, PE and PA lipids. We compare the results with the polar lipid profile of known *Anoxybacillus* strains from other geochemical areas.

## **6.2 Materials and Methods**

### **6.2.1 Cell growth**

The microorganism was grown on PAE2 medium on static mode, at 58°C and pH 7.0. The medium contains xylan 0.7% (w/v), yeast extract 0.2% (w/v), NaCl 0.25% (w/v), NH<sub>4</sub>Cl 0.5% (w/v), KH<sub>2</sub>PO<sub>4</sub> 0.15% (w/v), K<sub>2</sub>HPO<sub>4</sub> 0.3% (w/v), MgSO<sub>4</sub> 0.0025% (w/v) (3).

### **6.2.2 Materials**

HPLC grade acetonitrile, water, chloroform, methanol and formic acid were obtained from either Sigma (St. Louis, MO, USA) or Fisher Scientific (Waltham, MA, USA). All chemicals were used as received.

### 6.2.3 Extraction of polar lipids

Total polar lipids were extracted by the method of Lo and Chang (5). In brief, dried cells (143.8 mg) were soxhlet-extracted with chloroform/methanol (1:1, v/v) for 24 h. The crude lipids were fractionated by reversed-phase column chromatography using C-18 PrepSep columns (Fisher Scientific, Fair Lawn, NJ) eluted first with methanol: water (1:1, v/v) (filtrate A) and then with chloroform: methanol: water (0.8:2:0.8, v/v/v) (filtrate B). Filtrate B was further separated by thin-layer chromatography (TLC) using chloroform: methanol: water (65:25:4, v/v/v) as the solvent system. Four bands were detected after iodide vapor exposure (Figure 6.1). The  $R_f$  values of those fractions are: 0.493 for fraction I, 0.635 for fraction II, 0.736 for fraction III, 0.970 for fraction IV. These four bands were scraped and extracted with chloroform: methanol: water (5:10:4, v/v/v). All four fractions were collected, evaporated to dryness under nitrogen, and stored at -20 °C before structure analysis.

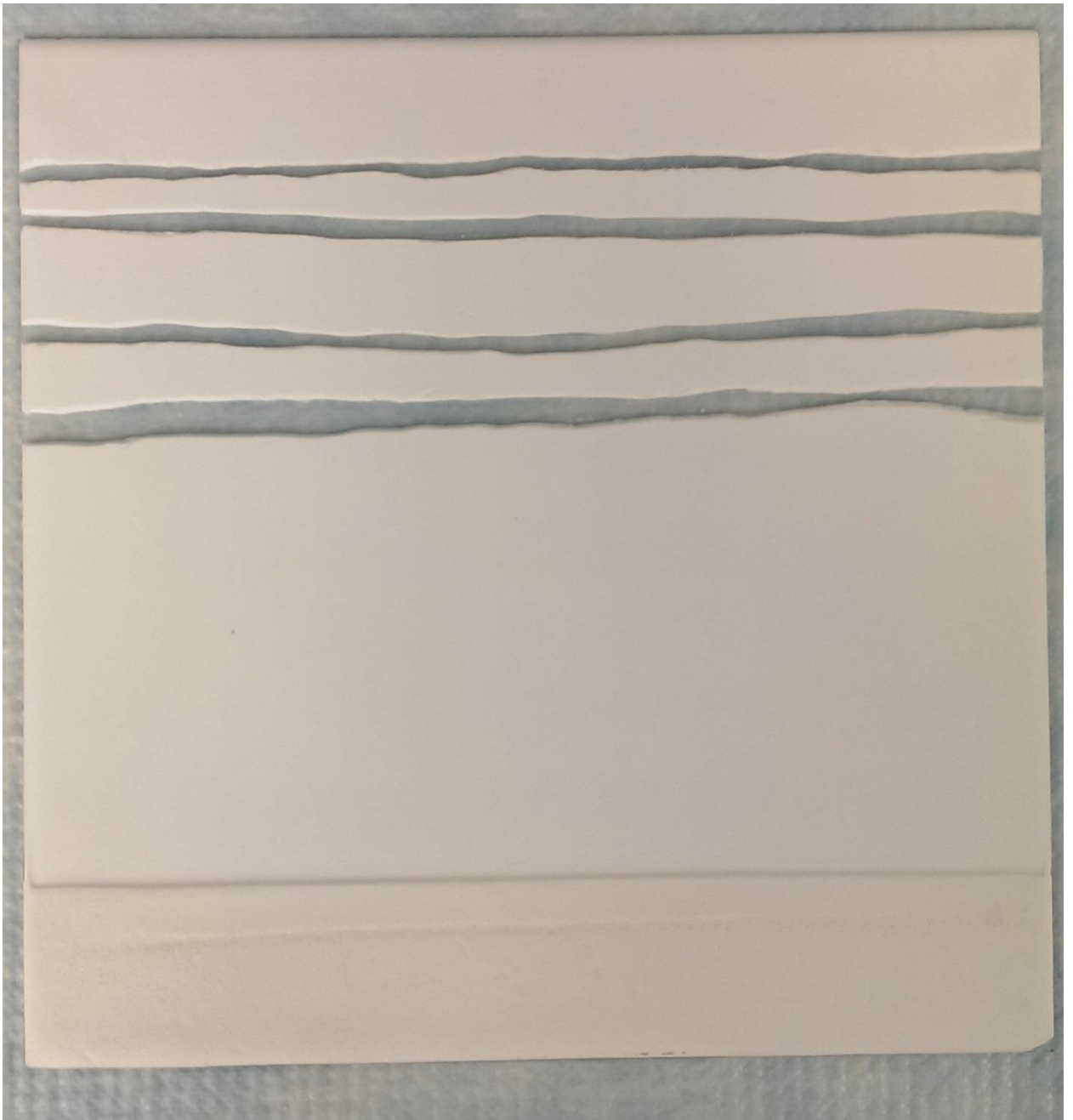


**Figure 6.1: Thin layer chromatography of lipids extracted from 7L strain.**

#### **6.2.4 Gas Chromatography**

FAME analysis was performed by following instructions of Microbial Identification System (MIDI, Microbial ID Inc.) (6). In brief, 1 ml of reagent 1 (45 g sodium hydroxide, 150 ml methanol, and 150 ml distilled water) was added to freeze dried bacterial cells to cleave fatty acids from lipids. Addition of 2 ml of reagent 2 (325 ml certified 6.0 N hydrochloric acid and 275 ml methyl alcohol) caused methylation of cleaved fatty acids. FAMEs were extracted using 1.25 ml of reagent 3 (200 ml hexane and 200 ml methyl tert-butyl ether). Obtained sample was further cleaned with reagent 4 (10.8 g NaOH dissolved in 900 ml distilled water). About 2/3 of the organic phase was pipetted and injected into Agilent 6890 Gas Chromatography system coupled with flame ionization detector (FID). A 25m × 0.2mm phenyl methyl silicone fused capillary column was used for separation by using temperature program, which increases from 170 °C to 270 °C at 5 °C per minute. Sherlock MIS data analysis software was used to qualify and quantify FAME peaks.

#### **6.2.5 Mass Spectrometry**

Portion of each sample was transferred to separate Eppendorf tube and was evaporated to dryness under nitrogen. About 1 mg fraction was dissolved in methanol and used for experiment. ESI/MS analyses were performed on Agilent 1200 LC-6520B Q-TOF high resolution Mass Spectrometer with Dual ESI as ion source in both positive and negative ionization mode. About 15 µl sample was injected with Agilent 1200 G1376B HiP autosampler. Full scan spectra were obtained by scanning masses between 100-1000 m/z. Other parameters were set as follows: sheath gas temperature, 300 °C; sheath gas flow, 5

l/min; nebulizer, 30 psi; and capillary entrance voltage, 3500 V. Fragmentor and skimmer1 were operated at 150 V and 65 V, respectively. The MS scan data were collected at a rate of 1 spectra/s in range of 100-1500 m/z. In the targeted MS/MS mode, the MS and the MS/MS information were collected in the 50-1500 m/z range at the same rate as the MS scan and the collision energy was 25-35 V. All the MS and MS/MS data were collected with MassHunter Data Acquisition (Agilent) and MassHunter Qualitative Analysis B.02.00 (Agilent) was applied to identify lipid species.

## **6.3 Results and Discussion**

### **6.3.1 Gas Chromatography**

Gas chromatography provided valuable information about fatty acid chain length and their proportions in 7L strain (Table 1). Fatty acid analysis revealed that strain 7L synthesized mainly iso- and anteiso-branched saturated fatty acids. The major cellular fatty acids identified from whole cell fatty acid analysis were iso-15:0 (52.29 %), iso-17:0 (18.64 %), 16:0 (7 %), anteiso-17:0 (5.30 %) and anteiso-15:0 (4.17 %). Total percentage of iso-branched fatty acids was about 80 % of the total fatty acids and anteiso-branched fatty acids comprised about 10 % of the total fatty acids. Fatty acid profile obtained was similar to that of other strains within the same genus (7). The major fatty acid of strain 7L and other strains from same genus *A. ayderensis*, *A. flavithermus* and *A. gonensis* was iso-15:0, followed by iso 17:0 (7).

<b>Fatty Acid</b>	<b>% Composition</b>
Iso-13:0	0.12
Iso-14:0	0.39
14:0	1.34
Iso-15:1	0.10
Iso-15:0	52.29
Anteiso-15:0	4.17
15:0	0.41
Iso-16:1	0.16
Iso-16:0	3.57
16:1( $\omega$ 7)	1.28
16:1( $\omega$ 6)	0.76
16:1( $\omega$ 5)	0.12
16:0	7.00
Iso-17:1 ( $\omega$ 5)	1.30
Anteiso-17:1	0.29
Iso-17:0	18.64
Anteiso-17:0	5.30
17:0	0.15
Iso-18:0	0.11
Iso-18:1 ( $\omega$ 9)	1.21
Iso-18:1 ( $\omega$ 7)	0.33
18:0	0.68
Iso-19:0	0.22

**Table 6.1: Whole cell fatty acid Profile for 7L strain**

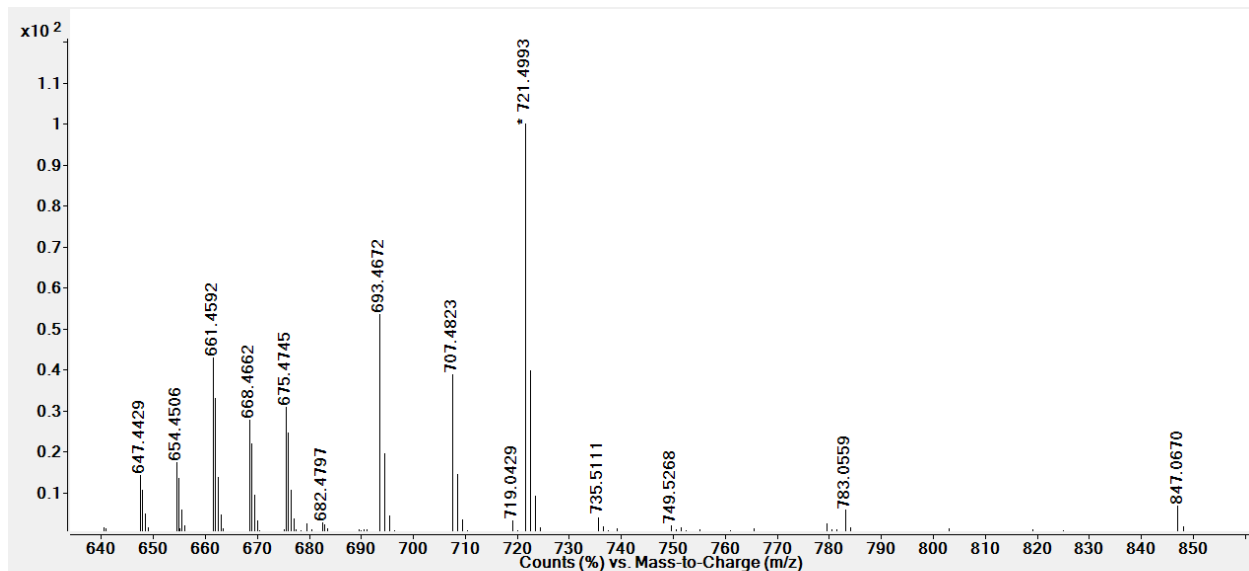
### **6.3.2 Mass Spectrometry**

Mass spectrometry analysis of extracted fractions revealed PA, PG, PE and CL type of lipids. Result of mass spectrometry is summarized in table 6.2. The ESI full scan mass spectrum of fraction II (figure 6.2), obtained with LC-6520B Q-TOF high resolution Mass Spectrometer in the negative ion mode showed presence of several lipid molecules.

	[M-H] <sup>-</sup>	[M+Na] <sup>+</sup>	Lipid	Proposed structure <i>sn1/sn2</i>
Fraction 2	647.46		PA	C17:0/15:0 C16:0/16:0 C18:0/14:0
	693.47		PG	C16:0/14:0 C15:0/15:0
	721.50		PG	C17:0/15:0 C16:0/16:0
	707.49		PG	C16:0/15:0 C17:0/14:0
	735.52		PG	C17:0/16:0 C18:0/15:0 C19:0/14:0
	749.53		PG	C17:0/17:0 C18:0/16:0 C20:0/14:0 C19:0/15:0
	1323.94		CL	C17:0/15:0, C16:0/14:0 (647,619)
	1309.93		CL	
	1337.96		CL	C17:0/15:0, C16:0/15:0 (647,633) C17:0/16:0, C16:0/14:0 (661,619)
	1351.98		CL	C15:0/17:0, C15:0/17:0 (647,647) C17:0/16:0, C15:0/16:0 (661,633)
Fraction 3	647.4573		PA	C17:0/15:0 C16:0/16:0
	633.4481		PA	C14:0/17:0 C15:0/16:0
	662.4733	686.4706	PE	C15:0/15:0 C14:0/16:0
	676.4878	700.4916	PE	C16:0/15:0 C14:0/17:0
	690.5018	714.5075	PE	C17:0/15:0 C16:0/16:0

**Table 6.2 Lipid analysis and lipid composition of major phospholipids from 7L strain fraction II and III**

a)



b)

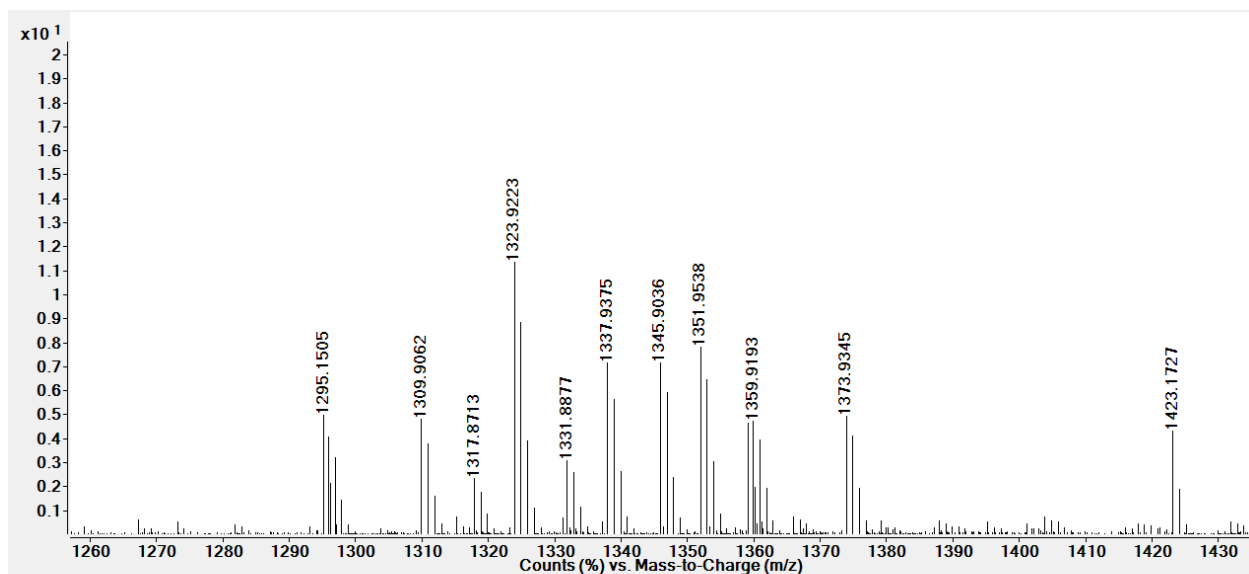
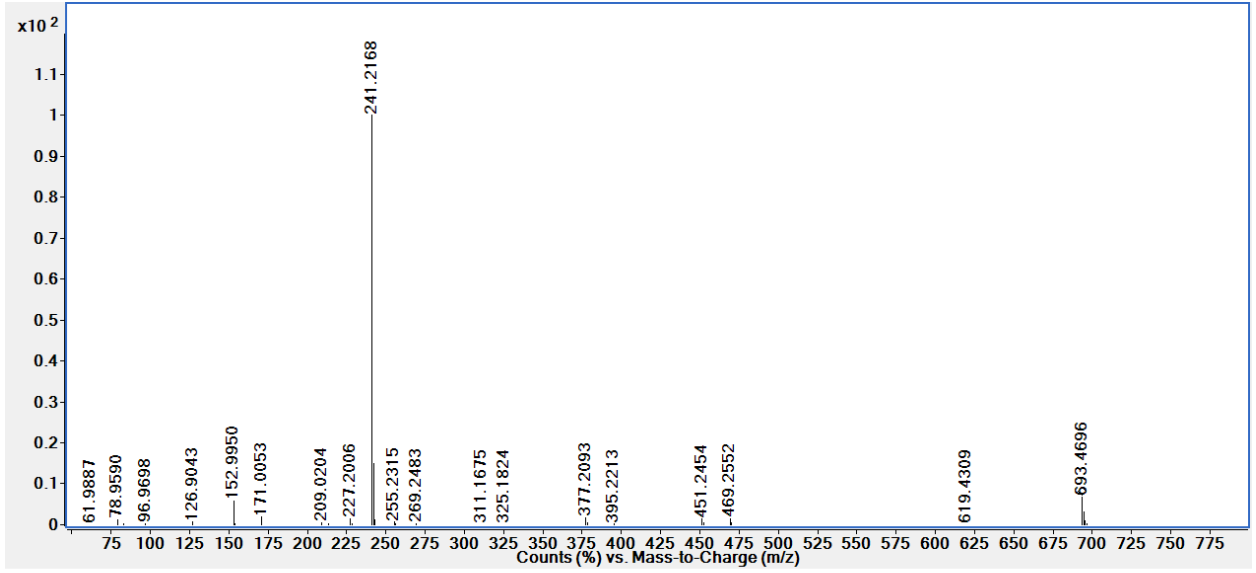


**Figure 6.2: Negative ESI-MS spectrum of fraction II a) Shows region from m/z range 600-900 b) Shows region from m/z range 1200-1450**

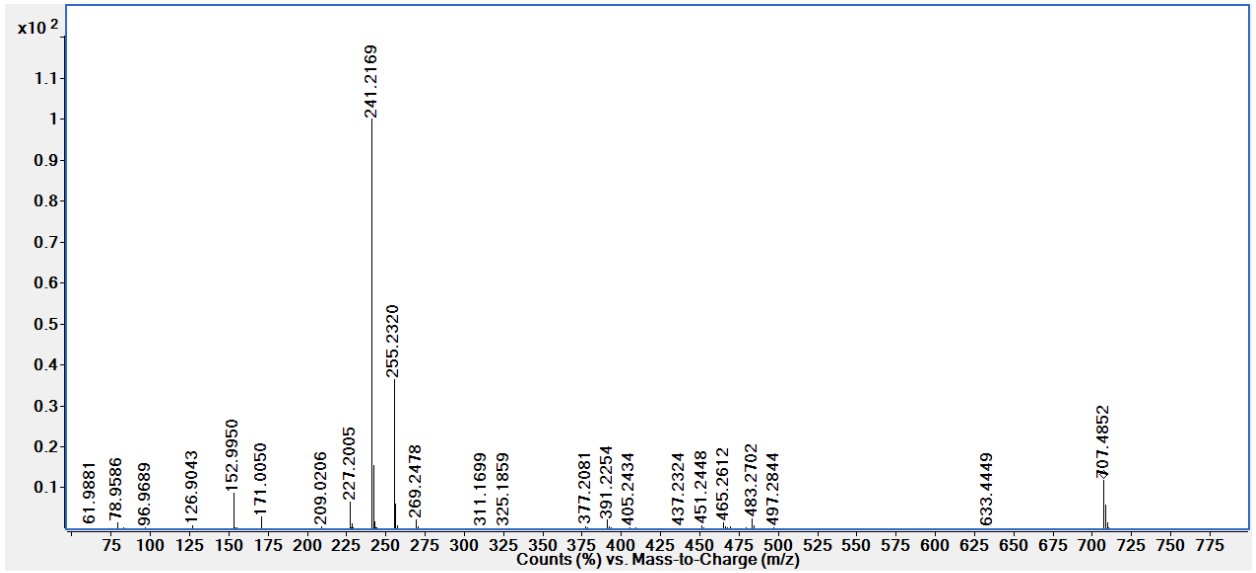
Mainly, we observed presence of  $[M-H]^-$  ions at  $m/z$  693.47, 707.49, 721.50, 735.52, and 749.53 (figure 6.3) which indicated presence of glycerophosphoglycerol (PG) lipids. We have confirmed this assignment using fragmentation characterization of individual molecules.

PG molecule ( $m/z$  721.50) fragmentation analysis (Figure 6.3c) showed fragments at  $m/z$  241.21 (C15:0) and  $m/z$  269.24 (C17:0) which are fatty acid molecules  $R_2-COO^-$  and  $R_1COO^-$  ions, respectively (8, 9). Higher abundance of one fatty acid over another indicates sterically favorable elimination of one over another and this helps us to identify their relative position in individual lipids. Higher abundance of C15:0 compared to C17:0 indicates that the latter is a fragment from the *sn*1 position (8, 9).  $[M-H-R_2CHCO]^-$  (497.28) and  $[M-H-R_2CHCO-H_2O]^-$  (479.27). Ions result from ketene elimination followed by neutral loss of water. Lower abundance of  $[M-H-R_1CHCO-H_2O]^-$  (451.24) also confirms preferred elimination of ketene from the *sn*2 position. Additional ions include  $m/z$  647.46 which forms after neutral loss of 74  $-C_3H_6O_2$ /glycerol moiety. After losing glycerol structure remaining ion looks similar to glycerophosphate (PA) lipid class, which further loses fatty acid molecule as acid rather than ketene which is confirmed by higher abundance of  $m/z$  405  $[M-H-74- R_2COOH]^-$  compared to  $m/z$  423  $[M-H-74-R_2CHCO]^-$  (8,9). Similarly we have identified other PG lipids from fragmentation analysis.

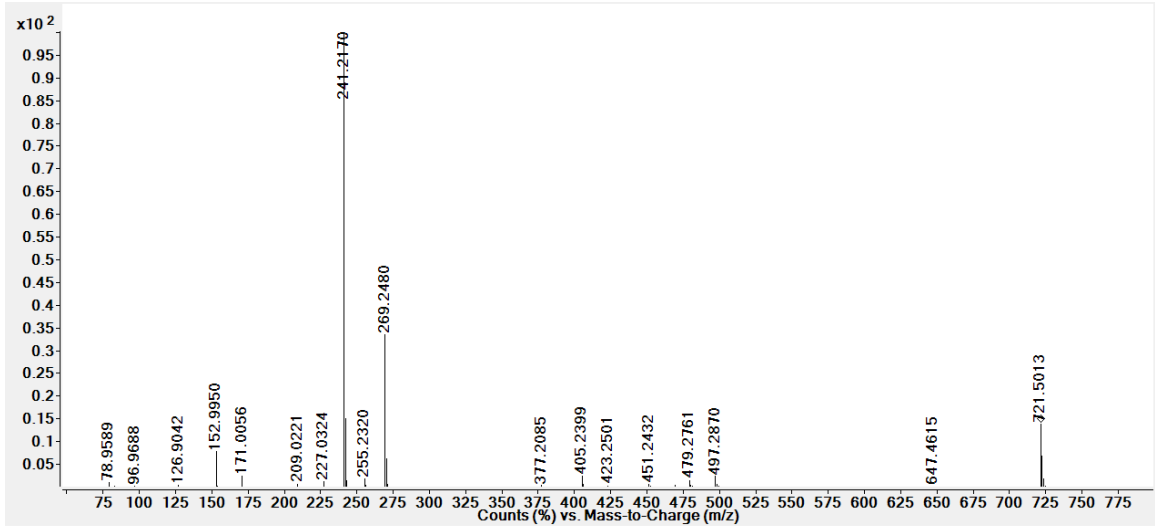
a)



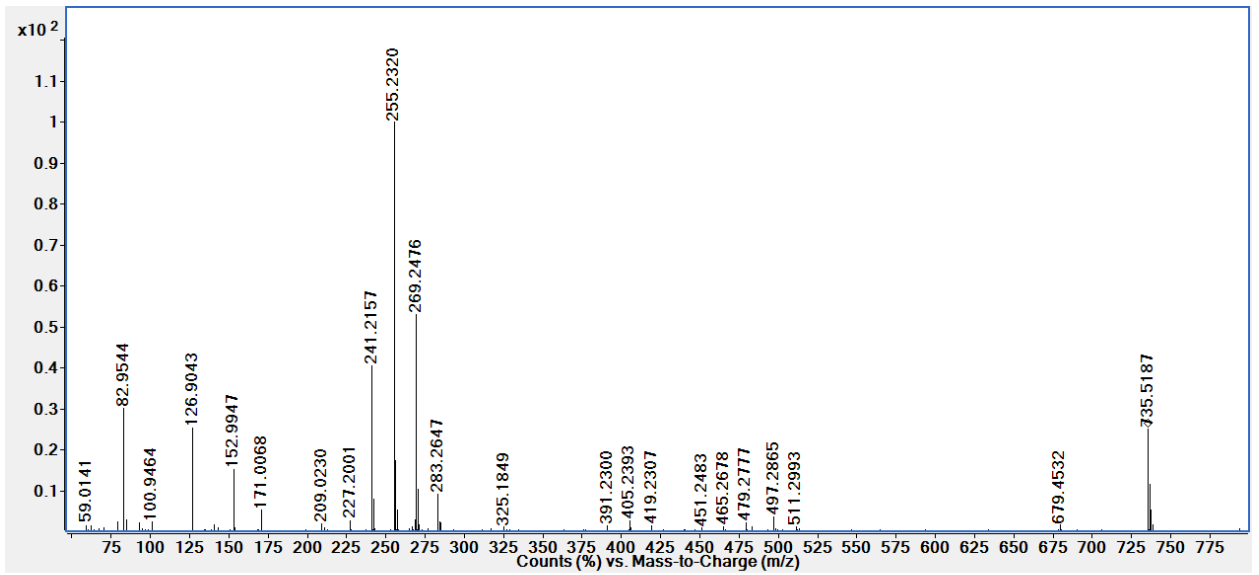
b)



c)



d)



e)

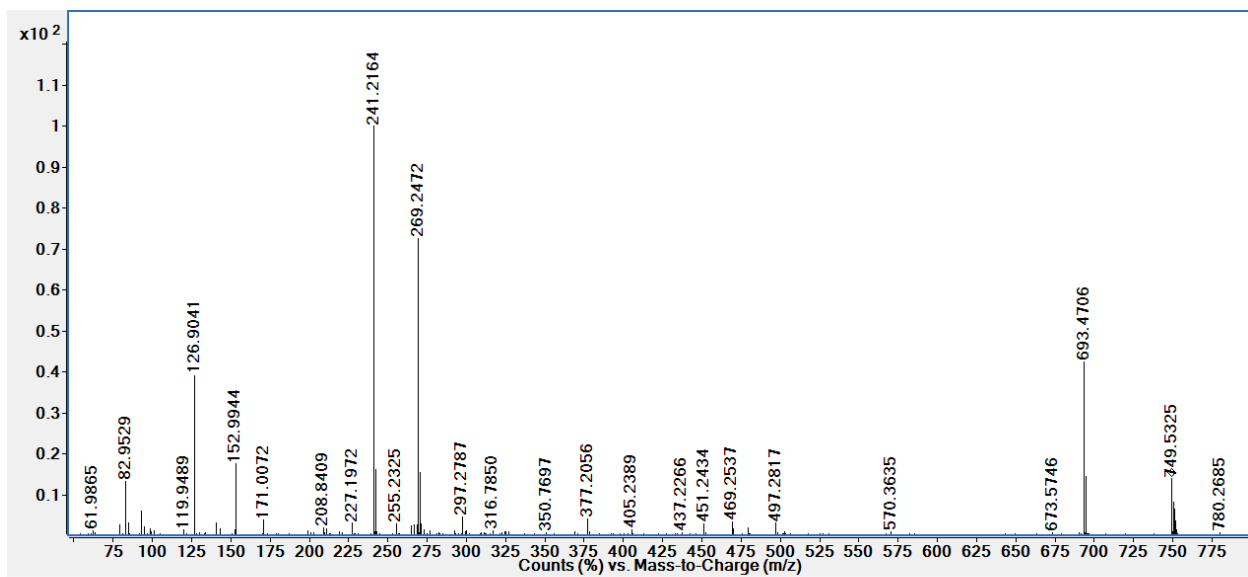


**Figure 6.3 ESI MS-MS (-ve) fragmentation spectra of PG lipids**

a) m/z 693.47, b) m/z 707.49, c) m/z 721.50 c) m/z 735.52, and d) m/z 749.53

We have also observed cardiolipins in fraction II at  $m/z$  1309.93, 1323.94, 1337.96 and 1351.98. MS-MS fragmentation spectra for these lipids are shown in figure 6.4 and figure 6.5. Cardiolipins follow complex and characteristic fragmentation pattern in tandem mass spectrometry (10). There are two major pathways for fragmentation of cardiolipins at  $m/z$  1323.9 (Figure 4a).

1) Formation of daughter ions  $m/z$  619.43 (a) and 647.46 (b) comes from  $m/z$  755 and 783 daughter ions, respectively by neutral loss of 136 as a tricyclic glycerophosphate ester moiety. Daughter ions  $m/z$  619.43 and  $m/z$  647.46 have structures similar to glycerophosphate (PA) lipid class and follow the fragmentation pattern similar to PA lipids (10).

2) Formation of phospholipid molecule with cyclic glycerol structure which undergoes fragmentation similar to glycerophosphoethanolamine (PE) lipids (losing fatty acyl chain as ketene rather than acid), and generates characteristic daughter ions at  $a+56$  ( $m/z$  675) and  $b+56$  ( $m/z$  703) (10).

Isobaric interferences (different lipid structures with same nominal masses) have made the assignment of *sn1* and *sn2* position difficult for cardiolipins. We have also observed a trace amount of PA lipids (confirmed with fragmentation analysis) as  $m/z$  647.46 in fraction II. (Figure 6.6)

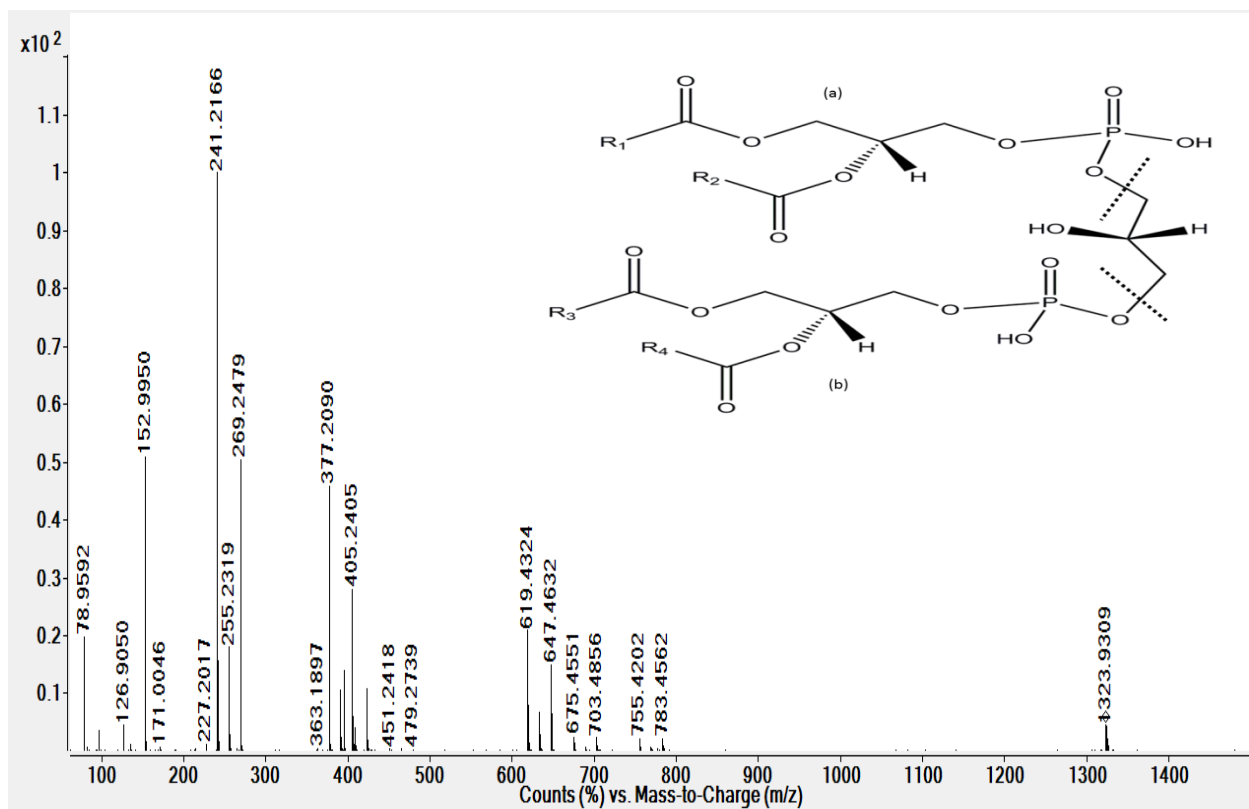
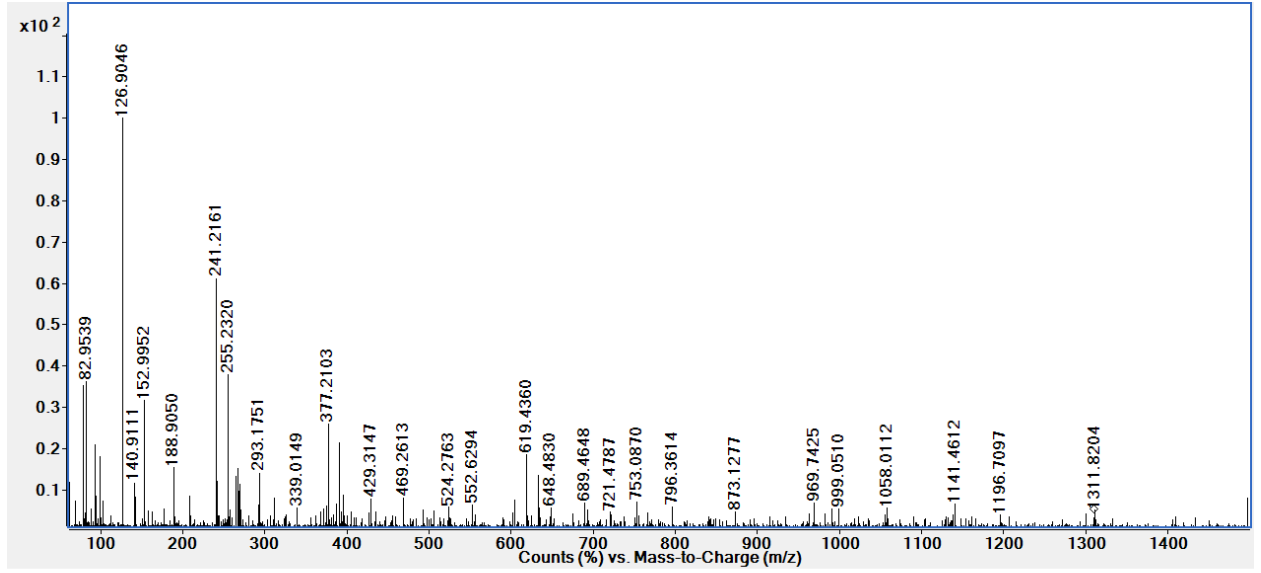
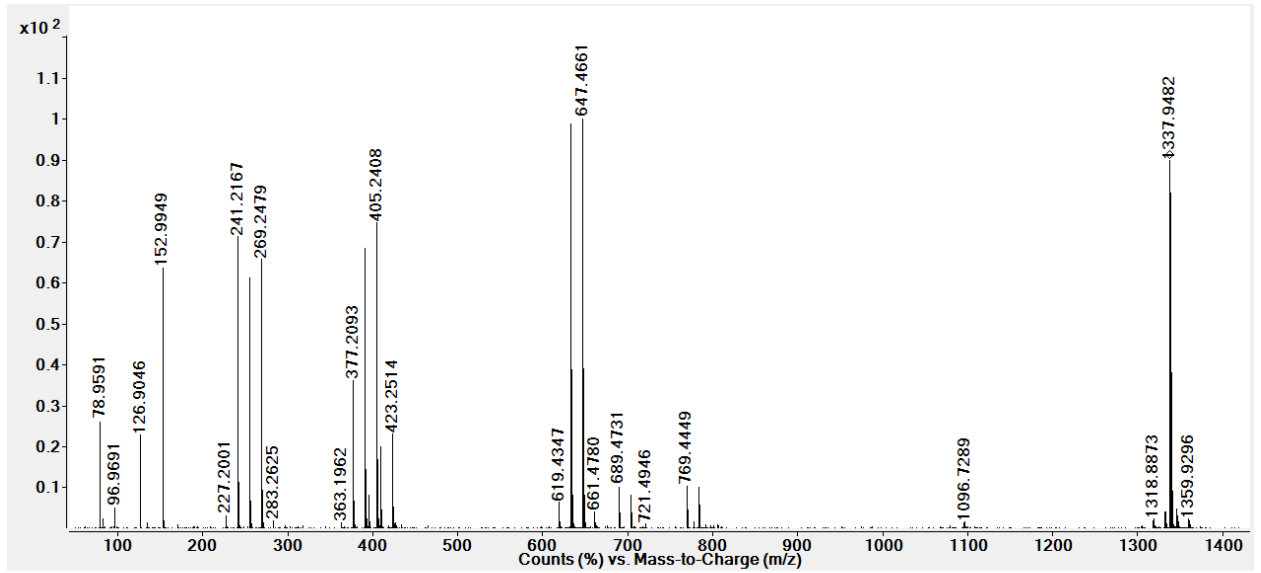


**Figure 6.4 Negative ESI- MS-MS analysis of Cardiolipin lipid at  $m/z$  1323.9**

a)



b)



c)

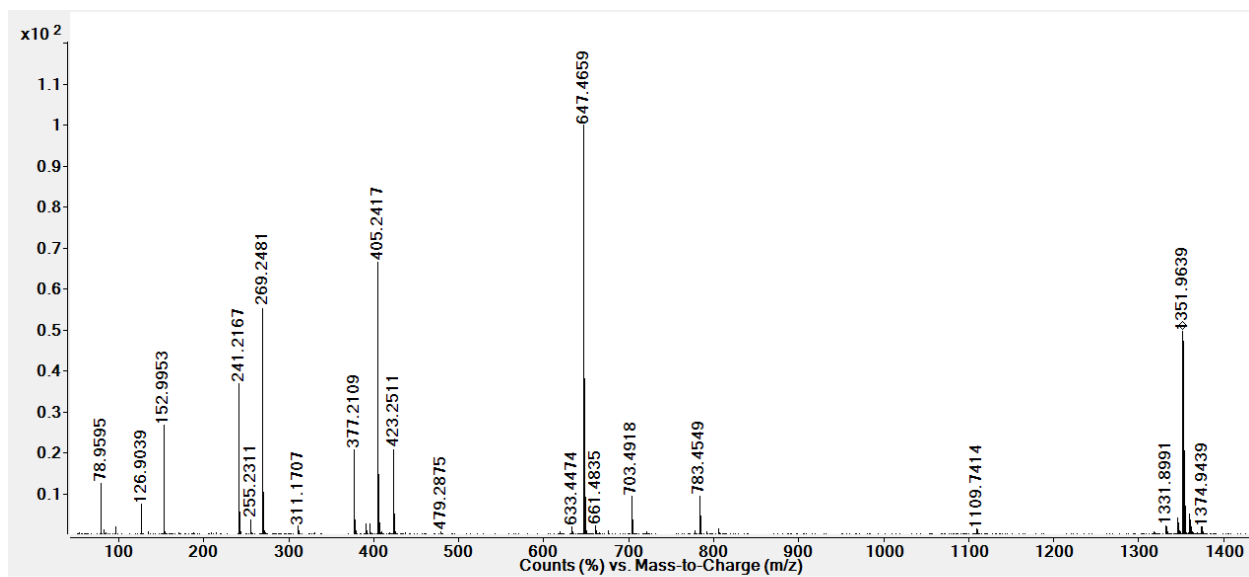


**Figure 6.5 ESI MS-MS (-ve) fragmentation spectra of cardiolipin lipids**  
a) 1309.93, b) 1337.96 and c) 1351.98

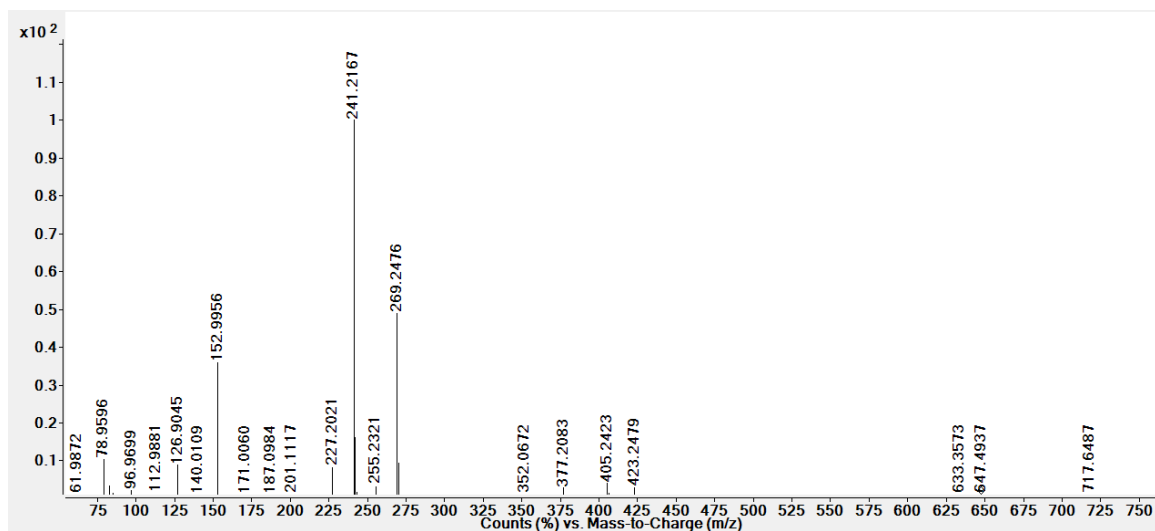
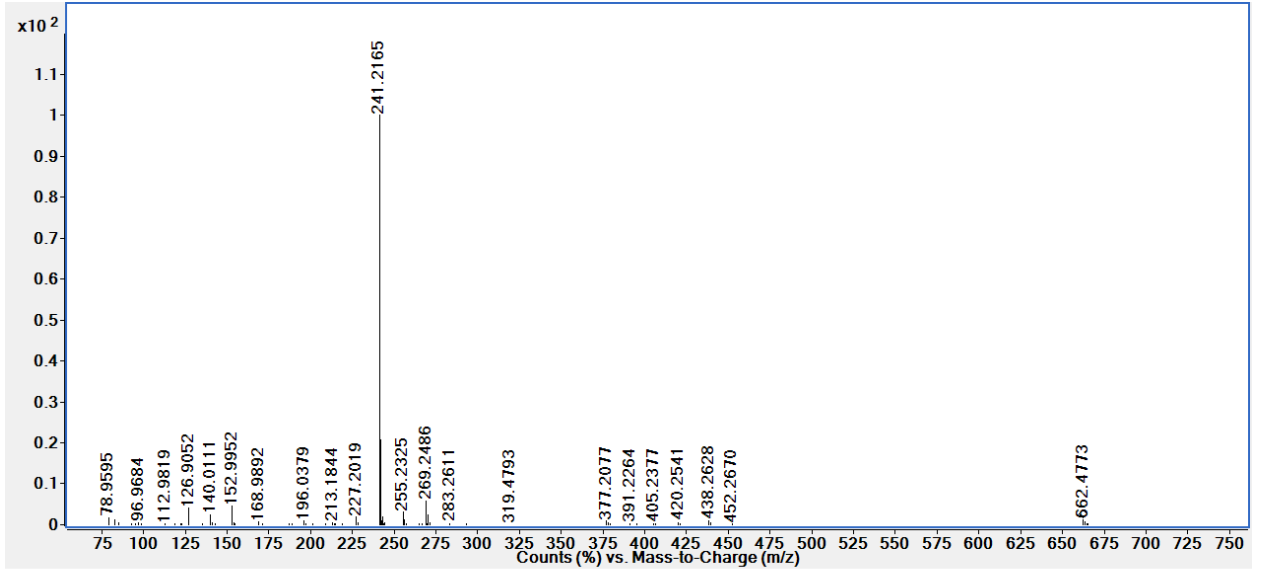


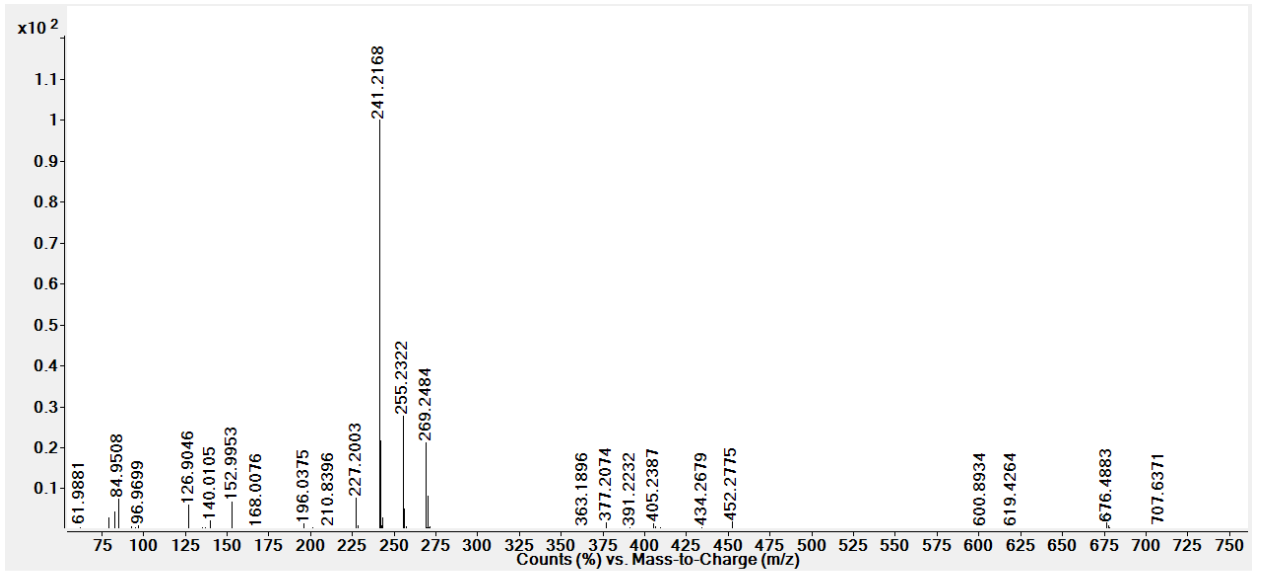
**Figure 6.6 ESI MS-MS (-ve) fragmentation spectra of PA lipid at m/z 647.49.**

Fraction III shows the presence of saturated polar lipids in ESI-MS spectrum which includes PE lipid ions at m/z 662.47, 676.48, 690.50 and traces of saturated PA lipids (m/z 647 and m/z 633) (figure 6.7). All the predicted lipid structures were also confirmed by comparing them with exact mass of predicted molecule with sub ppm level accuracy (Table 3).

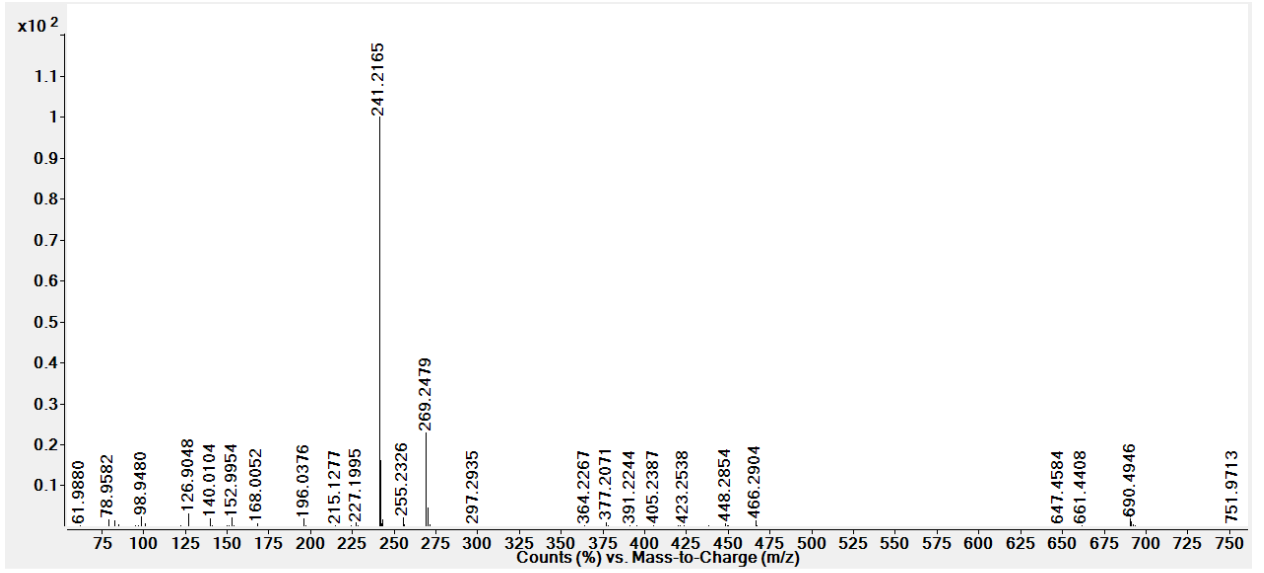
a)



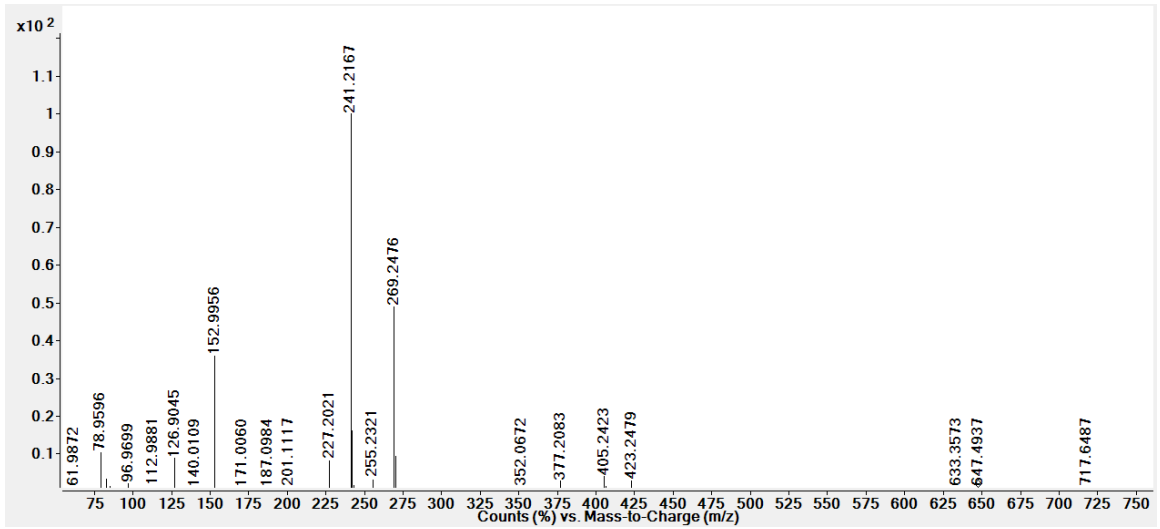
b)



c)



d)



e)

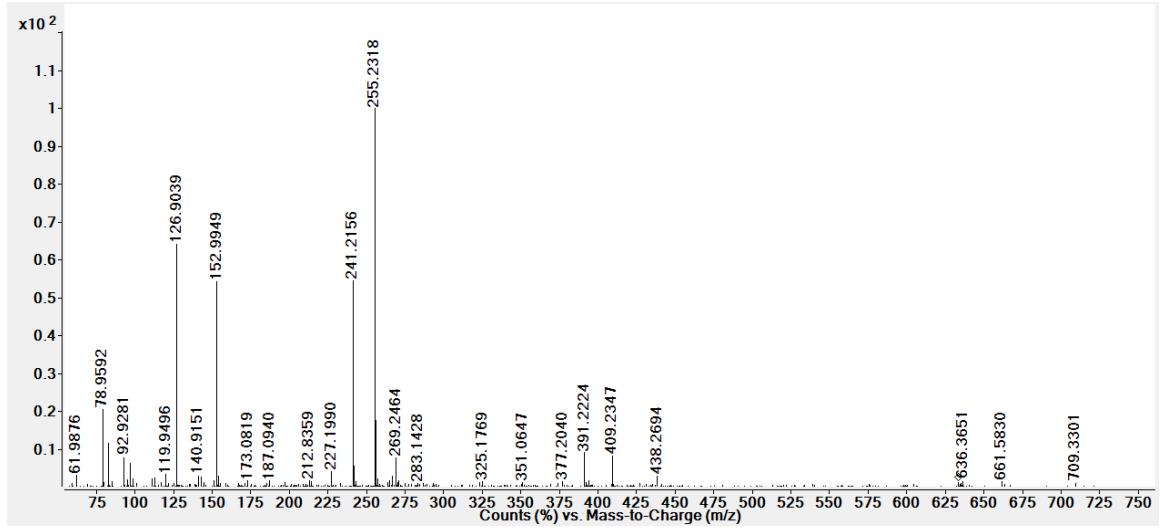


**Figure 6.7 ESI MS-MS (-ve) fragmentation spectra of fraction III lipids**  
a) 662.47, b) 676.48, c) 690.50 d) 647.4 and e) 633.4

Type	(M-H) <sup>-</sup>		
	Observed m/z	Exact m/z	Error (ppm)
PG	693.4701	693.4712	2.3
	707.4852	707.4869	2.4
	721.5013	721.5025	1.7
	735.5187	735.5182	0.7
	749.5325	749.5338	1.7
PA	633.4481	633.4501	3.1
	647.4635	647.4656	3.2
CL	1309.9200	1309.9180	1.53
	1323.9336	1323.9337	0.1
	1337.9482	1337.9488	0.4
	1351.9639	1351.9650	0.88
PE	662.4773	662.4766	1.0
	676.4896	676.4923	4.0
	690.5046	690.5079	4.8

**Table 6.3 Comparison of observed mass with exact mass of the predicted molecule.**

In summary, through analysis of fractions derived from thermophile *Anoxybacillus* sp. strain 7L, we have identified lipid and fatty acid compositions. The major cellular fatty acids identified from whole cell fatty acid analysis were iso-15:0 (52.29 %) and iso-17:0 (18.64 %). These data were similar to those from other *Anoxybacillus* sp. strains (7). Through tandem mass spectrometry we have observed a higher amount of PG lipids followed by cardiolipins and PE. A trace amount of PA lipids was also present in both Fraction II and III.

It is of interest to mention that Rezanka et al. performed a polar lipid characterization study on *Anoxybacillus* spp. strain *A. bogrovensis*. and *A. rupiensis* isolated from Bulgarian hot springs (7, 11). They reported unique lipid pattern with alanyl-, lysyl-, and glucosyl-phosphatidylglycerols (PG) and cardiolipins (CL). They also reported the presence of plasmalogens, characterized by the presence of a vinyl ether linkage at the *sn*-1 position (11). Deep et al. reported the presence of PG, cardiolipins, phosphatidylethanolamine (PE), phosphatidylcholine (PC) in *A. suryakundensis* a moderately thermophilic, alkalitolerant bacterium (12). *A. pushchinoensis* also contains CL, PG, PE, PC and unknown aminolipid in the cell membrane (13). Lipid profile of 7L strain was similar to that reported for other *Anoxybacillus* strains (11-13). However, we did not observe any amino lipids or plasmalogens in 7L, which appeared as unique pattern in *A. bogrovensis* and *A. rupiensis* (11). We observed similar trend for thermostability in *Geobacillus* strain *GWE1*, however, major lipid content for *GWE1* was PE followed by PG, PA and cardiolipins (14). *Bacillus* spp. fatty acyl ester lipids also behave in same way and increase iso fatty acid chains with increase in growth

temperature (15). These properties are known to increase the phase transition temperature of cell membrane and allow activities to survive at high temperatures (16-18). These lipid structural features could partially explain how the *7L* strain thrives at high temperatures.

#### **6.4. Conclusion**

Bacteria survive at higher temperature through several modifications. Thermophilic lipids compared to mesophilic lipids contain specific properties that allow the organism to survive at higher temperatures. We have observed these properties in lipids isolated from *7L* strain which includes the increase of saturated fatty acids and iso branched fatty acid chains with an iso/anteiso ratio of about 8:1.

## 6.5 References

- 1) Urbeita, M.S., Porati, G.W., Segretin, A.B., González-Toril, E., Giaveno, M.A. & Donati, E.R. Copahue Geothermal System: A Volcanic Environment with Rich Extreme Prokaryotic Biodiversity. *Microorganisms* **3**, 344-363 (2015).
- 2) Urbietta, M. S., Rascovan, N., Castro, C., Revale, S., Giaveno, M. A., Vazquez, M., & Donati, E. R. (2014). Draft Genome Sequence of the Novel Thermoacidophilic Archaeon *Acidianus copahuensis* Strain ALE1, Isolated from the Copahue Volcanic Area in Neuquén, Argentina. *Genome Announcements* **2(3)**, e00259-14 (2014).
- 3) Correa-Llantén, D. & Blamey, J.M., Isolation and characterization of a *Anoxybacillus* sp. strain 7l. (Manuscript in progress).
- 4) Pikuta, E., Lysenko, A., Chuvilskaya, N., Mendrock, U., Hippe, H., Suzina, N., Nikitin, D., Osipov, G. & Laurinavichius, K. (2000). *Anoxybacillus pushchinensis* gen. nov., sp. nov., a novel anaerobic, alkaliphilic, moderately thermophilic bacterium from manure, and description of *Anoxybacillus flavithermus* comb. nov. *IJSEM*. **50**, 2109-2117 (2000).
- 5) Lo, S.L. & Chang, E.L. Purification and characterization of a liposomal forming tetraether lipid fraction. *Biochem. Biophys. Res. Commun.* **167**, 238-243 (1990).
- 6) Sasser, M., *Bacterial identification by gas chromatographic analysis of fatty acids methyl esters (GC-FAME)*. (Technical note for MIDI, Microbial ID Inc., 2006)
- 7) Atanassova, M., Derekova, A., Mandeva, R., Sjøholm, C. & Kambourova, M. *Anoxybacillus bogrovensis* sp. nov., a novel thermophilic bacterium isolated from a hot spring in Dolni Bogrov, Bulgaria. *IJSEM* **58**, 2359-2362 (2008).

- 8) Oursel, D., Loutelier-Bourhis, C., Orange, N., Chevalier, S., Norris, V. & Lange, C.M. Lipid composition of membranes of *Escherichia coli* by liquid chromatography/tandem mass spectrometry using negative electrospray ionization. *Rapid Commun. Mass Spectrom.* **21**, 1721-1728 (2007).
- 9) Hsu, F.F. & Turk, J. Studies on phosphatidylglycerol with triple quadrupole tandem mass spectrometry with electrospray ionization: fragmentation processes and structural characterization. *J. Am. Soc. Mass Spectrom.* **12**, 1036-1043 (2001).
- 10) Hsu, F.F. & Turk, J. Structural characterization of cardiolipin by tandem quadrupole and multiple-stage quadrupole ion-trap mass spectrometry with electrospray ionization. *J. Am. Soc. Mass Spectrom.* **16**, 491-504 (2004).
- 11) Rezanka, T., Kambourova, M., Derekova, A., Kolouchova, I. & Sigler, K., (2012) LC–ESI–MS/MS Identification of Polar Lipids of Two Thermophilic *Anoxybacillus* Bacteria Containing a Unique Lipid Pattern. *Lipids* **47**, 729-739 (2012).
- 12) Deep, K., Poddar, A. & Das, S. *Anoxybacillus suryakundensis* sp. nov, a Moderately Thermophilic, Alkalitolerant Bacterium Isolated from Hot Spring at Jharkhand, India. *Plos one* **8(12)**, 1-11 (2013).
- 13) Miñana-Galbis D, Pinzón D, Lorén J, Manresa À & Oliart-Ros R. Reclassification of *Geobacillus pallidus* (Scholz *et al.* 1988) Banat *et al.* 2004 as *Aeribacillus pallidus* gen. nov., comb. nov. *Int J Syst Evol Microbiol* **60(7)**, 1600-1604 (2010).
- 14) Shah, S.P., Jansen S.A., Taylor, L.J., Chong P.L., Correa-Llantén D.N. & Blamey J.M. Lipid composition of thermophilic *Geobacillus* sp. strain *GWE1*, isolated from sterilization oven. *Chemistry and Physics of Lipids* **180**, 61-71 (2014).

- 15) Rilfors, L., Wieslander, A. & Stahl, S. Lipid and protein composition of membranes of *Bacillus megaterium* variants in the temperature range 5 to 70°C. *Journal of Bacteriology* **135**, 1043-1052 (1978).
- 16) Daniel, R.M. & Cowan, D.A. Biomolecular stability and life at higher temperatures. *Cell. Mol. Life Sci.* **57**, 250–264 (2000).
- 17) Koga, Y. Thermal adaptation of bacterial and archael lipid membranes. *Archaea* **2012**, 1-6 (2012).
- 18) Konings, W.N., Albers, S.V., Koning, S. & Driessen, A.J.M.,. The cell membrane plays a crucial role in survival of bacteria and archaea in extreme environments. *Antonie van Leeuwenhoek* **81**, 61-72 (2002).

## CHAPTER

### 7. LIPID COMPOSITION SUMMARY

#### 7.1 Introduction

In present work we have extracted and identified lipids from three different microorganisms:

- 1) *GWE1*, a gram positive thermophile isolated from sterilization oven
- 2) *7L*, a gram positive thermophile isolated from Copahue Volcano
- 3) *IIP* (Psychrophile) from Antarctica

*GWE1* microorganism belongs to genus *Geobacillus*, *7L* belongs to genus *Anoxybacillus* and *IIP* belongs to genus *Serratia*. In particular, this chapter focuses on comparing lipid composition of isolated extremophiles and understanding its implication on cell membrane stability.

#### 7.2 Lipid Composition

In microorganism cell, lipid bilayer exist in the form of liquid crystalline state phase in which, the original bilayer is conserved due to electrostatic interaction between polar head groups and hydrophobic interaction of nearby acyl chains. At the same time there is some disorder in acyl chains which allows them to progressively increase motion from hinged carbonyl carbon to terminal methyl group (1). Compositions of fatty acids affect this liquid crystalline structure stability. Increasing longer chain fatty acid molecules and/or having iso branched fatty acid molecule increase the hydrophobic forces in acyl chain and stabilizes the lipid bilayer at higher temperatures and allows cell to grow at

higher temperature. Degree of unsaturation or anteiso branched fatty acid generates a kink in acyl chain and destabilizes the liquid crystalline state and allows the cell to grow at lower temperatures (2, 3).

<b>7L</b>		<b>GWEI</b>		<b>IIP</b>	
<b>Fatty Acid</b>	<b>%</b>	<b>Fatty Acid</b>	<b>%</b>	<b>Fatty Acid</b>	<b>%</b>
Iso-13:0	0.12	Iso-14:0	0.5	12:0	1.8
Iso-14:0	0.39	14:0	3.1	14:0	5.39
14:0	1.34	Iso-15:0	13.6	14:0 3OH	6.72
Iso-15:1	0.10	Anteiso-15:0	3.6	15:0	0.41
Iso-15:0	52.29	15:0	3.2	16:1( $\omega$ 7/6)	29.34
Anteiso-15:0	4.17	16:1( $\omega$ 7)	12.8	16:1( $\omega$ 5)	0.25
15:0	0.41	Iso-16:0	28.5	16:0	34.20
Iso-16:1	0.16	Iso-17:0	13.5	17:0 CP <sup>1</sup>	7.61
Iso-16:0	3.57	Anteiso-17:0	12.3	17:0	0.5
16:1( $\omega$ 7)	1.28	17:0	2.9	18:2 ( $\omega$ 6)	0.22
16:1( $\omega$ 6)	0.76	18:1	2.6	18:1 ( $\omega$ 7)	10.10
16:1( $\omega$ 5)	0.12	18:0	3.5	18:0	1.68
16:0	7.00			19:0 (Cyclo $\omega$ 8)	0.23
Iso-17:1 ( $\omega$ 5)	1.30			19:0	0.13
Anteiso-17:1	0.29				
Iso-17:0	18.64				
Anteiso-17:0	5.30				
17:0	0.15				
Iso-18:0	0.11				
Iso-18:1 ( $\omega$ 9)	1.21				
Iso-18:1 ( $\omega$ 7)	0.33				
18:0	0.68				
Iso-19:0	0.22				

<sup>1</sup>CP: Cyclopentane Group

**Table 7.1 Fatty acyl composition for microorganism 7L, GWEI and IIP.**

Data of fatty acyl composition of *GWEI* is used from reference 4.

	<i>7L</i>	<i>GWE1</i>	<i>IIP</i>
Saturated FA chain (%)	94.39	59.3	58.67
Unsaturated FA chain (%)	5.55	15.9	39.66
Iso branched chain (%)	78.44	84.7	NA
Anteiso branched chain (%)	9.76	15.4	NA
Iso/Anteiso ratio	8.04	3.73	NA
Saturated/Unsaturated ratio	17.01	5.5	1.48

**Table 7.2: Summary of fatty acyl composition**

Table 7.1 and 7.2 summarizes the fatty acyl components present in these microorganisms. Microorganism *7L* shows fatty acyl iso to anteiso branching ratio of 8.04 to 1 and fatty acyl saturated to unsaturated ratio of about 17.00 to 1. *GWE1* organism shows fatty acyl iso to anteiso ratio of 3.73 to 1 and fatty acyl saturated to unsaturated ratio of about 5.5 to 1. This allows both *7L* and *GWE1* to grow at higher temperatures. In *IIP* organism we didn't observe any iso to anteiso branching but we observed much lower fatty acyl saturated to unsaturated ratio (1.48 to 1). This unsaturated fatty acyl chain produces kink in bilayer structure and decrease the hydrophobic forces between the chains, which supports its growth at lower temperature.

Shen et al. reported fatty acyl compositions for three mesophilic *Bacillus* strains (*B. pumilus*, *Bacillus sp. (XI)*, *B. licheniformis*) and three thermophilic bacillus (*B. stearothermophilus FJW*, *B. stearothermophilus 10*, *B. stearothermophilus 2184*) strains. This comparison is summarized in table below (5).

	<i>A</i>	<i>B</i>	<i>C</i>
Saturated FA chain (%)	69.4	68.8	62.3
Unsaturated FA chain (%)	5.4	2.1	<1%
Iso branched chain (%)	72.9	71.3	59.2
Anteiso branched chain (%)	25.3	27.5	37.8
Iso/Anteiso ratio	2.881	2.593	1.566
Saturated/Unsaturated ratio	12.852	32.762	NR

**Table 7.3 Fatty acyl composition for mesophilic strains *A. B. pumilus*; *B. Bacillus sp. (XI)*; *C. B. licheniformis***

	<i>D</i>	<i>E</i>	<i>F</i>
Saturated FA chain (%)	100	94.5	88.4
Unsaturated FA chain (%)	Trace	5.4	11.5
Iso branched chain (%)	74.4	86.5	80.5
Anteiso branched chain (%)	18.8	11.6	14.5
Iso/Anteiso ratio	3.957	7.457	5.552
Saturated/Unsaturated ratio	NA	17.500	7.657

**Table 7.4 Fatty acyl composition for mesophilic strains *D. B. stearothermophilus FJW*; *E. B. stearothermophilus 10*; *F. B. stearothermophilus 2184***

Genus bacillus mesophilic and thermophilic strains also have shown the higher iso/anteiso ratio of 3.95 or higher compare to mesophilic strains in which the same was less than 2.9. This observation was consistent with the findings of this research.

This result shows that higher fatty acyl Iso branching to anteiso branching ratio or higher fatty acyl saturation vs unsaturation ratio is indicator of microorganism's ability to survive at higher temperature. We didn't observe significant difference in lipid headgroup structure for these three microorganisms to compare its role in thermostability of individual microorganism. Results obtained from fatty acyl composition study confirm the previously reported theory of lipid packing (2, 3).

### **7.3 Contribution to the field**

In this dissertation we have successfully isolated and identified major polar lipid molecules of three different extremophiles in order to understand the thermostability of individual microorganism in both high and low temperatures. This research work includes use of multiple complementary analytical techniques with step by step guidance to isolate and identify polar lipids from three novel microorganisms. Each of the analytical technique provides additional information about the structure and gives us more confidence about the identified polar lipid structure in microorganisms with biotechnological potential. Different bacterial species display different lipid composition based on the environmental conditions exposure. Understanding lipid composition also helps in taxonomical classification of microorganisms and also provides valuable information about synthesis pathways and enzymes involved (6). Understanding lipid profile also helps understanding the antimicrobial drug efficacy (7).

#### 7.4 Reference

- 1) Eze, M.O. Phase Transitions in Phospholipid Bilayers: Lateral Phase Separations Play Vital Roles in Biomembranes. *Biochemical education* **19(4)**, 204-208 (1991).
- 2) Koga, Y. Thermal adaptation of bacterial and archaeal lipid membranes. *Archaea* **2012**, 1-6 (2012).
- 3) Daniel, R.M. & Cowan, D.A. Biomolecular stability and life at higher temperatures. *Cell. Mol. Life Sci.* **57**, 250–264 (2000)
- 4) Correa-Llantén, D., Larraín-Linton, J., Muñoz, P.A., Castro M., Boehmwald, F. & Blamey, J.M. Characterization of the thermophilic bacterium *Geobacillus* sp. strain *GWE1* isolated from a sterilization oven. *Kor. J. Microb. Biotech.* **41(3)**, 278-283 (2013).
- 5) Shen, P.Y., Coles, E., Foote, J.L. & Stenesh J. Fatty acid distribution in mesophilic and thermophilic strains of the genus *Bacillus*. *J. Bacteriol.*, 479-481 (1970)
- 6) Sohlenkamp, C. & Geiger, O. Bacterial membrane lipids: Diversity in structure and pathways. *FEMS Microbiology reviews* **40(1)**, 133-159 (2016).
- 7) Epanand, R.F., Savage, P.B. & Epanand, R.M. Bacterial lipid composition and the antimicrobial efficacy of cationic steroid compounds (Ceragenins). *Biochim biophys acta* **1768(10)**, 2500-2509 (2007).

## BIBLIOGRAPHY

- Adosraku, R.K., Anderson, M.M., Anderson, G.J., Choi, G., Croft, S.L., Yardley, V., Phillipson, J.D. & Gibbons, W.A. Proton NMR lipid profile of *Leishmania donouani promastigotes*. *Mol. Biochem. Parasitol.* **62**, 251-262 (1993).
- Adoskaru, K.R., Choi, G., Kokotos, V.C., Anderson, M.M. & Gibbons, W.A. NMR lipid profiles of cells, tissues, and body fluids: proton NMR analysis of human erythrocyte lipids. *J. Lipid Res.* **35**, 1925-1931 (1994).
- Aluyi, H.S., Boote, V., Drucker, D.B., Wilson, J.M. & Ling, Y.H., Analysis of polar lipids from some representative enterobacteria, *Plesiomonas* and *Acinetobacter* by fast atom bombardment-mass spectrometry. *Journal of Applied Bacteriology* **73(5)**, 1365-2672 (1992).
- Amenabar, M.J. & Blamey, J.M. Purification and characterization of a thermostable glutamate dehydrogenase from a thermophilic bacterium isolated from a sterilization drying oven. *BMB reports* **45**, 91-95 (2012).
- Araki, S., Sakurai, T., Oohusa, T. & Kayama, M. Distribution of phosphatidylcholine in brown algae. *Nippon Suisan Gakkaishi* **55**, 2049 (1989).
- Atanassova, M., Derekova, A., Mandeva, R., Sjøholm, C. & Kambourova, M. *Anoxybacillus bogrovensis* sp. nov., a novel thermophilic bacterium isolated from a hot spring in Dolni Bogrov, Bulgaria. *IJSEM* **58**, 2359-2362 (2008).
- Barria, C., Malecki, M. & Arraiano, C. Bacterial adaptation to cold. *Microbiology* **159(12)**, 2437-2443 (2013).
- Beveridge, T.J. Structures of gram-negative cell walls and their derived membrane vesicles. *J. Bacteriol.* **181**, 4725-4733 (1999).
- Birdsall, N.J., Feeney, J., Lee, A.G., Levine, K. & Metcalfe, J.C. Dipalmitoyl-lecithin: assignment of the <sup>1</sup>H and <sup>13</sup>C nuclear magnetic resonance spectra, and conformational studies. *J. Chem. Soc., Perkin Trans.* **2**, 1441-1445 (1972).
- Bloom, M., Evans, E. & Mouritsen, O.G. Physical properties of the fluid lipid-bilayer component of cell membranes: A perspective. *Q. Rev. Biophys.* **24**, 293-297 (1991).
- Brock, T. Life at high temperatures. *Science* **230**, 132-138 (1985)
- Brown, J.R. & Lupas, A.N. 1998. What makes a thermophile?. *Trends in Microbiology* **6**, 349-351 (1998).
- Carty, S.M., Sreekumar, K.R. & Raetz, C.R.. Effect of cold shock on lipid A biosynthesis in *Escherichia coli*. Induction At 12 degrees C of an acyltransferase specific for palmitoleoyl-acyl carrier protein. *J. Biol. Chem.* **274**, 9677-9685 (1999).

- Casu, M., Anderson, G.J., Choi, G. & Gibbons, W.A. NMR lipid profiles of cells, tissues and body fluids-1D and 2D proton NMR of lipids from rat liver. *Magnet. Reson. Chem.* **29**, 594-602 (1991).
- Chintalapati, S., Kiran, M.D. & Shivaji, S. Role of membrane lipid fatty acids in cold adaptation. *Cell Mol Biol (Noisy-le-grand)* **50**, 631-642 (2004).
- Cooper G.M., *The Cell: A Molecular Approach. 2nd edition.* (Sinauer Associates, Sunderland (MA), 2000).
- Chong, P.L. Archaeobacterial bipolar tetraether lipids: Physico-chemical and membrane properties. *Chem. Phys. Lipids.* **163**, 253-265 (2010).
- Correa-Llantén, D., Larraín-Linton, J., Muñoz, P.A., Castro M., Boehmwald, F. & Blamey, J.M. Characterization of the thermophilic bacterium *Geobacillus* sp. strain *GWE1* isolated from a sterilization oven. *Kor. J. Microb. Biotech.* **41(3)**, 278-283 (2013).
- Correa-Llantén, D. & Blamey, J.M. Isolation and characterization of a *Serratia* sp. strain *IIP*. (Manuscript in progress)
- Correa-Llantén, D. & Blamey, J.M., Isolation and characterization of a *Anoxybacillus* sp. strain *7l*. (Manuscript in progress).
- D'Amico, S., Collins, T., Marx, J.C., Feller, G. & Gerday, C. Psychrophilic microorganisms: challenges for life. *EMBO reports* **7**, 385–389 (2006).
- Daniel, R.M. & Cowan, D.A. Biomolecular stability and life at higher temperatures. *Cell Mol. Life Sci.* **57**, 250-264 (2000).
- Danson, M.J. & Hough, D.W. Structure, function and stability of enzymes from the Archaea. *Trends Microbiol.* **6**, 307-314 (1998).
- De la Vega-Hernandez, K. & Antuch, M., The Heteronuclear Single-Quantum Correlation (HSQC) Experiment: Vectors versus Product Operators. *J. Chem. Educ.* **92**, 482-487 (2015).
- De Rosa, M., Trincone, A., Nicolaus, B. & Gambacorta A. Archaeobacteria: lipids, membrane structures, and adaptation to environmental stresses. In *Life under Extreme Conditions*. pp.61-87. (Springer, Heidelberg, 1991).
- Deep, K., Poddar, A. & Das, S. *Anoxybacillus* suryakundensis sp. nov, a Moderately Thermophilic, Alkalitolerant Bacterium Isolated from Hot Spring at Jharkhand, India. *Plos one* **8(12)**, 1-11 (2013).
- Dufour, E. *Infrared Spectroscopy for Food Quality Analysis and Control*, (Elsevier Inc., Burlington (MA), 2009).

- Ellen, A.F., Zolghadr, B., Driessen, A.J.M. & Albers, S.V. Shaping the Archaeal Cell Envelope. *Archaea* **2010**, 1-13 (2010).
- Epanand, R.F., Savage, P.B. & Epanand, R.M. Bacterial lipid composition and the antimicrobial efficacy of cationic steroid compounds (Ceragenins). *Biochim biophys acta* **1768(10)**, 2500-2509 (2007).
- Eze, M.O. Phase Transitions in Phospholipid Bilayers: Lateral Phase Separations Play Vital Roles in Biomembranes. *Biochemical education* **19(4)**, 204-208 (1991).
- Fenn, J.B., Mann, M., Meng, C.K., Wong, S.F. & Whitehouse, C.M. Electrospray ionization-principles and practice. *Mass Spectrom Rev* **9**, 37-70 (1990).
- "FT-IR Spectroscopy - Attenuated Total Reflectance (ATR)". *Perkin Elmer Life and Analytical Sciences*. 2005.
- Gambacorta, A. *et. al.* Unique features of lipids of archaea. *Systems of Applied Microbiology* **16**, 518-527 (1994).
- Gennis, R.B., *Biomembranes. Molecular Structure and Function*. (Springer-Verlag, New York, 1989).
- Gilbert, J.A., Hill, P.J., Dodd, C.E. & Laybourn-Parry, J. Demonstration of antifreeze protein activity in Antarctic lake bacteria. *Microbiology* **150**, 171-180 (2004).
- Grimont, P.A.D., Grimont, F. & Dulong de Rosnay, H.L.C. 1976. Taxonomy of the Genus *Serratia*. *Journal of General Microbiology* **98**, 39-46 (1976).
- Guan, Z., Tian, B., Perfumo, A., & Goldfine, H. 2013. The polar lipids of *Clostridium psychrophilum*, an anaerobic psychrophile. *Biochimica et Biophysica Acta* **1831(6)**, 1108-1112 (2013).
- Hoffmann, E.De, Charette, J. & Stroobant, V. *Mass spectrometry: Principles and applications*. (John Wiley and Sons Inc., Hoboken(NJ), 1996).
- Hsu, F.F. & Turk, J. Characterization of phosphatidylethanolamine as a lithiated adduct by triple quadrupole tandem mass spectrometry with electrospray ionization. *J. Mass Spectrom.* **35**, 595-606 (2000).
- Hsu, F.F. & Turk, J. Studies on phosphatidylglycerol with triple quadrupole tandem mass spectrometry with electrospray ionization: fragmentation processes and structural characterization. *J. Am. Soc. Mass Spectrom.* **12**, 1036-1043 (2001).
- Hsu, F.F. & Turk, J. Electrospray ionization/tandem quadrupole mass spectrometric studies on phosphatidylcholines: the fragmentation processes. *J. Am. Soc. Mass Spectrom.* **14**, 352-363 (2003).

- Hsu, F.F. & Turk, J. Structural characterization of cardiolipin by tandem quadrupole and multiple-stage quadrupole ion-trap mass spectrometry with electrospray ionization. *J. Am. Soc. Mass Spectrom.* **16**, 491-504 (2004).
- Hsu, F.F., Turk, J., Shi, Y. & Groisman, E.A. Characterization of acylphosphatidylglycerols from *Salmonella typhimurium* by tandem mass spectrometry with electrospray ionization. *J. Am. Soc. Mass Spectrom.* **15**(1), 1-11 (2004).
- Johns, G.C. & Somero, G.N. Evolutionary convergence in adaptation of proteins to temperature: A4-lactate dehydrogenases of Pacific damselfishes (*Chromis* spp.). *Mol Biol Evol.* **21**, 314-320 (2004).
- Khachane, A.N., Timmis, K.N. & dos Santos, V.A. Uracil content of 16S rRNA of thermophilic and psychrophilic prokaryotes correlates inversely with their optimal growth temperatures. *Nucleic Acids Res* **33**, 4016-4022 (2005).
- Klein, W., Weber, M.H. & Marahiel, M.A. Cold shock response of *Bacillus subtilis*: isoleucine-dependent switch in the fatty acid branching pattern for membrane adaptation to low temperatures. *J. Bacteriol.* **181**, 5341-5349 (1999).
- Koga, Y. & Nakano, M., A dendrogram of archaea based on lipid component parts composition and its relationship to rRNA phylogeny, *Systematic and Applied Microbiology* **31**(3), 169-182 (2008).
- Koga, Y. Thermal adaptation of bacterial and archael lipid membranes. *Archaea* **2012** 1-6 (2012).
- Konings, W.N., Albers, S.V., Koning, S. & Driessen, A.J.M. The cell membrane plays a crucial role in survival of bacteria and archaea in extreme environments. *Antonie van Leeuwenhoek* **81**, 61-72 (2002).
- Lai, D., Springstead, J.R. & Monbouquette, H.G. Effect of growth temperature on ether lipid biochemistry in *Archaeoglobus fulgidus*. *Extremophiles* **12**, 271-278 (2008).
- Leone, S., Molinaro, A., Lindner, B., Romano, I., Nicolaus, B., Parrilli, M., Lanzetta, R. & Holst, O. The structures of glycolipids isolated from the highly thermophilic bacterium *Thermus thermophilus* Samu-SA1. *Glycobiology* **16**, 766-775 (2006).
- Lewis, R.N.A.H., Mantsch, H.H. & McElhaney, R.N. Thermotropic phase behavior of phosphatidylcholines with  $\omega$ -tertiary-butyl fatty acyl chains. *Biophys. J.* **56**, 183-193 (1989).
- Lo, S.L. & Chang, E.L. Purification and characterization of a liposomal forming tetraether lipid fraction. *Biochem. Biophys. Res. Commun.* **167**, 238-243 (1990).
- Macomber, R.S. *A complete introduction to modern NMR spectroscopy*. (John Wiley and Sons Inc., Hoboken(NJ), 1998)

- March, R. An Introduction to Quadrupole Ion Trap Mass Spectrometry, *Journal of Mass Spectrometry* **32**(4), 351-369 (1997).
- Mancuso-Nichols, C.A.; Guezennec, J. & Bowman, J.P. Bacterial exopolysaccharides from extreme marine environments with special consideration of the southern ocean, sea ice, and deepsea hydrothermal vents. *Mar. Biotechnol.* **7**, 253-271 (2004).
- Milosevic, M. *Internal Reflectance near Critical Angle, in Internal Reflection and ATR Spectroscopy*. (John Wiley & Sons, Inc., Hoboken(NJ), 2012).
- Mirabella, FM Jr. *Practical Spectroscopy Series; Internal reflection spectroscopy: Theory and applications*, (Marcel Dekker, Inc., New York, 1993).
- Miñana-Galbis D, Pinzón D, Lorén J, Manresa À & Oliart-Ros R. Reclassification of *Geobacillus pallidus* (Scholz *et al.* 1988) Banat *et al.* 2004 as *Aeribacillus pallidus* gen. nov., comb. nov. *Int J Syst Evol Microbiol* **60**(7), 1600-1604 (2010).
- Morita, R.Y. Psychrophilic Bacteria. *Bacteriol Rev* **39**, 144-167 (1975).
- Morell, V. Microbiology's Scarred Revolutionary. *Science* **276**, 669-702 (1997).
- Murari, R., Abd El-Rahman, M.A., Wedmid, Y., Parthasarathy, S. & Baumann, W.J. Carbon-13 nuclear magnetic resonance spectroscopy of phospholipids in solution. Spectral and stereochemical assignments based on  $^{13}\text{C}$ - $^{31}\text{P}$  and  $^{13}\text{C}$ - $^{14}\text{N}$  couplings. *J. Org.Chem.* **47**, 2158-2163 (1982).
- Nan, L., Zhuangde, J. & Xueyong, W. Emerging microfluidic devices for cell lysis: a review. *The Royal Society of Chemistry* **14**(6), 1060-1073 (2013).
- Neuhaus, F. C. & Baddiley, J. A continuum of anionic charge: structures and functions of d-alanyl-teichoic acids in gram-positive bacteria. *Microbiol Mol Biol Rev* **67**, 686-723 (2003).
- Nichols, F. C., Riep, B., Mun, J., Morton, M. D., Kawai, T., Dewhirst, F. E. & Smith, M. B. Structures and biological activities of novel phosphatidylethanolamine lipids of *Porphyromonas gingivalis*. *J. Lipid Res.* **47**, 844-853 (2006).
- Nzai, J.M. & Proctor, A. Soy lecithin phospholipid determination by Fourier transform infrared spectroscopy and the acid digest/Aarseno-molybdate method: A comparative study. *JAACS* **76**, 61-66 (1999).
- Oursel, D., Loutelier-Bourhis, C., Orange, N., Chevalier, S., Norris, V. & Lange, C.M. Lipid composition of membranes of *Escherichia coli* by liquid chromatography/tandem mass spectrometry using negative electrospray ionization. *Rapid Commun. Mass Spectrom.* **21**, 1721-1728 (2007).
- Pack, S.P. & Yoo, Y.J. Protein thermostability: structure-based difference of amino

acid between thermophilic and mesophilic proteins. *Journal of Biotechnology* **111**, 269-277 (2004).

- Phadtare, S. & Inouye, M. Genome-wide transcriptional analysis of the cold shock response in wild-type and cold-sensitive, quadruple-csp-deletion strains of *Escherichia coli*. *J Bacteriol.* **186**, 7007-7014 (2004).
- Pikuta, E., Lysenko, A., Chuvilskaya, N., Mendrock, U., Hippe, H., Suzina, N., Nikitin, D., Osipov, G. & Laurinavichius, K. (2000). *Anoxybacillus pushchinensis* gen. nov., sp. nov., a novel anaerobic, alkaliphilic, moderately thermophilic bacterium from manure, and description of *Anoxybacillus flavithermus* comb. nov. *IJSEM.* **50**, 2109-2117 (2000).
- Ramos, J.L., Gallegos, M.T., Marques, S., Ramos-Gonzalez, M.I., Espinosa-Urgel, M. & Segua, A. Responses of Gram-negative bacteria to certain environmental stressors. *Curr. Opin. Microbiol.* **4**, 166-171 (2001).
- Rascoe, J., Berg, M., Melcher, U., Mitchell, F. L., Bruton, B. D., Pair, S. D. & Fletcher, J. Identification, phylogenetic analysis, and biological characterization of *Serratia marcescens* strains causing cucurbit yellow vine disease. *Phytopathology* **93**, 1233-1239 (2003).
- Rezanka, T., Kambourova, M., Derekova, A., Kolouchova, I. & Sigler, K., (2012) LC-ESI-MS/MS Identification of Polar Lipids of Two Thermophilic *Anoxybacillus* Bacteria Containing a Unique Lipid Pattern. *Lipids* **47**, 729-739 (2012).
- Rilfors, L., Wieslander, A. & Stahl, S. Lipid and protein composition of membranes of *Bacillus megaterium* variants in the temperature range 5 to 70°C. *Journal of Bacteriology* **135**, 1043-1052 (1978).
- Rothschild, L.J. & Mancinelli, R.L. Life in extreme environments. *Nature* **409**, 1092-1101 (2001).
- Roberts, P. Chapter 8: One-Dimensional (1D) NMR Experiments [PowerPoint slides]. Retrieved from <http://www.bionmr.unl.edu> (2014).
- Roberts, P. Chapter 9: 2D NMR Experiments [PowerPoint slides]. Retrieved from <http://www.bionmr.unl.edu> (2014).
- Russi, M., Buzzini, P., Cordisco, L., Amaretti, A., Sala, M., Raimondi, S., Ponzoni, C., Pagnoni, U.M. & Matteuzzi, D. Growth, lipid accumulation, and fatty acid composition in obligate psychrophilic, facultative psychrophilic, and mesophilic yeasts. *FEMS Microbiol. Ecol.* **69**, 363-372 (2009).
- Sardesai, Y. N. & Bhosle, S. Organic solvent-tolerant bacteria in mangrove ecosystem. *Curr. Sci.* **82**, 622-623 (2002).
- Sasser, M., *Bacterial identification by gas chromatographic analysis of fatty acids*

*methyl esters (GC-FAME)*. (Technical note for MIDI, Microbial ID Inc., 2006)

- Saunders, N.F *et al.* Mechanisms of thermal adaptation revealed from the genomes of the Antarctic Archaea *Methanogenium frigidum* and *Methanococcoides burtonii*. *Genome Res* **13**, 1580–1588 (2003).
- Schäffer, C. & Messner, P. The structure of secondary cell wall polymers: how Gram-positive bacteria stick their wall together. *Microbiology* **151**, 643-651 (2005).
- Shah, S.P., Jansen S.A., Taylor, L.J., Chong P.L., Correa-Llantén D.N. & Blamey J.M. Lipid composition of thermophilic *Geobacillus* sp. strain *GWE1*, isolated from sterilization oven. *Chemistry and Physics of Lipids* **180**, 61-71 (2014).
- Shimada, H., Nemoto, N., Shida, Y., Oshima, T. & Yamagishi, A. Effects of pH and temperature on the composition of polar lipids in *Thermoplasma acidophilum* HO-62. *J. Bacteriol.* **190**, 5404-5411 (2008).
- Singer, S.J. & Nicholson, G.L. The fluid mosaic model of the structure of cell membranes. *Science* **175**, 720-731 (1972).
- Sohlenkamp, C. & Geiger, O. Bacterial membrane lipids: Diversity in structure and pathways. *FEMS Microbiology reviews* **40(1)**, 133-159 (2016).
- Sparling, M.L., Zidovetzki, R., Muller, L. & Chant, S.I. Analysis of membrane lipids by 500 MHz NMR <sup>1</sup>H NMR. *Analytical Biochemistry* **178**, 67-76 (1989).
- Stetter, K. A brief history of the discovery of hyperthermophilic life. *Biochemical Society Transactions* **41(1)**, 416-420 (2013).
- Stuart, B. *Infrared Spectroscopy: Fundamentals and Applications*, John Wiley & Sons Inc., Hoboken (NJ), 2004).
- Urbieto, M. S., Rascovan, N., Castro, C., Revale, S., Giaveno, M. A., Vazquez, M., & Donati, E. R. (2014). Draft Genome Sequence of the Novel Thermoacidophilic Archaeon *Acidianus copahuensis* Strain ALE1, Isolated from the Copahue Volcanic Area in Neuquén, Argentina. *Genome Announcements* **2(3)**, e00259-14 (2014).
- Urbeita, M.S., Porati, G.W., Segretin, A.B., González-Toril, E., Giaveno, M.A. & Donati, E.R. Copahue Geothermal System: A Volcanic Environment with Rich Extreme Prokaryotic Biodiversity. *Microorganisms* **3**, 344-363 (2015).
- Van de Vossenberg, J. *et al.* The essence of being extremophilic: the role of the unique archaeal membrane lipids. *Extremophiles* **2**, 163-170 (1998).
- Vasilyeva, L., Omelchenko, M., Berestovskaya, Y., Lysenko, A., Abraham, W., Dedysh, S. & Zavarzin, G., 2006. *Asticcacaulis benevestitus* sp. nov., a psychrotolerant,

dimorphic, prosthecate bacterium from tundra wetland soil. *Int J Syst Evol Microbiol* **56(9)**, 2083-2088 (2006).

- Violot, S., Aghajari, N., Czjzek, M., Feller, G., Sonan, G.K., Gouet, P., Gerday, C., Haser, R. & Receveur-Brechot, V. Structure of a full length psychrophilic cellulase from *Pseudoalteromonas haloplanktis* revealed by X-ray diffraction and small angle X-ray scattering. *J Mol Biol* **348**, 1211-1224 (2005).